Daniel Chung

Green Templeton College
University of Oxford

Supervised By:
Prof. Constantin-C. Coussios
Prof. Fergus Gleeson

QUANTITATIVE ASSESSMENT OF TUMOUR RESPONSE TO THERAPY BY DIAGNOSTIC ULTRASOUND

A thesis submitted to the Department of Medical Science
for the degree of Doctor of Philosophy

Trinity 2015

Abstract

Quantitative assessment of tumour response to therapy by diagnostic ultrasound
Daniel Chung, Green Templeton College
Submitted for degree of DPhil, 2015

Chemotherapy forms the mainstay of treatment for patients with liver tumours, which has a number of significant side effects. Treatment response is often assessed some time after commencement of treatment. A quantitative method to detect early liver tumour response to chemotherapy would be beneficial to facilitate termination of ineffective treatment and to minimise unnecessary side effects. This thesis investigated firstly whether fractal analysis of contrast enhanced computed tomography (ceCT) images of colorectal liver metastases could be used to detect early response to chemotherapy. Secondly, a technique based on Nakagami imaging of ultrasound radio-frequency (RF) signals was developed, initially using data from a xenograft mouse tumour model, as a potential early predictor of tumour response. This was subsequently tested using clinical ultrasound data collected from patients undergoing chemotherapy treatment for liver tumours.

Mean fractal dimension (FD) obtained from fractal analysis of volumetric ceCT images of colorectal liver metastases was confirmed as a reliable quantitative parameter to detect tumour tissue changes. There was however no significant difference in the interval change of mean FD from baseline between responding and non-responding metastases. Based on the current study, fractal analysis is unable to detect early liver tumour response to chemotherapy.

Development of an ultrasound-based tissue assessment technique was then performed, owing to the advantages of ultrasound imaging. A Nakagami imaging-based volumetric tissue assessment technique was developed using backscattered RF ultrasound data from xenograft mice tumour treated in an investigation of high intensity focused ultrasound mediated chemotherapy delivery. The percentage of pre-Rayleigh regions (%PRR) obtained from the new analysis technique demonstrated an indirect correlation with the tumour volume. Interval reduction in %PRR from baseline was also found to be significantly greater in tumours that responded to treatment. These observations confirmed the potential of Nakagami imaging-based techniques to detect early tumour response to treatment.

The technique was subsequently used to analyse volumetric ultrasound datasets collected from patients undergoing chemotherapy treatment for liver tumours. The %PRR was found to indirectly correlate with the axial diameter of the liver tumour. Additionally, interval increase in the %PRR between follow-up and baseline study was found to be significantly higher in responding compared to non-responding tumours.

These preliminary results demonstrated the potential of the Nakagami imaging-based volumetric tissue assessment technique to detect early response of liver tumour to chemotherapy. Further work is recommended prior to translation into clinical practice.

Statement of Originality

I hereby declare that this submission is my own work and, to the best of my knowledge, it contains no materials previously published or written by another person, or substantial proportions of material which have been accepted for the award of any other degree or diploma at the University of Oxford or any other educational institution, except where due acknowledgement is made in the thesis.

Any contribution made to the research by others, with whom I have worked at the University of Oxford or elsewhere, is explicitly acknowledged in the thesis.

I also declare that the intellectual content of this thesis is the product of my own work, except to the extent that assistance from others in the project's design and conception or in style, presentation and linguistic expression is acknowledged.

Daniel Chung
Trinity 2015

Acknowledgements

I am indebted to my supervisors, Professor Constantin-C. Coussios and Professor Fergus Gleeson, for their mentorship, wisdom, encouragement and support. I am extremely grateful to them for giving me the opportunity to study for a DPhil, and keeping faith in my ability to complete this work. I am also grateful to my other unofficial supervisors Professor J. Alison Noble and Professor Julia Schnabel, though not as directly involved with my research, has advised and encouraged me throughout.

I would like to express my sincere thanks to Dr. Omar Al-Kadi, providing me with invaluable assistance to develop and implement the image analysis software, without which this work would not have been possible. I am also grateful to Dr.Amalia Cifor for her assistance with some of the image post processing. I would like to thank Dr. Eleonora Mylonopoulou and Professor Robert Calisle for their kind assistance in the animal experiments, without their expertise this part of the experimental work would not have been successful. I am also extremely grateful for the support from past and present members of the Biomedical Ultrasonics, Biotherapy and Biopharmaceuticals Laboratory (BUBBL). I would like to thank them for their entertaining company, and for welcoming and helping me during the three years I spent in the lab. I would also like to acknowledge the help of the nurses in the Churchill Hospital Day Treatment Unit and the help of the oncology consultants for their assistance in patient recruitment to the clinical study.

I would like to gratefully acknowledge the funding for this research from the Oxford Medical Engineering Centre, a collaboration between the Wellcome Trust and the Engineering and Physical Sciences Research Council (EPSRC).

I would like to take this opportunity to thank my parents for all their efforts and sacrifices, to always provide me with the best opportunities to succeed, and for their love and encouragement throughout the years. I am also grateful for the moral support provided by my fiancé's family during my research.

I would like to dedicate this thesis to my fiancé Dipanjali for her support and precious love, who was always standing by me and supporting me in my hard times during this work.

Content

Table of Contents

List of abbreviations

%PRR	Percentage of pre-Rayleigh regions
Akt	Protein kinase B
ARFI	Acoustic radiation force impulse
ASPA	Animals Scientific Procedures Act
ceCT	Contrast enhanced computed tomography
CT	Computed tomography
dce	Dynamic contrast enhanced
EGFR	Epidermal growth factor receptor
FD	Fractal dimension
FDG	2-[fluorine-18] fluoro-2-deoxy-D-glucose
HER2	Human epidermal growth factor receptor 2
HIF	Hypoxia inducible factor
HIFU	High intensity focused ultrasound
K^{Trans}	Transfer coefficient
MRI	Magnetic resonance imaging
mTOR	Mammalian target of rapamycin
PBS	Phosphate buffer solution
PDGF	Platelet-derived growth factor
PDGFR	PDGF receptor
PET	Positron emission tomography
PI3K	Phosphatidylinositol 3-kinase
PR	Partial response
RECIST	Response Evaluation Criteria in Solid Tumours
RF	Radiofrequency
SD	Stable disease
SUV	Standardised uptake value
SWE	Shear wave elastography
TD	ThermoDox®
TE	Transient elastography
US	Ultrasound
VEGF	Vascular endothelial growth factor
VEGFR	VEGF receptor

CHAPTER 1

INTRODUCTION

1. Introduction

1.1. Overview

In order to develop a novel quantitative method of detecting early response of liver tumour to chemotherapy, it is important to firstly understand the burden of liver tumour and the mechanisms through which chemotherapy act on tumours. The problems associated with systemic chemotherapy are then discussed to justify the need for a novel method of detecting early response to treatment. Current and emerging methods to assess liver tumour response to treatment will be reviewed in order to identify candidate strategies for subsequent investigation.

1.2. The burden of liver tumour

Liver tumour can be broadly divided into primary and secondary, the former originating from cells within the liver, and the latter spreading from primary tumours elsewhere in the body.

The two major types of primary liver tumours are hepatocellular carcinoma and intrahepatic bile duct cancer. In 2011, primary liver cancer was the 18th most common cancer with around 4300 new cases diagnosed [1]. This incidence varies worldwide, being more common in sub-Saharan Africa and Southeast Asia owing to the prevalence of hepatitis B, a risk factor for the development of hepatocellular carcinoma. Liver cancer is the sixth most common cancer worldwide with more than 782,000 new cases diagnosed in 2012, and the second most common cause of death from cancer worldwide, responsible for nearly 746,000 deaths in 2012 [2]. The incidence of hepatocellular carcinoma in western countries has increased over the last two decades [3, 4], which has been attributed to the increase in hepatitis C infection [5]. The rise in obesity in the western world has resulted in an increase in the

incidence of diabetes. As diabetes is associated with hepatocellular carcinoma [6], it is anticipated that the incidence of HCC may also increase in the future.

Breast, lung, and bowel cancers are the most common primary cancers that spread to the liver. These cancers represent three of the top four most common cancer diagnosed in the UK in 2012, responsible for approximately 135,000 new diagnoses [7]. 5.2% of breast cancer patients [8] and 50% of colorectal cancer patients [9] are reported to develop liver metastases during the course of their disease. These findings combined with the low prevalence of risk factors for primary liver cancer explains why the majority of tumours diagnosed in the liver are secondary rather than primary liver cancers in the UK.

Surgical resection of liver tumours offers the best chance of cure and long-term survival. This has been demonstrated in both primary [10], as well as various secondary liver tumours [11-14]. The lack of symptomatology in primary liver cancer means patients often present at an advanced stage of disease. When this is combined with the fact that the majority of patients have pre-existing liver damage, surgery may not be possible. In the case of secondary liver tumour, anatomical location, the presence of extra-hepatic disease, co-morbidity and the burden of metastases means only 15 – 20% of patient may be suitable for curative surgery at the time of presentation [15, 16]. However, advances in surgical technique and the use of down staging chemotherapy [17, 18] mean that liver resection may still be possible in patients with initially unresectable colorectal metastases, increasing the number of patients suitable for surgical resection. Despite increasing evidence to support the use of percutaneous ablation of both primary [19, 20] and secondary liver tumours [21], and transarterial chemoembolization of hepatocellular carcinoma [22], both remain unsuitable in patients with significant burden of disease. As a result, chemotherapy

continues to be the mainstay of treatment in the majority of patients with primary and secondary liver tumours.

1.3. Chemotherapy

A brief overview of the mechanisms through which chemotherapy act on tumours is provided to understand changes to the tumour that can be used to detect response to treatment.

Chemotherapy can be divided into those that are cytotoxic, killing cells that divide rapidly, or targeted therapy, targeting proteins expressed abnormally on the surface of tumour cells that are essential for tumour growth.

Most chemotherapy is delivered intravenously, usually as part of a chemotherapy regime involving a combination of drugs with additive or synergistic effects. Since only a proportion of the tumour is killed with each treatment, repeated administration is necessary to ensure on-going tumour shrinkage. Chemotherapy regimes are usually delivered in cycles, with regular interruption allowing time for major organs to recover from drug toxicity. The frequency and duration of each cycle is determined by the drug toxicity, which may need to be adjusted for individual patients.

1.3.1. Cytotoxic chemotherapy

There are several groups of cytotoxic chemotherapy acting on different parts of the cell cycle to interrupt cell replication necessary for tumour growth, their actions are briefly outlined below [23]:

Alkylating agents- induce binding of DNA strands resulting in cross-linked DNA. Attempt by the cell to repair or replicate these cross-linked DNA will result in breakage.

Antimetabolites- resembles the structure of nucleotides, which are the building blocks of DNA and RNA, to block enzymes required for DNA synthesis, or produce DNA damage by their incorporation during DNA synthesis.

Anti-microtubules- prevent formation or disassembly of microtubules, which are important cellular structures necessary to achieve cell replication.

Topoisomerase inhibitors- these drugs affect the action of topoisomerase enzymes responsible for unwinding of DNA during replication and transcription.

Cytotoxic antibiotics- a group of drugs with various mechanisms of action: including DNA intercalation, generation of toxic free radicals to damage intercellular molecules and topoisomerase inhibition.

The actions of cytotoxic chemotherapy ultimately result in programmed cell death or apoptosis.

1.3.2. Targeted therapy

Advances in molecular biology have increased our understanding of the pathophysiological processes common to tumours including: sustaining proliferative signalling, evading growth suppressors, resisting cell death, enabling replicative immortality, inducing angiogenesis, and activating invasion and metastasis [24]. These processes are caused by dysregulation of the cell signalling pathways, providing targets for the development of this novel group of anticancer therapy (**Table 1**). Targeted therapy drugs are either monoclonal antibodies that directly block circulating growth factors and growth factor receptors expressed on the surface of tumour cells, or inhibitor of tyrosine kinases, which are responsible for the downstream propagation of cell signalling pathway following activation of growth factor receptors.

Pathway	Action
VEGFR, PDGFR	Activates malignant angiogenesis
EGFR-HER2	Activates proliferation, angiogenesis, invasion, metastasis, and evasion of apoptosis
PI3K/Akt/mTOR	Activates cancer cell growth and proliferation, evasion of apoptosis, synthesis of proteins necessary for cell growth, cell cycle progression, and cell metabolism
cKIT	Plays a critical role in cell proliferation and differentiation
Hormonal	Cell growth and survival

Table 1-1. Functions of biological pathways targeted by novel anticancer therapy. Akt is a serine-threonine protein kinase, cKIT is a proto-oncogene. EGFR = epidermal growth factor receptor, HER2 = human epidermal growth factor receptor 2, mTOR = mammalian target of rapamycin, PDGF = platelet-derived growth factor, PDGFR = PDGF receptor, PI3K = phosphatidylinositol 3-kinase, VEGF = vascular endothelial growth factor, VEGFR = VEGF receptor.

There are several classes of target therapies and their actions are outlined in the context of the biological pathways they act upon:

Antiangiogenesis therapy- angiogenesis, formation of new blood vessels, is essential for growth of tumours beyond 2-3 mm^3, when diffusion alone is not sufficient to deliver oxygen and nutrient to supply tumour cells. Hypoxia secondary to growth of the tumour mass is believed to be the main driver for angiogenesis, inducing the expression of HIF (hypoxia inducible factor) which promote the expression of other factors such as VEGF (vascular endothelial growth factor), PDGF (platelet-derived growth factor) and carbonic anhydrase IX. Targeted therapy acting on this pathway either directly inhibit the growth factors or receptors responsible for the formation of new blood vessel, angiogenesis inhibitor, or target established tumour vasculature to disrupt blood flow to induce tumour necrosis, vascular disrupting agent [25, 26].

Drugs interfering with EGFR-HER2 or KIT receptors and PI3K/Akt/mTOR pathway inhibitors- the majority of human epithelial cancers are marked by functional activation of the growth factors and receptors of the EGFR (epidermal growth factor receptor) family, including EGFR and HER2 (human epidermal growth factor receptor 2) [27-29]. The activation of EGFR-HER2 triggers intracellular pathways

including the RAS-RAF-MEK-MAPK and the PI3K/Akt/mTOR which may result in cancer cell proliferation, blocking of apoptosis to prolong cell survival, activation of invasion and metastasis, and stimulation of angiogenesis, cell metabolism, and synthesis of proteins necessary for growth. Targeted therapy in this group either act directly on the EGFR-HER2 receptor or the associated tyrosine kinase triggering the intracellular pathways. Specific drugs are also available to directly target the downstream PI3K/Akt/mTOR pathway [30]. Inhibitor of KIT kinase activity is also available to block the KIT receptor, which has oncogenic function in haematological and solid tumours, controlling cell proliferation and differentiation, apoptosis, and metabolic tumour activity [31].

Hormonal therapy- Steroid hormone growth factors act on nuclear receptors to activate transcription of genes whose product stimulate growth and viability of hormone dependent malignancies including breast and prostate cancers [32, 33]. Treatment of breast cancer is dominated by the used of oestrogen receptor antagonist, or by depletion of oestrogens by aromatase inhibitor, while androgen blockade is used as hormonal therapy for prostate cancer.

1.3.3. Problems with chemotherapy

Cell proliferation is essential for both normal and cancer cells. As the action of chemotherapy is non-discriminatory, both cell populations can be affected. The higher cellular proliferation of tumour cells, and their defective ability to repair damaged DNA confers selectivity of chemotherapy towards cancer cells. The rapidly dividing cells within the bone marrow, gastrointestinal mucosa, hair follicles and gonads are the most sensitive to chemotherapy with resultant myelosuppression, nausea and vomiting, hair loss and reduced fertility respectively. Although nausea and vomiting is ranked as the most distressing in a survey of patients receiving chemotherapy [34],

myelosuppression can be life-threatening owing to increased vulnerability to infection and overwhelming sepsis. Toxicity can also develop some time after completion of treatment including cardiomyopathy associated with doxorubicin, pulmonary fibrosis associated with bleomycin, as well as possible development of secondary primary malignancy [35].

Despite the high selectivity of targeted therapies compared to cytotoxic chemotherapy, a range of previously unknown side effects are now becoming apparent. The biological basis of these side effects are not well established, but are likely related to the inhibition or modulation of the specific molecular target in normal tissue by targeted therapies. Below are examples of common sides effects and their associated therapies:

Antiangiogenic therapy- hypertension, proteinuria, thrombotic events, bleeding, gastrointestinal perforation, delayed wound healing [36, 37].

Anti-EGFR therapy- acneiform eruption, nausea, vomiting, and diarrhoea [38-41].

Anti- HER2 therapy- reversible cardiotoxicity [42].

Multitargeted kinase inhibitor- acral erythema associated with sorafenib [43], hypothyroidism [44].

Apart from the side effects of chemotherapy, it is also important to recognise that chemotherapy is not effective in all patients with the same type of cancer. In the case of liver cancers, contrasting examples include colorectal liver metastases with response to chemotherapy reported in up to 60% of patients [45], compared to the poor response rate of hepatocellular carcinoma to sorafenib observed in 2% of patients [46]. With a typical course of chemotherapy lasting several weeks to months, and first response assessment carried out at halfway through treatment, patients may be subjected to toxic and ineffective treatment for a prolonged time period before

treatment failure is recognised. Commencement of alternative potentially effective treatment may also be delayed owing to late recognition of treatment failure. Given the high proportion of patients with liver tumour undergoing treatment with chemotherapy, a reliable method to detect early response to treatment will be advantageous to minimise unnecessary toxic effects to the patient in cases where the tumour does not respond to treatment, and consider alternative therapy where available.

1.4. Current and emerging methods of liver tumour response assessment

Early response of solid organ tumours to chemotherapy can potentially be detected with histological analysis of tissue samples obtained from needle biopsies. Serial biopsies of the tumour throughout treatment are however not feasible due to a number of limitations. Firstly, needle biopsy requires local anaesthesia or sedation, and the invasive nature of needle biopsy carries risks of bleeding and infection. Secondly, needle biopsy can potentially stimulate neo-angiogenesis by damaging tumour tissue, and also increase the risk of metastases by increasing circulating tumour cells [47]. Furthermore, sampling from only a small proportion of the tumour may not be representative of the overall tumour response, resulting in erroneous interpretation.

Imaging techniques are favoured for response monitoring, permitting non-invasive, serial assessment at multiple time points throughout treatment, and can also be used to evaluate the entire three-dimensional volume of the tumour.

Emerging functional and molecular imaging techniques using ultrasound (US), computed tomography (CT), magnetic resonance imaging (MRI) and positron emission tomography (PET) have shown promising results to interrogate functional aspects of liver tumours affected by treatment beyond size and morphology alone.

Review of these techniques is provided with the aim of identifying candidates that may be used to detect early response to treatment in the subsequent investigation.

1.4.1. Current methods of liver tumour response assessment

Anatomic objective response evaluation using Response Evaluation Criteria in Solid Tumours (RECIST 1.1) provides a reliable and standardised methodology for assessment both in the research setting, as well as daily patient care [48]. The criteria established fixed and forced categories that use tumour size as the only criterion. Although the use of uni-dimensional measurement of tumour on cross-sectional imaging including CT and MRI makes the technique simple, reproducibility of the measurement by different observers represents a major drawback of the technique. Other limitations of the criteria are less relevant to liver tumours, including the need for modification in certain types of tumour, e.g. mesothelioma [49], disease that are deemed to be too small by the criteria for follow up assessment (small lesions with diameter less than 10mm and lymph nodes measuring less than 15mm), as well as diseases that are truly non-measurable by parametric parameters, such as leptomeningeal disease, ascites, pleural or pericardial effusion, inflammatory breast disease, and lymphangitic involvement of the skin and lung [48]. While reduction in tumour size would suggest cytoreduction in response to chemotherapy, applicable to both cytotoxic chemotherapy and targeted therapies, tumour shrinkage is a late indicator of response since it is increasingly recognised that cellular and molecular changes of tumours precede size change.

Furthermore, the use of novel molecular targeted agents inhibiting aberrantly activated cellular pathways results in a predominant cytostasis effect [50, 51]. Tumour shrinkage cannot therefore be used as an indicator of response in patients undergoing such treatments. This has lead to the development of functional and molecular

imaging techniques for response assessment, increasing the repertoire of imaging techniques that can be used to assess tumour changes.

Although ultrasound is able to visualise and provide accurate size measurement of liver tumours, ultrasound is not recommended as a method of measurement according to RECIST 1.1, since the whole examination cannot be reproduced for independent review. In addition the technique is operator-dependent, and it cannot be guaranteed that the same technique and measurement can be taken from one examination to the next. Furthermore, new disease may not be visible due to the lack of suitable acoustic window, e.g. para-aortic lymph node [48], resulting in failure of the operator to appreciate disease progression. Despite this, liver tumours are usually well visualised by ultrasound and since the current investigation is aimed at detecting the response of liver tumours to chemotherapy, some of the novel ultrasound-based imaging techniques with potential for detecting tumour response to chemotherapy are reviewed for further consideration.

Apart from size, qualitative assessment of liver tumour morphological changes on ceCT has also been shown to correlate with response to treatment [52]. In this study, the Choi criteria originally studied in the setting of gastrointestinal stromal tumour treated with imatinib [53], were expanded to investigate morphological changes in colorectal liver metastases undergoing treatment with bevacizumab (monoclonal antibody against vascular endothelial growth factor). Similar to the prior study, reduction in tumour density, as well as increased sharpness of the tumour borders was found to have improved correlation with pathological response and overall survival than size alone (**Figure 1-1**). The authors attributed the reduction in tumour density to the replacement of treated tumour with fibroconnective tissue, demonstrated in a prior study by Rubbia-Brandt et al. [54]

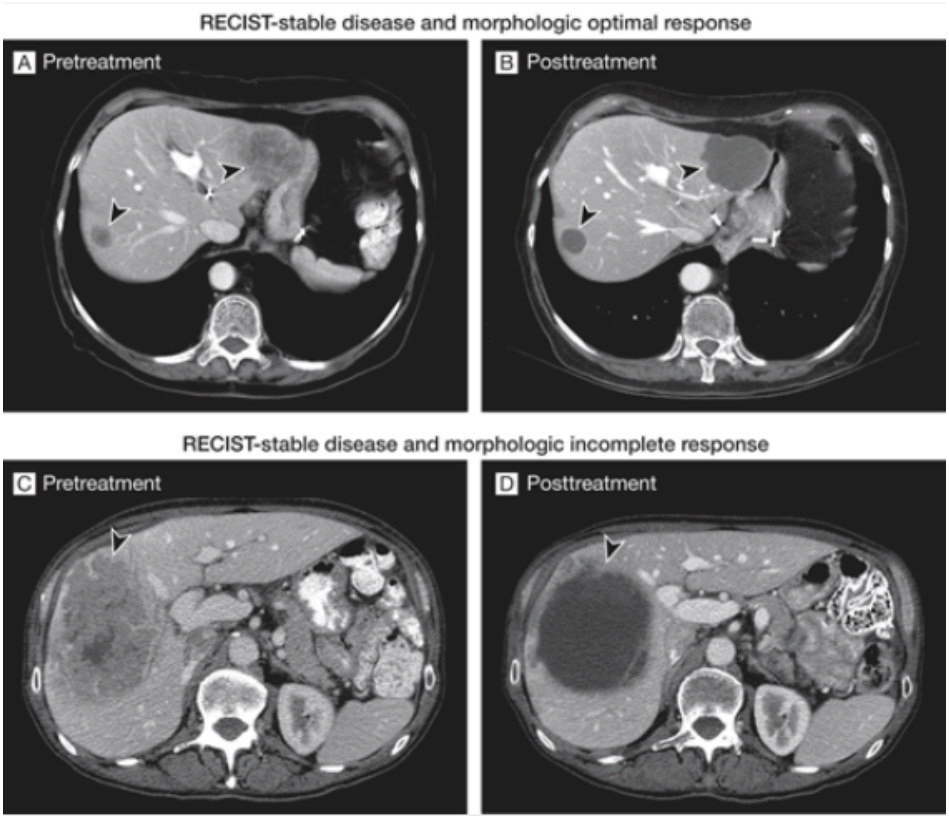

Figure 1-1: Representative pre and post-treatment contrast enhanced CT evaluated by morphological response and RECIST criteria. Arrowheads indicate the tumour-liver interface. Morphological optimal response is characterised by decrease in density and sharp tumour-liver interface (B); morphological incomplete response is characterized by decrease in density but persistent ill-defined tumour-liver interface remaining after treatment (D). Image adapted from [52].

1.4.2. Emerging methods of liver tumour response assessment

Improvements in imaging techniques have led to novel functional and molecular imaging, allowing non-invasive quantitative assessment of physiological and molecular features of the tumour [55]. Parameters from these quantitative techniques, albeit based on different biological properties, can be correlated with pathophysiology of the tumour. These techniques can indirectly demonstrate cancer hallmarks including angiogenesis, tumour cellularity and metabolism, with potential use in predicting and monitoring tumour response to chemotherapy. These novel techniques are briefly reviewed in categories based on different aspects of tumour pathophysiology assessed by the technique.

1.4.2.1. Imaging evaluation of angiogenesis

Non-invasive imaging techniques including US [56], CT [57] and MR [58] are able to provide indirect measurement of angiogenesis. In all the techniques, sequential images are acquired dynamically, through a volume of interest before, during and after administration of contrast agents to allow quantification of the dynamic tissue enhancement. The US contrast agents used in dynamic contrast enhanced (dce)US uses gas-containing microbubbles with mean diameter of 0.5 – 10 μm, which resonate non-linearly when exposed to an US pulse to enhance visualisation of vasculature. Since US contrast agents remain intravascular, any echoes visualised in the volume of interest are related to flow within functional vessels. dceUS data acquired using conventional US scanners can be analysed using dedicated software offline to obtain quantitative parameters of tumour perfusion. Regions of interest within the study volume can be selected to produce time-intensity curves to study tumour perfusion. Fitting of data to a kinetic model can determine volume and flow rate and semi-quantitative parameters including peak intensity, time to peak intensity, mean transit time and area under the total enhancement curve [59]. Early changes in tumour perfusion have been identified using this technique following treatment of liver tumours with anti-angiogenic therapy [60, 61].

Dynamic CT obtains information based on the first pass of iodinated contrast material to generate quantitative parameters including blood volume, blood flow, and mean transit time. Reduction in these parameters has been reported in several small studies looking at patients with liver metastases from metastatic carcinoid tumour [62, 63] and colorectal cancer treated with antiangiogenic therapies [64].

dceMRI technique relies on changes in signal intensity on T1-weighted gradient echo sequence following intravenous injection of gadolinium-based contrast agents to

create a time versus enhancement curve. This can be used to calculate semi-quantitative parameters describing the shape of the enhancement curve including, slope of the initial enhancement, time to peak, slope of the washout curve and initial area under gadolinium curve. By applying pharmacokinetic modelling, calculation of quantitative parameters such as the transfer coefficient (K^{trans}) can be obtained, which is the most widely reported parameter in dceMRI and represents a combination of blood flow and vessel permeability. Interval reduction in transfer coefficient area under the contrast enhancement curve at 180 sec from baseline 1 week post colorectal metastasis treatment with bevacizumab-containing chemotherapy regime predicted response and favourable prognosis [65].

Most recently, fractal analysis, a quantitative measurement of tumour heterogeneity has also been found to reduce from baseline in patients with hepatocellular carcinoma that responded to treatment with sunitinib [66]. The authors attributed their finding to normalization of the tumour vasculature reducing the tumour heterogeneity, thus fractal analysis of contrast enhanced CT image is able to evaluate angiogenesis of liver tumours.

1.4.2.2. Imaging evaluation of tumour cellularity

The movement of water in biological tissue is restricted because their motion is influenced and limited by interaction with cell membrane and macromolecules [67, 68]. Malignant tissue being more cellular impedes water diffusion. Since diffusion-weighted imaging is sensitive to water content and movement, it facilitates the detection and characterisation of tumours. The quantitative parameter derived from diffusion-weighted imaging, ADC (apparent diffusion coefficient), has previously been correlated with histological findings, including tumour proliferation index, tumour grade, the presence of necrosis, and tumour cell apoptosis [67-69]. Treatment

that causes necrosis or cellular lysis will therefore increase water diffusion in the extracellular space, in turn increasing the ADC value. Early interval increase in ADC value from baseline of colorectal and gastric hepatic metastases has shown promise in predicting and monitoring response to chemotherapy [70].

There are several ultrasound techniques that may offer an insight into tumour cellularity, although not previously investigated. Ultrasonic backscattered signals are dependent upon the shape, size, density and other properties of scatterers in a tissue [71-73], information that may be lost on the B-mode images due to signal processing, which may be valuable for tissue characterisation. Increasing availability of US research interfaces permits researchers to access the pre-processed ultrasonic backscattered signals, also known as the radiofrequency (RF) signals. The Nakagami statistical distribution, originally proposed to describe the statistics of radar echoes, has been used to analyse US backscattered signals [74]. The quantitative Nakagami parameter, derived from this analysis has shown good ability to differentiate different scatterer concentrations in a medium [74], and has also demonstrated use in the classification of benign and malignant breast tumours [75]. That study attributed their correlation to the more complex scatterer arrangement and composition seen in malignant tumours. Construction of Nakagami images based on the Nakagami parameter map [76] has also been shown in a more recent study to be useful in characterising breast lesions [77]. With changes to tumour cellularity in response to treatment, it is possible that scatterer composition and arrangement will alter with secondary impact on the backscattered signal that may be detectable with Nakagami imaging.

Ultrasound elastography offers an additional possible method to assess changes in tumour cellularity. The tortuous, dilated and disorganised vasculature in tumours are

hyper-permeable, resulting in an increase in tumour interstitial fluid pressure [78], a characteristic which may also contribute to the increased stiffness observed in malignant lesions. This has been also been confirmed recently when viscoelastic properties of post-surgical specimens were studied [79]. The changes in response to chemotherapy including tumour structure, and interstitial fluid pressure through normalization of tumoural vasculature [80, 81], and necrosis or reduction in tumour cells secondary to apoptosis may alter the stiffness of liver tumours. Ultrasound elastography has previously been studied in liver tissue. The technique quantifies tissue stiffness by monitoring the degree of tissue displacement resulting from shear waves generated at a focal point within the tissue. Based on the velocity of laterally propagating waves from the focal point, an estimate of tissue stiffness can then be calculated [82]. Three methods have been used to implement the shear wave technique to study liver lesions: transient elastography (TE), acoustic radiation force impulse (ARFI) and shear wave elastography (SWE).

Although TE (Fibroscan; Echosens, Paris, France) has been used to examine the stiffness of liver lesions, this method is limited by the lack of real time imaging guidance, examination of only superficially placed tumours and the assumption that the estimate of elasticity is uniform throughout a large fixed region of interest [83].

Both ARFI and SWE are now integrated into commercially available diagnostic US systems. Unlike TE, a region of interest (ROI) can be accurately selected for assessment using imaging guidance with these methods. Transient focused acoustic radiation force from modified diagnostic transducer excites tissue within the chosen ROI inducing tissue displacement, resulting in shear waves that propagate away from the tissue. The velocity of the shear waves can be measured using ultrafast algorithms, and used to evaluate and quantify tissue stiffness [84]. Both methods have previously

been applied to clinical studies of focal liver lesions [85-90], with ARFI also having been used to monitor changes in an animal model following anti-angiogenic treatment [91]. In the latter study, reduction in xenograft tumour stiffness was demonstrated, correlating with changes in interstitial fluid pressure in response to treatment, providing further evidence for the use of ultrasound elastography techniques to detect tumour response to treatment.

1.4.2.3. Imaging evaluation of tumour metabolism

PET allows assessment of tissue metabolism by using radiolabelled molecules to image biological processes in vivo. Tumour cells increase glucose utilization secondary to overexpression of membrane glucose transporter, increased hexokinase activity and decreased levels of glucose-6-phosphtatase [92]. 2-[fluorine-18] fluoro-2-deoxy-D-glucose (FDG), the most widely used radiotracer is taken up by the tumour cells. Subsequent PET imaging allows visualization and quantification of FDG uptake and provides a quantitative parameter of tumor glucose metabolism, the specific uptake value (SUV). As tumour cells reduce in response to treatment, reduction in SUV of the tumour would be expected. Increasing use of FDG-PET to monitor treatment response has led to the development of the PERCIST criteria [93]. The metabolic response measured by FDG-PET/CT after a single course of chemotherapy in colorectal liver metastasis has been shown to identify patients who will not benefit from the treatment [94]. Although promising, the cost, limited availability and high radiation associated with FDG-PET limits frequent scanning and its wider clinical application.

1.5. Implications for the present work

Liver tumours represent an important disease worldwide. Large portions of patients are not suitable for curative surgery, requiring treatment with chemotherapy. Treatment with chemotherapy is associated with a number of toxic side effects, some of which are life threatening. With response assessment performed some time after commencement of treatment, treatment failure is recognised late, with patients potentially being subjected to unnecessary side effects in cases of treatment failure, whilst being denied the opportunity for earlier commencement of a potentially effective alternative therapy.

Given the wide variety of conventional and emerging imaging techniques available, the selected strategy should be quantitative, with little or no additional cost, should not necessitate additional scan acquisitions or equipment, and should not expose patients to additional risks.

Since CT is the most commonly used imaging modality to assess liver tumour response to treatment, any CT-based technique could be immediately translated into clinical practice. Fractal analysis of contrast-enhanced CT is thus first investigated in the present work, to determine whether it can act as a clinically useful predictor of response to chemotherapy.

Should CT not provide the required solution, the only form of additional imaging that could be contemplated in this context is ultrasound, by virtue of its low cost, widespread availability, lack of ionizing radiation and speed with which examinations can be carried out. Since Nakagami imaging-based technique requires only analysis of the RF signal with no need for equipment upgrade or the use of ultrasound contrast, confirmation of a Nakagami imaging-based technique to detect early tumour response would permit rapid adoption into clinical practice.

In summary, this thesis focuses on validation of fractal analysis of contrast enhanced CT of liver tumour to detect early response to chemotherapy. A Nakagami imaging based technique is also developed, initially using a small animal model, and validated using clinical data to analyse ultrasound images with the aim of detecting early liver tumour response to chemotherapy.

The main hypotheses for this project are:

1. Fractal analysis of contrast enhanced CT of liver tumour can detect early tumour changes in response to chemotherapy.
2. A Nakagami imaging-based technique can detect early tumour response to chemotherapy in animal tumour models using diagnostic ultrasound.
3. A Nakagami imaging-based technique can detect early liver tumour response in patients undergoing chemotherapy treatment using diagnostic ultrasound.

CHAPTER 2

FRACTAL ANALYSIS OF CONTRAST ENHANCED CT TO ASSESS LIVER TUMOUR RESPONSE TO CHEMOTHERAPY

2. Fractal analysis of contrast enhanced CT to assess liver tumour response to chemotherapy

2.1. Introduction

With the exception of assessing the density and morphology of tumour treated with chemotherapy targeting the angiogenesis pathway, CT is mainly used to monitor interval changes in tumour size as a marker of response to chemotherapy. Since CT is the most common imaging modality used for tumour response assessment, development of a CT-based quantitative marker of early response to treatment in liver tumours would be advantageous. The quantitative assessment of tumour texture using fractal analysis has shown promise in the classification of tumour aggressiveness. Early response of tumour to treatment may result in changes to tumour texture that can be detected with fractal analysis. This chapter will examine the feasibility of this hypothesis using CT studies from patients undergoing chemotherapy for colorectal liver metastasis.

2.1.1. Texture analysis

It is recognised that tumours are heterogeneous both at the genetic and at the cellular level, with considerable intra-tumoural spatial variation [95, 96]. Previous histological studies have demonstrated intra-tumoural heterogeneity correlates with aggressiveness of tumour and resistance to treatment [97-99]. Texture analysis can quantitatively assess tumour heterogeneity, which may change in response to chemotherapy thus providing a method of detecting early response.

Quantitative assessment of medical images in clinical practice is currently limited to assessing the mean density on CT, signal intensity on MRI or SUV on PET in a selected region of interest of the tumour. Although these parameters offer information about the content of the tumour, more detailed assessment of the acquired imaging

data with texture analysis could offer insight into intra-tumoural heterogeneity that may facilitate clinical management.

Texture analysis is a group of mathematical techniques that evaluate variation in the grey-level intensity, and the spatial location of a pixel on a medical images, to obtain 'texture features' that measures intra-tumour heterogeneity [100]. These techniques interrogate the image beyond what can be perceived by the reader visually to extract features that may improve tumour assessment. They also have the advantage of using information from routinely acquired clinical images, without extra cost associated with additional acquisitions or hardware.

Texture analysis techniques can be divided into statistics-, model-, and transform-based methods. Statistics-based techniques are the most commonly applied describing the distribution and relationship of grey level values in the image. Model-based techniques utilised sophisticated mathematical models including fractal analysis. Transform based techniques, such as Fourier, Gabor, and wavelet transforms, analyse texture in a frequency or the scale space. While texture analysis has been studied in all medical imaging modalities, this chapter will focus on its application to CT images.

2.1.2. Current clinical application of texture analysis to CT images

Texture analyses of CT have demonstrated benefit in previous studies to the detection, diagnosis, characterisation, and response assessment of tumours in various organs.

Previous studies have attempted to correlate texture features with imaging and biological parameters to better understand the biological aspect of the tumour assessed with texture analysis. Studies in lung cancer demonstrated higher mean fractal dimension (FD) amongst aggressive tumours confirmed on FDG PET-CT [101]. At a histological level, texture features in lung tumours have also demonstrated

correlation with percentage of tumour hypoxia and angiogenesis vasculature [102]. In that study, the standard deviation and mean positive pixel quantified from medium to coarse texture on contrast enhanced CT showed significant association with the percentage of tumour stained for pimonidazole hydrochloride (exogenous marker of hypoxia). The same parameters obtained from unenhanced CT also showed significant inverse association with the average intensity of the tumour stained CD34 (marker of angiogenesis). Despite the findings of these studies indicating the potential for texture analysis, further research remains necessary in this area.

Based on the hypothesis that texture differences exist between benign and malignant lesions, a number of studies have identified greater heterogeneity and higher FD in lung [103, 104], liver [105] and colonic [106] tumours, as well as lymph node metastasis [107] compared to benign lesions. Despite these promising findings, few studies have investigated the use of texture analysis to assess tumour response to chemotherapy.

In a study of kidney tumours treated with a form of targeted therapy, namely tyrosine kinase inhibitor (antiangiogenic and antiproliferative agent), increase in uniformity, denoting reduction in tumour heterogeneity from baseline was found to correlate with longer time to progression [108]. Primary oesophageal tumour was also found to become more homogeneous following neoadjuvant chemotherapy in a separate study, indicated by decrease in entropy and increase in uniformity with texture analysis [109]. Fractal analysis has also been used to analyse contrast enhanced CT of hepatocellular carcinoma treated with sunitinib, a tyrosine kinase inhibitor with antiangiogenic activity [66]. It was found that tumours with greater reduction in the FD on portal venous phase CT after one cycle of therapy showed longer overall survival.

The findings of prior studies suggest texture features obtained from texture analysis correlate with tissue changes within the tumour. These features can identify tumours that are malignant, more aggressive, as well as demonstrating treatment related tumour tissue changes indicating more favourable outcome. While these results are promising, most studies have focused on statistical texture analysis methods. There remains a gap in knowledge concerning other techniques including fractal analysis. Although interval change in FD of hepatocellular carcinoma treated with targeted therapy have been shown to correlate with overall survival, changes in FD of other types of liver tumours responding to conventional chemotherapy may also be detectable, providing a potential biomarker of early response to treatment. Since the correlation of tumour changes with FD has not previously been studied, this will be necessary prior to confirming its role as a biomarker of early response. In particular, the effect of tumour size, the degree of tumour necrosis and the presence of chemotherapy may alter FD, their impact must be established to ensure any changes in FD detected following treatment is truly representative of tissue changes resulting from response to treatment.

2.1.3. Fractal analysis

FD obtained from fractal analysis provides a quantitative measure of texture complexity. In the case of CT images, density of pixels on an image is likened to buildings in a city resulting in an uneven surface. Fractal analysis can examine this surface to quantify its texture or degree of heterogeneity. Since biological and natural features tend to have FD [110], changes of tumour tissue in response to treatment may follow similar pattern that could be detected with fractal analysis of CT images to indicate early response to treatment.

The term fractal was first introduced by Benoit Mandelbrot to describe non-Euclidean objects that possesses self-similarity at all scales and level of magnification [111]. Fractals are often irregular shapes and surfaces created by a series of successive iterations. The complexity of fractal objects mean they cannot be adequately represented by traditional Euclidean or topological dimensions. Fractal geometry is used to describe the underlying process supporting the generation of structures and measures irregular and fragmented structures quantitatively in terms of FD.

For instance, the theoretical FD of a set describing ordinary geometric shapes will equal its 'normal' or Euclidean or topological dimension: i.e. 0 dimension for sets describing a point; 1 dimension for sets describing lines (length only); 2 dimension for sets describing surfaces (length and width); and 3 dimensions for sets described volumes (length, width and height). In the case of fractals sets, the theoretical FD exceeds its topological dimension, e.g. a curve with FD of 1.1 will behave close to an ordinary line, but one with FD of 1.9 will wind convolutedly in space and behaving more like a surface. Therefore, FD can take non-integer values and may be considered an extension of classical geometry.

Mandelbrote stated that one criterion for a surface being fractal is self-similarity. Self-similarity can be explained as follows. Consider a bounded set S in Euclidean n-space. The set would be self-similar if *S* is the union of *Nr* distinct (non-overlapping) copies of itself with similarities to S with respect to a scaling factor r, each of which is of the form *r(Sn)* where the *Nr* and *Sn* sets are congruent in distribution to S. The FD of the bounded set *S* could then be used to characterise the geometric complexity of *S* in the same way that lengths is used as a measurement tool in Euclidean space. The FD can be computed as follows:

$$\mathrm{FD} = \frac{\log\,(N_r)}{\log\,(1/r)} \qquad (1)$$

where *Nr* is the number of self similar shapes and r is the scaling factor.

Most natural and mathematical self-similar fractals are random, meaning they scale in a statistical fashion. The resemblance between shapes seen at different scales in natural fractals is usually approximate and random rather than self- similar. In theory, the FD of a structure examined should have self- similar fragments at all scales reaching to infinity. However, in biological structures, this can only be true within a finite range of scales, below and above which the structure either becomes smooth or completely rough and non-self-similar.

When fractal analysis is applied to medical image analysis, the FD provides an additional image classifier to measure surface roughness. A variety of methods exist to compute FD resulting in different values being obtained with different methods. The reason lies in the fact that FD cannot be computed directly using equation *1*. Instead, FD is approximated using different algorithm to estimate the parameter N. Each of the methods follows the same three basic steps:

a. Measure the quantities of the object using various step sizes.
b. Plot log (measured quantities) versus log (step size) and fit a least- squares regression line.
c. Estimate FD as the slope of the regression.

In this chapter, contrast-enhanced CT images are transformed to FD images using the differential box counting algorithm [112-115] at various different scales then displayed for the identification of tumour region of interest, followed by texture analysis. The differential box counting approach is capable of dealing with large number of data values [116], thus suitable for analysis of CT images generated from a large number of pixels, i.e. 512 x 512 pixels. Further details of the technique are provided in section 2.4.3.

2.2. Gap in knowledge

Fractal analysis of contrast-enhanced CT images of tumours and the resulting FD offer a quantitative method of assessing tumour heterogeneity. Liver tumour tissue changes in response to chemotherapy may alter tumour heterogeneity, which could be quantitatively assessed with FD. The detection of changes in FD from baseline may offer a novel indicator of liver tumour response to treatment. The impact of tumour tissue changes on FD will also need to be established to ensure it represents a reliable indicator of early tumour response to treatment.

2.3. Aim

- To determine if mean FD obtained from fractal analysis of secondary liver tumour is affect by the tumour size, the degree of necrosis or the presence of chemotherapy.
- To determine if baseline mean FD obtained from fractal analysis of secondary liver tumours can predict response to chemotherapy.
- To determine if interval change in FD of secondary liver tumours from baseline on the first follow-up scan can be used to detect early response to chemotherapy.

2.4. Materials and methods

The texture analysis method described in this section was carried out in collaboration with Dr. Omar Al-Kadi based on his previous work assessing the aggressiveness of lung tumours [101]. His contribution to the development of the software for automated image analysis was instrumental to the success of these experiments.

2.4.1. Retrospective dataset collection

The chemotherapy prescription system (ARIA® Oncology Information System, Varian medical system, CA, USA) was interrogated to identify all patients that have been treated with Oxaliplatin based chemotherapy regimen for colorectal cancer at the Oxford Cancer and Haematology Centre at the Churchill hospital site of the Oxford University Hospitals NHS trust between March 2009 and June 2012. Since Oxaliplatin forms part of the first line combination chemotherapy for patients with colorectal cancer liver metastases [117, 118], the search criteria was designed to identify patients treated with conventional chemotherapy for colorectal liver metastases. The radiology records of these patients were retrospectively reviewed to identify those who had imaging confirmed secondary liver tumour at the start of their prescribed chemotherapy course. Patients were included in the current analysis if follow up contrast enhanced CT studies were available for a minimum of two further time points after the start of treatment. The final study group consisted of 30 patients (19 men, 11 women, mean age 64 years, range 25-83 years). A total of 49 secondary liver tumours were analyzed with mean size of 32.3 ± 17.6 mm. The mean follow up imaging period from the start of treatment was 110.22 ± 70.8 days.

2.4.2. CT imaging

Since the dataset was retrospectively collated for this study, two different CT scanners were used during the study period with 16 or 64 detector rows (GE Lightspeed 16 or LightSpeed VCT respectively; GE Healthcare, Milwaukee, Wisconsin) using the following parameters: 120 kV; 280 mAs; 0.6-second rotation time; 5-mm section collimation; field of view, 300; matrix, 512; 75-second delay after administration of 100 mL of 300 mg/mL iodinated contrast material (Omnipaque, GE healthcare, Amersham, UK). CT studies for colorectal staging of the abdomen and pelvis were routinely performed in the portal venous phase to maximize conspicuity of the liver tumour. The baseline and all subsequent follow up CT studies up to 5mm slice thickness of the selected patients were retrieved from the radiology archive for analysis.

2.4.3. CT imaging review and texture analysis

All contrast-enhanced CTs retrieved for analysis were loaded onto a personal computer for further analysis with software developed in house. The imaging of all patients was initially reviewed to identify a suitable tumour for analysis using the following criteria: 1) axial dimension greater than 10 mm to permit accurate segmentation, and 2) present at baseline and follow up imaging to allow computation of FD from these time points for comparison. If more than one lesion was deemed to be suitable for analysis per patient, up to three tumours per patient were used for analysis.

The acquired CT images were transformed to FD images using the differential box-counting (DBC) algorithm at various scales using the technique described in the previous publication by Al-Kadi and Watson [101].

In brief, the contrast enhanced CT DICOM (Digital Imaging and Communications in Medicine) image *I (x, y)* of size *M* x *N* is transformed to a FD image by applying a varying size non-linear kernel *w(s,t)* of size *m* x *n* as in equation 3 that operates by block processing on the neighbouring pixels and finds the difference between the pixel with high density (*Pmax)* and the low lower density *(Pmin)*. The two variables a and b are positive integers that are computed to central the kernel *w(s,t)* on pixel *Pxy* in the original image. The kernel is calculated as in equation 3 and then applied to equation 4.

$$w(s,t) = \sum_{s=-a}^{a} \sum_{t=-b}^{b} \text{floor}\left[\frac{Pmax-Pmin}{r}\right] + 1 \qquad (3)$$

where r= 2, 3, 4,…, *j*

$$a = \text{ceil}\left(\frac{m-1}{2}\right), \qquad b = \text{ceil}\left(\frac{n-1}{2}\right)$$

and

$$Nd(x,y,d) = \sum_{s=-a}^{a} \sum_{t=-b}^{b} w(s,t)\, I(x+s, y+t) \left(\frac{j}{r}\right)^2 \qquad (4)$$

where *d*= 1, 2, 3, …, *j-1* is the dimension of matrix $Nd(x,y,d)$ that represents the necessary number of boxes necessary to overlay the image. In this case, the scaling factor *r* was chose to be in the range of between 2 and 9. Theoretically as seen in equation 1, *r* should represent how similar a specific structure of pixels is to its surroundings. In the previous study, operating with the same parameter of CT images, size= 512 x 512 pixel and resolution of 12 bits per pixel, the best scaling was found to be achieved in this range. Extension beyond this range results in inaccuracy of the estimated FD. The slope of the linear regression line of $Nd(x,y,d)$ and *r* represent the FD of the analyzed pixel. The method through which this is obtained is described in further details in Al-Kadi and Watson [101].

A mouse-controlled cursor was used to manually select a polygonal region of interest around the tumour from the sequential axial DICOM images until the entire tumour volume had been selected. This was necessary as the tumour was difficult to define clearly from background normal liver parenchyma on the transform images (**Figure 2-1**). The regions of interest from sequential axial images were subsequently superimposed onto the transformed images to compute the mean FD of the entire selected tumour volume. The same process was repeated with the subsequent follow up CT imaging.

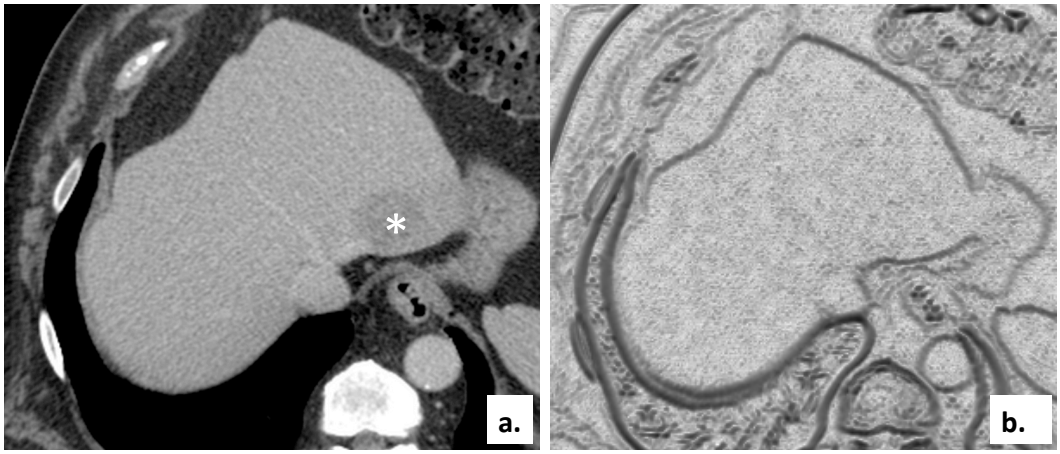

Figure 2-1: Transformation of CT images in preparation for fractal analysis. a.) Contrast enhanced CT demonstrated liver metastasis in the left liver lobe (asterix) and b.) Transformed image in readiness for selection of region of interest for analysis.

The mean FD for each tumour volume at follow-up imaging was compared against baseline to identify any interval change. Rather than only analyzing data from a selected region of interest within the tumour as reported in prior studies using fractal analysis [66, 101], analysis of data from the entire tumour volume should provide a more comprehensive understanding of any changes in heterogeneity throughout the entire tumour volume without the risk of potential error associated with selection bias. Tumours with the same response to treatment (further details below) were pooled for analysis to determine any significant difference in the mean interval change in FD between different tumour response groups.

2.4.4. Correlation of fractal dimension with tumour size, degree of tumour necrosis and presence of chemotherapy

The mean FD obtained from each tumour was correlated against the tumour size and the degree of tumour necrosis following estimation of these parameters using the manually selected polygonal region of interest. The area of the polygons on sequential axial images was multiplied by the image slice thickness to provide an estimation of each tumour volume. The percentage of pixels between 0 and 20 Hounsfield units, i.e. water density, enclosed within the tumour volume region of interest was used as an estimate of the degree of tumour necrosis. The mean FD of tumour volumes at baseline and follow up were plotted to identify any significant changes resulting from the presence of chemotherapy.

2.4.5. Correlation of interval change in fractal dimension with tumour response to chemotherapy

Interval change in mean FD of the tumour volume between baseline and follow up imaging was calculated for each analysed tumour. The interval change in mean FD of the tumour volume was compared between tumours that responded to chemotherapy and tumours that did not respond to chemotherapy. The tumour response to chemotherapy was determined by the change in tumour size at the end of the chemotherapy course compared to baseline as determined on routine clinical imaging with CT or MRI using the Response Evaluation Criteria in Solid Tumour (RECIST 1.1) [48]. For the purpose of the current study, tumour that responded to treatment were those that completely resolved or demonstrate reduction in axial diameter of >30% from baseline. Tumours that were classed as unresponsive to treatment if their axial diameter remained unchanged or increased by >20%.

2.4.6. Statistical analysis

Parametric data mean FD and interval change in FD compared to baseline in responders and non-responders were compared by Student independent-sample t test. A P value of 0.05 or lower was considered significant. Data were analysed by using commercially available statistical software (version 20.0; SPSS, Chicago, Illinois).

2.5. Results

2.5.1. Correlation of mean fractal dimension of whole tumour volume with tumour volume, degree of tumour necrosis and presence of chemotherapy

There was no correlation demonstrated between mean FD of the whole tumour volume with the volume of tumour (**Figure 2-1**) or the degree of tumour necrosis (**Figure 2-2**). When the mean fracture dimension of whole tumour volume was plotted against the tumour axial dimension (**Figure 2-3**), there was significant overlap of data from baseline imaging, before chemotherapy was started, and data from the first follow up imaging, after chemotherapy commenced. This observation suggests the presence of chemotherapy alone does not result in changes in the mean FD obtained from the whole tumour volume.

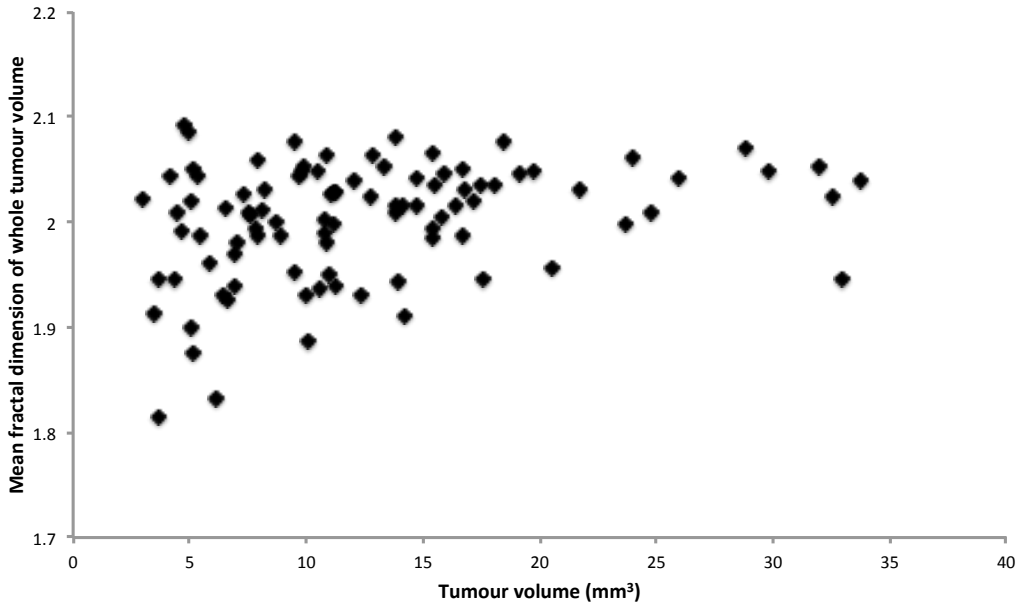

Figure 2-1: Graph showing the mean FD of whole tumour volume plotted against the tumour volume estimated from the manually selected region of interest.

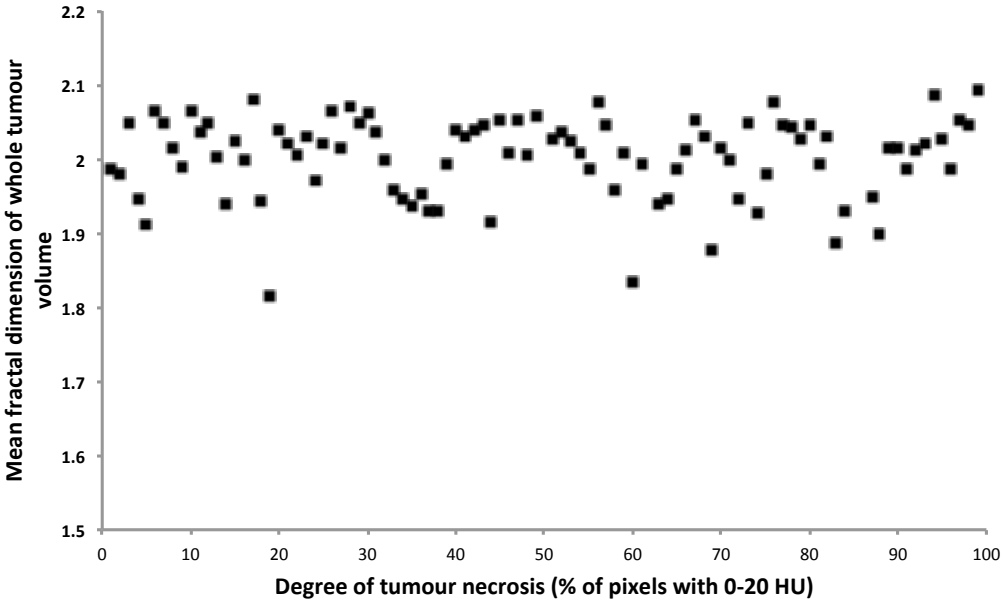

Figure 2-2: Graph showing the mean FD of whole tumour volume plotted against the degree of tumour necrosis estimated from the percentage of pixels within the manually selected region of interest between 0 and 20 Hounsfield unit.

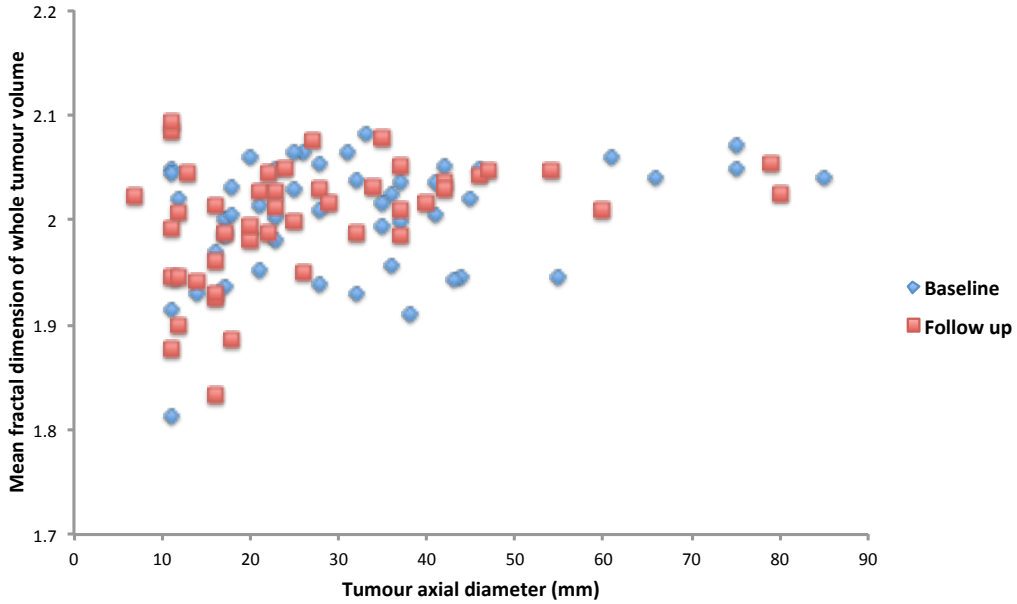

Figure 2-3: Graph showing the mean FD of whole tumour volume at baseline and at the first follow up imaging study plotted against the axial tumour dimension.

2.5.2. Comparison of mean fractal dimension of whole tumour volume between responders and non-responders

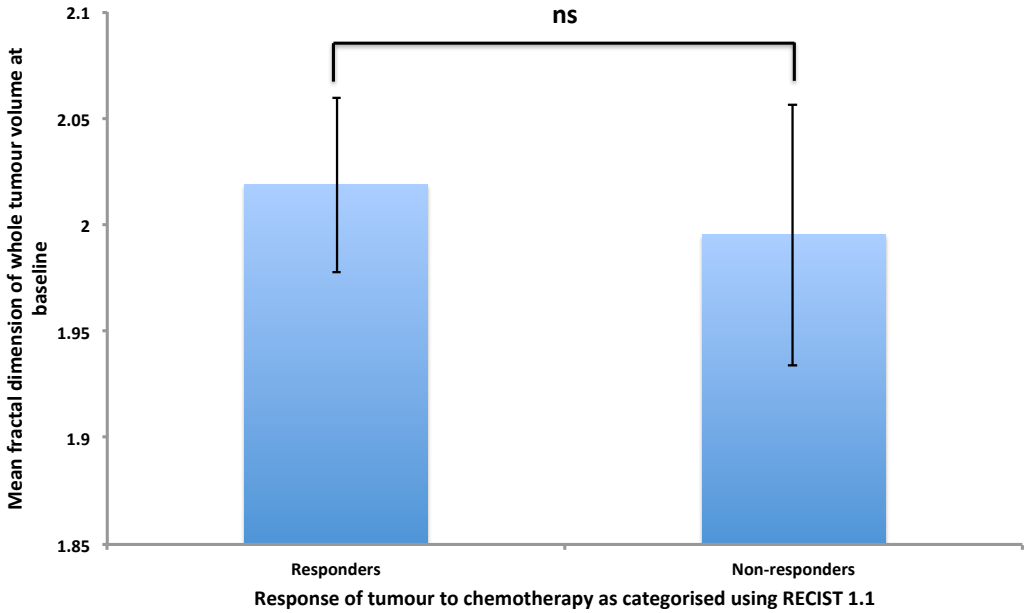

Figure 2-4: Graph showing the mean and standard deviation of mean FD of whole tumour volume at baseline between tumours that responded to chemotherapy and those that did not respond to chemotherapy. Groups compared using Student independent sample T test; ns= no significance

There was no significant difference demonstrated in the mean FD of whole tumour volume at baseline between tumours that responded and those that did not respond to chemotherapy, p=0.135 (**Figure 2-4**). Although reduction in mean FD of whole tumour was seen in tumours that responded to chemotherapy (**Figure 2-5**), a wide standard deviation was also demonstrated in the whole dataset. Statistically analysis confirmed no significant difference in the interval change of mean FD of whole tumour volume from baseline between tumours that responded and those that did not respond to chemotherapy, p=0.08.

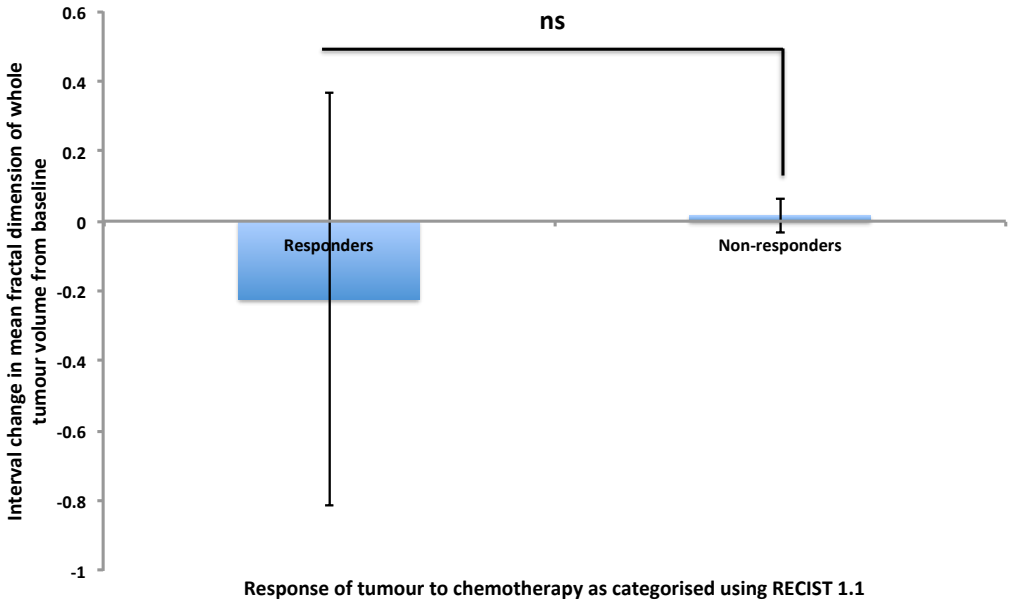

Figure 2-5: Graph showing interval change in the mean and standard deviation of mean FD of whole tumour volume from baseline to first follow up imaging between tumours that responded to chemotherapy and those that did not respond to chemotherapy. Groups compared using Student independent sample T test; ns= no significance.

2.6. Discussion

The current study confirmed mean FD from the whole tumour volume, a quantitative measure of tissue heterogeneity, is unaffected by the tumour volume, the degree of tumour necrosis or the presence of chemotherapy. These findings provide further support for mean FD being a reliable and independent measure of tumour tissue changes, thus a potential indicator of tumour response to treatment. However, interval changes in mean FD between the baseline imaging and the first follow up study were not found to be significantly different between responding and non-responding tumours. Therefore, while fractal analysis could detect changes to tumour tissue at follow up imaging, the extent of this observed early interval changes in mean FD is insufficient to confirm early response of tumour to chemotherapy based on the current analysis.

Since mean FD provides a quantitative measure of tumour heterogeneity, changes in tumour size and degree of necrosis may have been expected to alter the mean FD. There was however no correlation demonstrated between mean FDs from the whole tumour volume with either the tumour volume or the degree of tumour necrosis. While this may not be intuitive, previous authors have attributed chemotherapy-induced alteration in the underlying tumour vasculature to their observed changes in tumour mean FD [66, 101]. The development and branching structures of vessels is believed to follow fractal geometry, previous authors have therefore hypothesised that mean FD is mainly influenced by the heterogeneity of the tumour vasculature rather than all components of the tumour mass. This hypothesis would also explain why the presence of chemotherapy, i.e. at follow up imaging, did not significantly alter the mean FD from the whole tumour volume. Alternatively, since chemotherapy is only transiently present within the tumour, its presence will have limited potential impact

on the mean FD. This finding was important to validate the ability of mean FD to detect early tumour response to chemotherapy. If the presence of chemotherapy alone impacts upon the mean FD from the whole tumour volume, interval changes following treatment from baseline may simply indicate the presence of chemotherapy, and not representative of treatment related tumour tissue changes.

Based on previous studies demonstrating the ability of fractal analysis to assess the aggressiveness of lung tumour [101], and predict overall survival of patients with hepatocellular carcinoma treated with anti-angiogenic agent [66], it was hypothesised that changes in mean FD observed at the first follow up study may provide a quantitative indicator of subsequent tumour response to chemotherapy. While an interval change in mean FD from the whole tumour volume was seen at the first follow up study compared to baseline, confirmed in both responding and non-responding tumours, this was not found to be significantly different between the two groups. Therefore, this quantitative parameter cannot be reliably used to detect early response of secondary colorectal liver tumour treated with conventional chemotherapy. Assuming the findings in the previous studies are correct regarding the association between FD and tumour vascularity, it would explain the current experimental finding in the setting of secondary colorectal liver tumour, which are less vascular, treated with conventional chemotherapy, i.e. not specifically targeting the tumour vascularity. The fact that chemotherapy regime used for secondary colorectal liver tumours has predominantly cytotoxic effect, changes in tumour vasculature though may be present, is unlikely to be the dominant change that can be detected using fractal analysis. Therefore, although interval changes in mean FD from baseline was seen in the current setting, that may indicate changes in vasculature, this change cannot be used as an early indicator of tumour response to chemotherapy.

Even though mean FD of tumour volume has not demonstrated utility in the current setting, it may still be useful to detect early tumour response, if applied to other types of liver tumour treated with anti-angiogenic chemotherapy. Alternatively, it may still have utility in the setting of secondary colorectal liver tumour treated with anti-angiogenic chemotherapy regime, although these regimes are not currently used as the first line treatment [119], but could be considered in future investigation. This chapter has deliberately focused on secondary colorectal liver tumours to ensure a homogeneous study group. Additionally, this group of tumour represents a significant proportion of liver tumours treated with chemotherapy. The identification of a CT based biomarker to detect early response to chemotherapy in this group of patients would have conferred significant benefit to their clinical management.

2.7. Summary

We hypothesized that fractal analysis of CT images could provide a quantitative measure of secondary colorectal liver tumour tissue changes resulting from chemotherapy. Interval changes from baseline in the calculated mean FD from liver tumours was however not significantly different between responding and non-responding tumours. While a CT based technique for detecting early response of tumour to chemotherapy is highly desirable, the application of fractal analysis to CT images to detect early response of secondary colorectal tumours treated with conventional chemotherapy has not been confirmed in the current study.

Despite poor reproducibility, an alternative ultrasound imaging-based strategy should therefore be considered owing to its speed, relatively low cost, with no risk associated with ionizing radiation seen with CT imaging, as well as its suitability to perform repeated measurement throughout the course of chemotherapy. The identification of an ultrasound imaging-based quantitative parameter to detect early response of liver

tumour to chemotherapy would have significant benefit to patient's undergoing chemotherapy for liver tumours. Further investigation of a potential ultrasound imaging based technique is outlined in the subsequent chapters of this thesis: with initial experiments conducted using xenograft mice tumour (**Chapter 3**), and its validation in a prospective observation study (**Chapter 4**).

CHAPTER 3

QUANTITATIVE NAKAGAMI IMAGING-BASED VOLUMETRIC ASSESSMENT OF TUMOUR RESPONSE IN VIVO

3. Quantitative Nakagami imaging-based volumetric assessment of tumour response in vivo

3.1. Introduction

The use of current radiological techniques to monitor liver tumour response to chemotherapy, including CT and MRI, cannot be used for frequent repeat scanning during treatment due to the potential damage of ionizing radiation and high cost respectively. An alternative approach using ultrasound would be desirable with advantages including rapid scanning, wide availability, lower cost and no exposure to ionizing radiation, permitting frequent monitoring during a course of chemotherapy treatment. Previous research has suggested that the envelope statistics of the backscattered ultrasound signal can facilitate tissue characterization. This backscattered ultrasound signal is produced by complex interaction between the sound wave and scatterers within the tissue being examined. Tumour tissue changes in response to chemotherapy treatment may alter scatterers within the tissue that can be detected by analysing the backscattered ultrasound signal. The Nakagami distribution is one of the most frequently adopted mathematical statistical distributions to model the envelope statistics of the backscattered ultrasound signal. Nakagami imaging is an extension of this technique, exploiting the ability of Nakagami distribution to model backscattered ultrasound signal to construct parametric maps for tissue assessment. This chapter examines the ability of Nakagami imaging to detect early response of tumour to chemotherapy using a xenograft animal tumour model.

3.1.1. Nakagami Imaging

In order to appreciate the theoretical basis supporting the use of Nakagami imaging for tissue assessment, the relationship between ultrasound interactions with tissue, the

enveloped backscattered ultrasound signal and the Nakagami distribution is briefly reviewed. Current application of Nakagami imaging and its potential for detecting early tumour response to chemotherapy is then illustrated providing the background for the experimental study in this chapter.

3.1.2. Envelop of backscattered ultrasound signal

Following electrical stimulation of piezoelectric crystals at the surface of ultrasound transducers, mechanical distortion of the crystal occurs, resulting in vibration and the production of the ultrasound wave. This typically consists of a short duration sinusoid with 2-3 cycles of the same frequency. As this pulse propagates through tissue, reflections at interfaces produce an echo that propagates back to the transducer, and is in turn converted back into electrical energy. This echo signal is typically much longer than the transmitted pulse, because of the successive reflections of the incident pulse from structures and interfaces at different propagation distances from the transducer (**Figure 3-1**). The received waveform has variable amplitude due to attenuation of the transmitted and received signals resulting from absorption, reflection, scattering and refraction of the ultrasound pulse at a particular depth of tissue, and variable phase due to the varying distance of the reflective structures from the transducer. This echo signal is often called RF signal due to similarity of its temporal shape to RF signals used in telecommunication. The received data by the transducer is therefore called the RF data. In order to create the ultrasound image, envelope detection of the RF data is then performed following use of the Hilbert transform (**Figure 3-2**), whereby the signal is shifted by 90 degrees in phase. This modified signal is then combined with the original signal in order to minimise any ripples, improving estimation of the signal amplitude and image details.

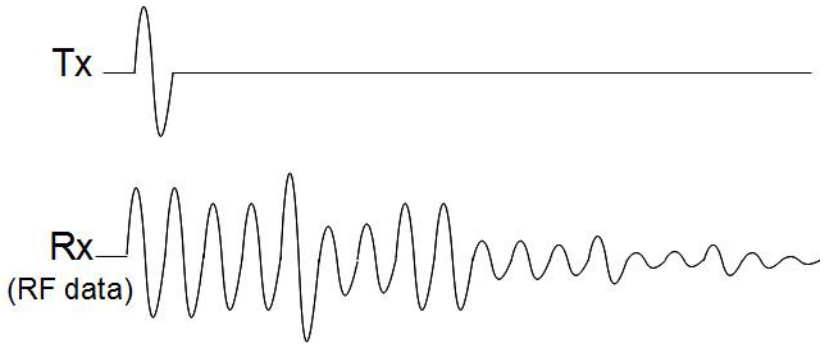

Figure 3-1: Time domain traces comparing the transmit (Tx) pulse compared to the radiofrequency (RF) echo signal following interaction with tissue

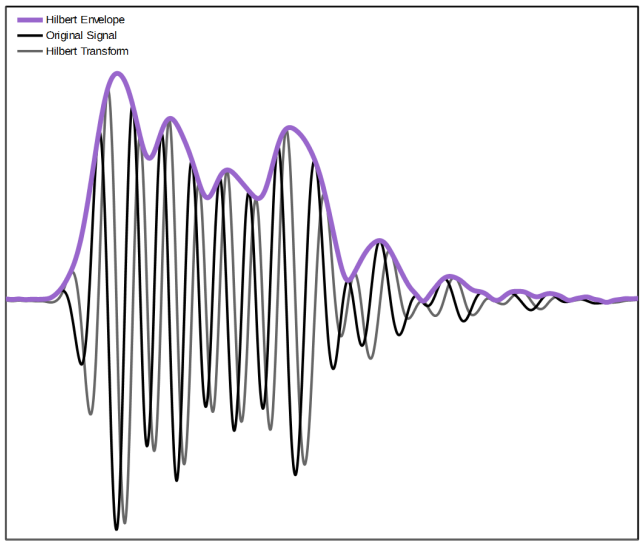

Figure 3-2: Time domain traces demonstrating Hibert transform of the original radiofrequency signal and subsequent envelope detection of the signal.

Apart from the larger structures on the ultrasound image, which are related to ultrasound reflection from objects larger than the wavelength of the insonated ultrasound, the rest of the image is characterised by a granular structure or 'speckle'. Speckle is deterministic as opposed to a random phenomenon, meaning that the same imaging pattern will be produced if the same arrangement of tissue is scanned under the same spatial and processing condition [120].

Tissues under investigation are generally considered as inhomogeneous, with density and compressibility that fluctuate in different sections about their mean value [121]. A

complete range of scatterers with different spacing is therefore present throughout the tissue, but only those comparable in size to the wavelength of the ultrasound are relevant to speckle. Individual cells, collections of cells, vascular structures and other inhomogeneities will individually scatter the incident ultrasound field, producing scattered wavelets that will interact either constructively (constructive interference) to produce a high amplitude echo, or destructively (destructive interference) to produce a low amplitude echo. These interactions contribute to the fluctuations observed in the backscattered RF signal and produce what is known as speckle. With this in mind, as the spatial distribution, density, compressibility or concentration of scatterers within the examined tissue changes, the envelope of the backscattered signal will also change. The Nakagami distribution, described in greater detail below, can model the statistical properties of the backscattered signal, thus providing a quantitative description of the underlying tissue texture, with potential use in the field of tissue characterization [122].

3.1.3. Nakagami distribution

The Nakagami distribution was initially defined in the field of wave propagation by Holfman [123], Shankar initially proposed that the model could describe the statistics of the envelope of the backscattered ultrasound signal. Additionally, the estimated Nakagami parameter could differentiate the various scattering conditions with varying densities of scatterers, varying cross sections, and the presence or absence of regularly spaced scatterers, supporting its use for tissue characterisation [124].

The Nakagami parameter is a shape parameter of the Nakagami statistical distribution. The distribution has the density function:

$$N(x|\mu,\omega) = 2\left(\frac{\mu}{\omega}\right)^{\mu}\frac{1}{\Gamma(\mu)}x^{(2\mu-1)}e^{-\frac{\mu}{\omega}x^2}, \qquad \forall x \in \Re \geq 0$$

Where x is the envelop of the RF signal, with the shape of the distribution defined by the μ parameter corresponding to the local scatterer conditions, and the local backscattered energy by the scale parameter ω>0, for x> 0 and Γ(-) is the Gamma function. If x has a Nakagami distribution N and parameters μ and ω, then x^2 has a gamma distribution Γ with shape μ and scale (energy) parameter ω/μ. The Nakagami distribution can model various backscattering conditions in medical ultrasound. As μ changes the envelope statistics range from pre-Rayleigh (μ <1), Rayleigh (μ =1), to post-Rayleigh (μ >1) (**Figure 3-2**). The statistics of the backscattered envelope follows the Rayleigh distribution when the examined tissue contains a large number of randomly distributed scatterers. If the examined tissue contains scatterers that have randomly varying scattering cross-sections with a comparatively high degree of variance, the envelope statistics are pre-Rayleigh distributions. If the examined tissue contains periodically located scatterers in addition to randomly distributed scatterers, the envelope statistics are post-Rayleigh distributions. The Nakagami parameters are generally estimated by the 2nd and 4th order moments, where given x is the backscattered envelope and *E*(-) denotes the statistical mean, the two Nakagami parameters can be calculated as:

$$\omega = E(x^2), and\ \mu = \frac{E(x^2)}{Var(x^2)} = \frac{E(x^2)^2}{E(x^4) - E(x^2)^2}$$

With its simplicity and low computation complexity [125], it is currently the most widely adopted model for tissue characterisation.

The concept of ultrasound Nakagami imaging was proposed by Shankar to facilitate clinical utilization of this technique for improved diagnosis [76]. This is achieved by calculating multiple local Nakagami parameters from a region of interest, which are then combined to generate a parametric image that can be interpreted simultaneously alongside the conventional B-mode ultrasound image [126].

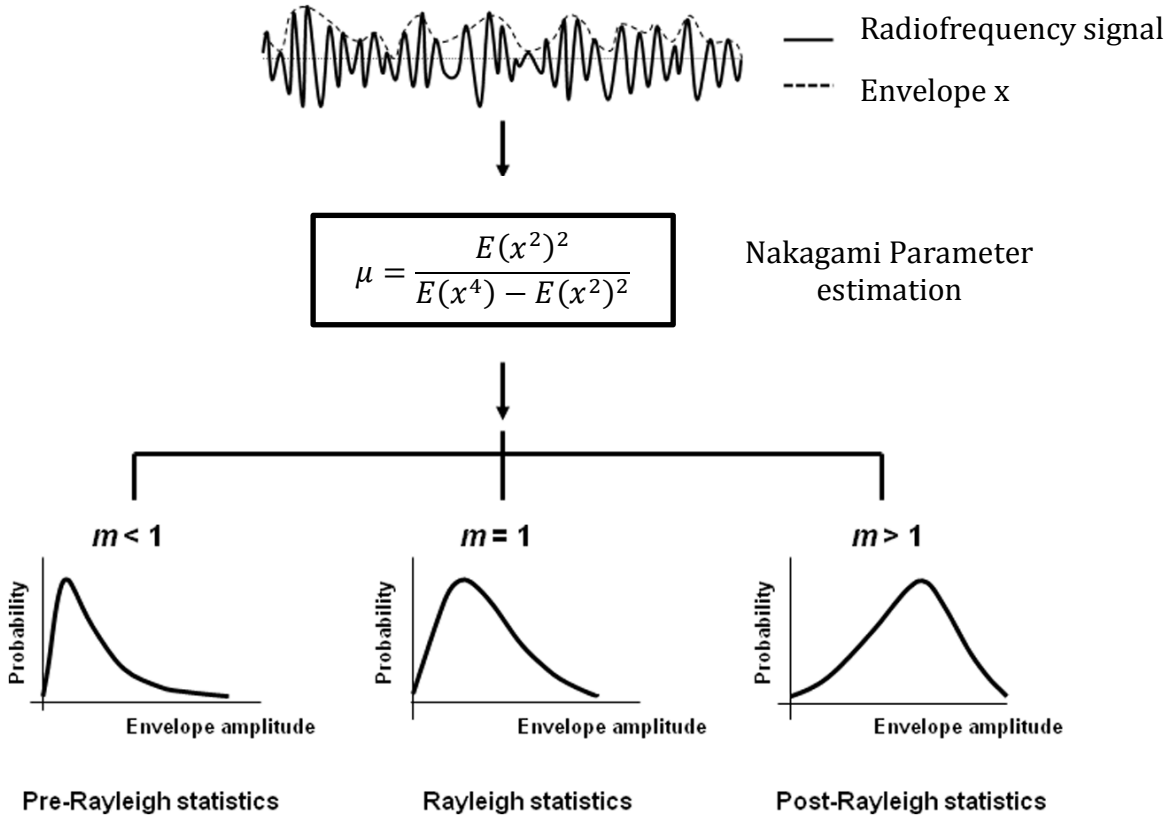

Figure 3-2: Adapted schematic diagram demonstrating the conversion of raw ultrasound backscattered signal for estimation of the Nakagami parameter. Raw ultrasound backscatter signals (i.e. radiofrequency signals) and the corresponding envelope signal used to estimate the Nakagami parameter μ for modelling the statistical distribution of backscatter envelope x. Different Nakagami parameters indicate varying envelope statistics caused by various properties of scatterers in the tissue. (Adapted from Zhou et al. [127]).

3.1.4. Current applications of Nakagami imaging

Nakagami imaging is a relatively novel technique that is yet to be adopted clinically. It has been investigated in a number of clinical applications with promising results, examples include: ophthalmology to assess the degree of lens hardening [128], classification of breast masses into benign or malignant lesions [77, 129, 130], assessing the degree of fat deposition within the liver [131] and severity of liver fibrosis [132, 133], assess the extent of burn [134], and identifying post radiotherapy damage to the vagina [135] and the parotid gland [136].

3.1.5. Potential of Nakagami imaging to detect tumour response to treatment

To date, Nakagami imaging has mainly been used to characterize soft tissue, due to its ability to effectively describe changes in the backscattered envelope statistics with structural changes. In malignant breast cancer, backscattered envelope was found to be more pre-Rayleigh distributed [77]. This was attributed to the development of calcification, dilatation of internal ducts and new vessels increasing the complexity of scatterer composition and arrangement. Liver fibrosis has also been shown to cause deviation towards more pre-Rayleigh distribution compared to normal liver [133]. The authors attributed this to the process of damage and regeneration resulting in the deposition of extracellular matrix, altering the organisation of scatterer cross sections with resulting changes in backscattered signal. While these studies demonstrated the potential for Nakagami imaging to distinguish normal and diseased human tissue, it may also identify changes in tissue characteristics, such as tumour with response to treatment or progression. To achieve this goal, the technique must account for the variety of tissue response to treatment and heterogeneity within tumours.

3.1.6. Tumour heterogeneity and response to treatment

The evidence supporting heterogeneity of tumours was initially found in an animal tumour, where separate cell lines with differing characteristics were identified in a single mouse mammary tumour using cell culture and separation methods [96]. Advances in analysis techniques have since confirmed tumour heterogeneity both on genetic and histological levels. This manifest through changes in cellular density, vascularity, extracellular matrix and necrosis throughout the tumour. Intra-tumour heterogeneity may in turn lead to the development of treatment resistance [137], resulting in a heterogeneous tumour response to a given treatment. Whilst cross sectional imaging with CT and MRI acquires information from the entire tumour

volume to overcome this potential problem, volumetric data is not routinely captured with ultrasound, since 3D scanning is rarely employed in clinical practice. Additionally, the larger acoustic window required for 3D ultrasound transducer may limit its wider application. Examples may include imaging of liver when the limited acoustic window between rib space may reduce the quality of the acquire images due to acoustic shadowing by the ribs.

3.2. Gap in Knowledge

Development of an ultrasound method to detect early tumour response to treatment is desirable and would have significant advantages over current methods. Nakagami imaging has demonstrated potential in previous studies to characterise soft tissue. The technique has not previously been used to assess interval change in tumour tissue. In this chapter the utility of the Nakagami parameter to quantitatively detect tumour response to chemotherapy is explored.

3.3. Aims

- To determine if an adapted Nakagami imaging-based volumetric ultrasound tissue assessment technique can provide a quantitative parameter that varies between tumours that respond differently to treatment.
- To determine if this quantitative parameter is affected by the tumour size or the presence of chemotherapy.
- To determine if interval change of this quantitative parameter from baseline is significantly different between responding and non-responding tumours.

3.4. Materials and Methods

The experimental procedures described in this section were carried out in collaboration with two highly skilled researchers, Dr. Eleonora Mylonopoulou and Professor. Robert Calisle. In particular, their expertise with high intensity focused ultrasound (HIFU) mediated chemotherapy delivery were instrumental to the success of these experiments.

The xenograft tumour model and treatment used in this part of the study was conducted as part of an extended investigation into HIFU-mediated drug release from low-temperature sensitive liposomes containing doxorubicin (lyso-thermosensitive liposomal doxorubicin - ThermoDox®, Celsion Corp.). The aims of the experiment were: 1) To identify the HIFU parameters required to induce sufficient intra-tumour hyperthermia necessary to release the encapsulated chemotherapy, 2) To demonstrate changes in tumour growth following HIFU-mediated release of chemotherapy using the parameters identified in part 1 of the study. These experiments also provided the opportunity to capture ultrasound images from xenograft mice tumours assigned to different treatment protocols in part 2 of the study. This data was used to develop a Nakagami imaging based volumetric tissue assessment technique to detect tumour response to chemotherapy. As tumour growth was hypothesised to vary in mice subjected to different treatment protocols, i.e. retarded growth or tumour shrinkage indicating response to treatment in the full treatment group, and tumour growth indicating no response or progressive tumour in the partially treated or control group, this experiment provided ultrasound data to address the aims and objectives of this part of the thesis.

3.4.1. Xenograft tumour model and animal welfare

Animal studies were performed in accordance with the Animals Scientific Procedures Act (ASPA) of 1986 (UK). Female CD1-nude mice (Charles Rivers) were used in all experiments as they lack a thymus gland, which renders them immunodeficient, hence suitable for implantation of xenografts. They were housed in individually ventilated cages (IVCs) at 21^0C with 12 h light/dark cycles and food and water available *ad lib* during experiments. HCT-116 cells ($5x10^6$) were implanted into the right hind leg of the 6- to 8- weeks old mice. After approximately 2 weeks, mice were used in the experiment when interval xenograft tumour growth reaches approximately $50mm^3$, as determined by calculated volume (length x width x depth)/2) using serial caliper measurements. All mice were monitored closely for any adverse effects during the course of an experiment and were euthanised if their condition became poor. All animals were euthanised after experiments by Schedule one methods.

3.4.2. Anaesthesia for treatment and ultrasound imaging

Anaesthesia in the experiments was induced and maintained using a mixture of isofluorane (Baxter) and room air. Whilst under anaesthetic mice were monitored for respiration rate (maintained at 60-100 respirations/min) and temperature (maintained at 37^0C). After the experiment, mice were either euthanised or recovered in isolation and monitored for 10 min to ensure recovery from anaesthesia and procedures.

3.4.3. HIFU exposures

Thermodox is a drug that contains low-temperature-sensitive liposomes at a liquid suspension of 2mg/ml. Upon heating to temperatures in the range 39^0C to 42^0C, the lipid bilayers destabilize and the anticancer agent that is encapsulated is locally

released within the heated area. The active drug in ThermoDox is doxorubicin HCl, a widely used chemotherapeutic agent.

In part 1 of the experiment, the HIFU exposure necessary to achieve chemotherapy release from Thermodox was identified (unpublished data). This was achieved by performing thermal measurements with a fine needle (0.2 mm) T-type thermocouples (HYP0, Omega) inserted into the tumour under anaesthesia during HIFU exposure. These parameters were subsequent employed in the second part of the experiment without the need for further thermal measurements.

A custom-manufactured spherically focused HIFU transducer with centre frequency of 1.06-MHz transducer (H-102B SN22; Sonic Concepts, Bothell, Wash) was used in this study. This has a 63-mm geometric focus, 64-mm active diameter, and an 18 × 45-mm^2 rectangular cutout to enable coaxial placement of a Zonare L10-5 linear imaging array (Zonare Medical Systems, Inc., Mountain View CA, USA) for image guidance. The transducer was calibrated in water by using a 0.5-mm needle hydrophone (SN 1203; Precision Acoustics, Dorchester, Dorset, England). The 6-dB longitudinal, transverse, and elevational beam widths were measured as 16, 2, and 1 mm, respectively. To generate the exposures, a signal generator (model 33250A; Agilent Technologies, Santa Clara, Calif) was connected to a power amplifier (model A300; ENI, Rochester, NY), which was in turn connected to the 50-Ω matching network supplied with the HIFU transducer.

Pulsed HIFU exposures were performed at pressure of 6.08 MPa ppk (175mV ppk), 25% duty cycle with 1Hz pulse repetition frequent and 5s duration in part 2 of the experiment, having been found in part 1 of the experiment to produce the temperature rise (5- 8^0C) necessary to release Doxorubicin from Thermodox (TD).

A three-dimensional stage mounted on a custom-built water tank containing degassed water, maintained at 37^0C, was used for both experiments. Individual mice were initially placed in a custom-built holder immersed into the water tank opposite the transducer, and the co-axially placed imaging transducer was used to localize the tumor that was to undergo exposure. The stage was initially used to position the mice so that the tumor was located in the center of the focal zone of the therapeutic transducer during exposure. The focal volume of the ultrasound exposure was then adjusted using the positioning system throughout the exposure to ensure hyperthermia was achieved in a large proportion of the tumour volume. This was performed at 3 separate cross sectional plane using a 3 x 3 raster grid, with a lateral and vertical spacing of 1mm per site. This provided a total of 27 separate sites of HIFU exposures throughout the tumour volume.

3.4.4. Treatment groups

Mice were randomly assigned into one of four treatment groups: phosphate buffered saline (PBS) (6), HIFU only (6), HIFU and TD (8) and TD only (8). For the purpose of addressing the aims and objective of the current study, tumour shrinkage indicating response to treatment was expected in the HIFU and TD group, and tumour growth indicating no response or progressive tumour was expected in the PBS only (control group). Stable tumour size was expected in HIFU only and TD only groups to represent partial response secondary to receiving only part of the treatment. In the case of HIFU, mild hyperthermia to the tumour may induce anti-tumour immune response and changes in the vasculature resulting in partial suppression of tumour growth [138]. Depending on the assigned treatment group, 100 µL of PBS or TD (containing approximately 80 µg of Doxorubicin) was injected into the tail vein. In the HIFU only group, HIFU exposures were performed without any prior injection.

HIFU exposure was performed immediately post injection in mice assigned to the combined HIFU and TD group.

3.4.5. Ultrasound imaging protocol

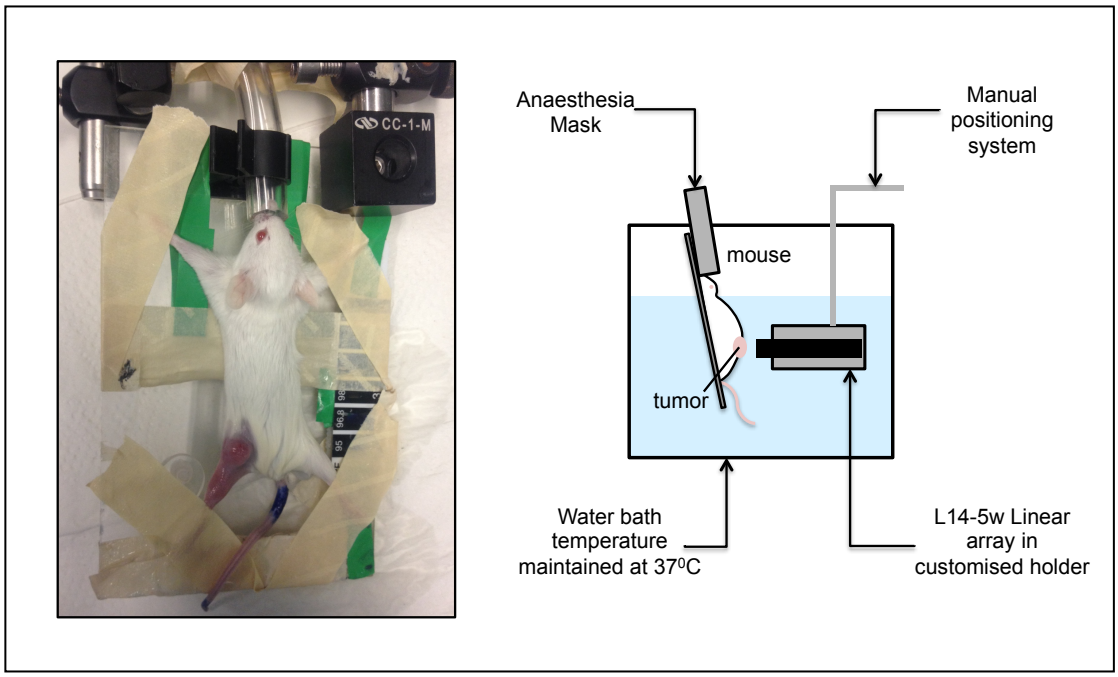

Figure 3-3: Photograph and schematic drawing demonstrating positioning of mice for HIFU exposure and ultrasound imaging.

RF ultrasound data was acquired using a diagnostic ultrasound system (z.one, Zonare Medical Systems, Mountain View, CA, USA), using the L14-5w linear 192 elements array with a central frequency of 10 MHz and a sampling rate of 50 MHz. The output 2D image size was 20 x 54 mm with a resolution of 289 x 648 pixels. Individual mice to be imaged were initially placed in a custom-built holder immersed into the water tank whilst under constant anaesthesia (**Figure 3-3**). The stage was then used to position the mice so that the tumour was located opposite the imaging transducer secured in a customized holder. Data from the whole tumour volume was obtained by acquiring sequential cross sections of the tumour, with a 1mm step-wise movement of the array using the manual positioning stage in a cranial to caudal direction, until the whole tumor volume was imaged. The 2D images were combined to create a

volumetric dataset. In order to ensure that nearby healthy tissue was not included in tumor tissue characterization, manual segmentation of the tumour from each image was initially performed (**Figure 3-4**).

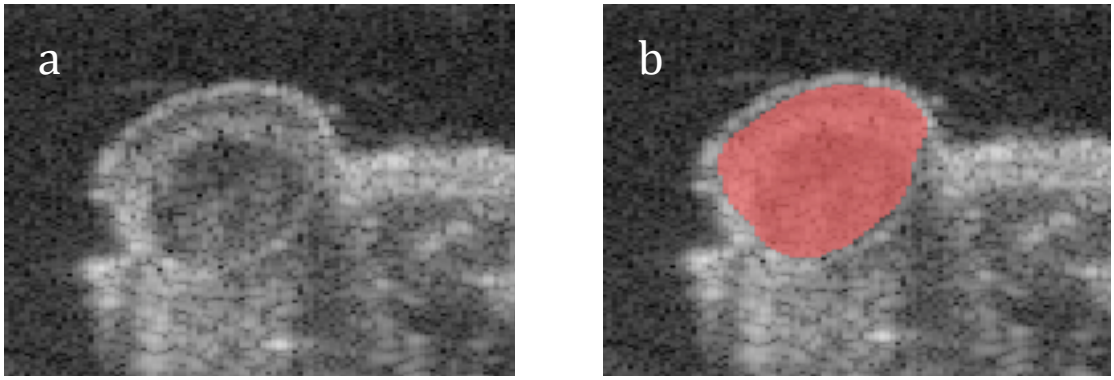

Figure 3-4: B mode ultrasound image of hindleg xenograft tumour pre (a) and post manual segmentation (b). Only data contained within the segmented region was then used for subsequent analysis.

Due to the small size of xenograft tumour, it was challenging to accurately segment smaller parts of the tumour without erroneously including normal tissue, raising the potential for inaccurate analysis when calculating the Nakagami parameter. To ensure the most representative data was analyzed for tissue characterization, tumour cross sections with an area less than the median area of all cross sections from a single tumour were removed from analysis. Following this elimination step, the remaining cross-sections from each tumour were used for subsequent analysis.

3.4.6. Tumour growth monitoring

Besides close monitoring of the general condition of each mouse and its weight post-treatment, tumour volume was measured every 2 days based on calculated volume (length x width x depth)/2) using serial caliper measurements. The tumour volume was also assessed by ultrasound imaging at the time of data acquisition on day 0, 7 and 14-post treatment as per protocol outlined below. Tumour volume was calculated using the area obtained from segmented tumour cross sections, and the assumption of

1mm image thickness, based on the distance of imaging transducer movement during data acquisition, i.e. 1 mm.

3.4.7. Nakagami parameter calculation for tumour volume

The image analysis method described in this section was carried out in collaboration with Dr. Omar Al-Kadi and Dr. Amalia Cifor. Their contribution to the development of the software for automated image analysis was instrumental to the success of this part of the experiment.

In order to calculate the Nakagami parameter for the whole tumour volume, each tumour cross section was initially analysed using the same procedure for construction of the Nakagami image [126]. In brief, the technique involves two steps: firstly, a square window within the envelope image is used to collect the local backscattered envelopes for estimating the local Nakagami parameter, which is then assigned to the pixel located in the centre of the window. This process is then repeated with the window moving throughout the entire envelope image in steps of one pixel, which yields the Nakagami parameter values for the entire image.

To ensure accurate estimation of the Nakagami parameter for the current analysis, the optimal size of the sliding window used to estimate the Nakagami parameter was initially assessed. A square-sliding window with sides containing 7 pixels was found to have the smallest error based on this initial analysis [139], thus this window size was adopted for subsequent automated image analysis. Estimation of the Nakagami parameter of the cancerous tissue has been reported to be erroneous owing to the inclusion of pixels from normal tissue adjacent to the tumour [77]. An additional safeguard was therefore introduced to ensure exclusion of pixels outside the tumour segmentation when analyzing data from the edge of the tumour.

Thus far, the calculation of the Nakagami parameter has only been developed to obtain data from a single cross section, i.e. two-dimensional region, of a tumour. In order to account for heterogeneous response within the tumour, a quantitative method was developed to represent the Nakagami parameter obtained from the whole tumour volume. This was necessary since data from a representative region of the tumour, e.g. maximal cross sectional area, is prone to selection bias and difficult to accurately replicate throughout the course of treatment for serial measurement. In addition, by obtaining quantitative data from the entire tumour volume, any intra-tumour heterogeneous response to treatment will also be taken into consideration as part of the overall response to treatment by the tumour.

Since previous studies demonstrated the deviation of backscattered envelope statistics towards pre-Rayleigh from malignant breast tumour [77] and liver fibrosis [133], tumour response to treatment may also result in similar changes. Following automated analysis of the segmented cross sections from each tumour as previously outlined, the percentage of square slide window with estimated Nakagami parameter < 1, i.e. pre-Rayleigh was then calculated, herein referred to as the percentage of pre-Rayleigh regions (%PRR). This percentage value thus provided a quantitative parameter based on data from the entire tumour volume overcoming some of the obstacles associated with the use of a single/representative region of the tumour for the purpose of monitoring response to treatment.

Interval change in the %PRR throughout the course of treatment was compared between different treatment groups, hypothesized to result in differential response to treatment. To ensure the validity of %PRR as a quantitative parameter for detecting tissue changes, further analysis was also performed to ascertain the influence of tumour size and the presence of chemotherapy on the %PRR.

3.4.8. Statistical analysis

Interval change in the %PRR compared to based between different response group was treated as parametric data and these were compared between the two response groups using Student independent-sample t test. A P value of 0.05 or lower was considered significant. Data were analysed by using commercially available statistical software (version 20.0; SPSS, Chicago, Illinois).

3.5. Results

3.5.1. Confirmation of treatment response in different treatment groups

The mean size of tumours within the different treatment groups based on caliper and ultrasound measurements throughout the duration of the experiment was initially analysed. This was necessary to establish if changes in tumour size within the different treatment groups was consistent with our hypothesis to provide groups of tumour with different response to chemotherapy treatment. For the purpose of addressing the aims and objective of the current study, tumour shrinkage indicating response to treatment was expected in the HIFU and TD group. Tumour growth indicating no response to treatment or progressive tumour was expected in the PBS only (control group). Stable tumour size was expected in HIFU only and TD only groups to represent partial response secondary to receiving only part of the treatment.

It is also important to bear in mind that the mean baseline tumour volumes of the different treatment groups were heterogeneous (**Figure 3-5, 3-6**). This was not due to experimental errors in tumour cell implantation, but related to ethics and animal license issues. The latter governs the need to terminate animals when implanted xenograft tumours reach an upper volume threshold to avoid suffering. Since the experiment continued for 14 days, during which tumours will continue to grow in the absence of effective treatment, small tumours at the start of the experiment were deliberately assigned to the control, TD only or HIFU only group. In this way, it was hoped that the tumours would not grow beyond the threshold volume necessary to prematurely terminate the animal prior to the end of the experiment. On the other hand, since tumours in the group receiving the combined HIFU and TD treatment will hypothetically be receiving the optimal treatment leading to tumour shrinkage, thus

large tumours at the beginning of the experiment were assigned to this combination treatment group.

Based on calculated tumour volume from caliper measurements, tumours in the combined HIFU and TD group demonstrated an initial reduction in mean tumour volume. This was followed by a reduced tumour growth rate compared to the other treatment groups (**Figure 3-5**). The growth rate of tumours in the group treated with HIFU only was lower compared to the PBS and TD only groups, though remained higher than the combined HIFU and TD group.

The mean volume of tumours in the combined HIFU and TD group was higher than other treatment groups at baseline due to the experimental protocol as previously discussed.

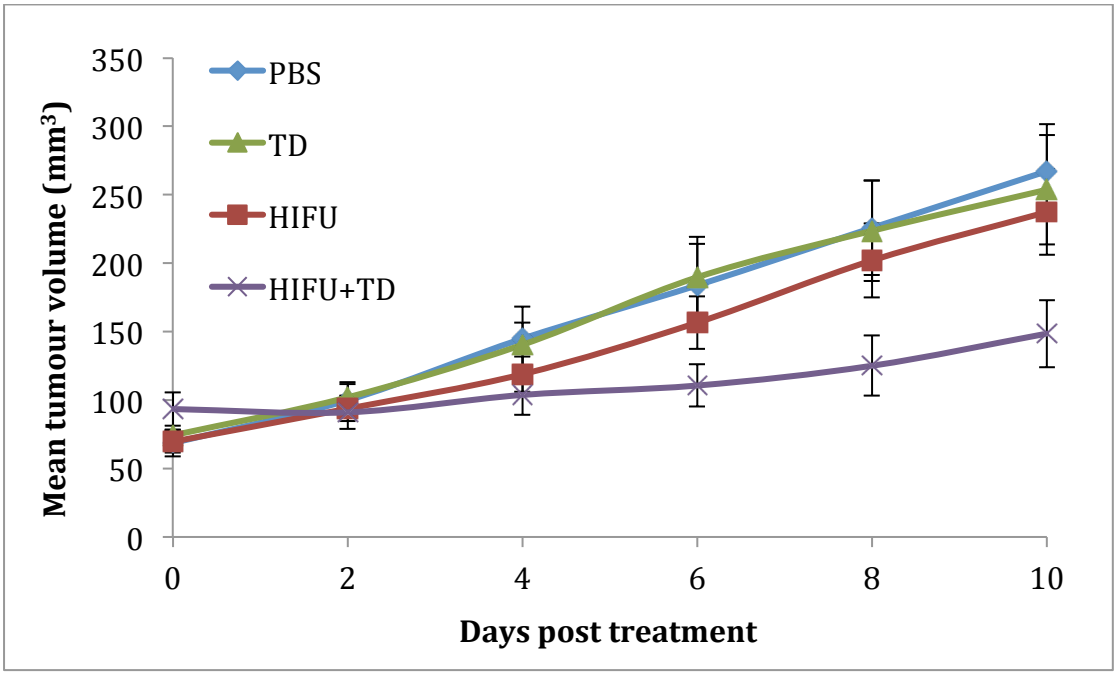

Figure 3-5: Graph showing the mean and standard deviation of tumour volume, calculated from caliper measurements, in different treatment groups against the number of days post treatment. PBS= phosphate buffer solution, TD= Thermodox only, HIFU= High intensity focused ultrasound only and HIFU+TD= combined treatment with High intensity focused ultrasound and Thermodox.

Our imaging protocol on day 0, 7 and 14 post treatment meant there were fewer data points for direct comparison with the results from calculated tumour volume based on caliper measurements.

Heterogeneity in the baseline mean tumour volume between different treatment groups was again confirmed on ultrasound measurement of tumour volume (**Figure 3-6**), secondary to experimental protocol as discussed earlier. Interval increases in mean tumour volume were seen in all treatment groups from baseline to day 7, this was however reduced in the HIFU and TD group, a trend that continued into day 14-post treatment. In the HIFU only group, the rate of tumour volume growth reduced compared to both the PBS and TD only groups between days 0 to day 14- post treatment.

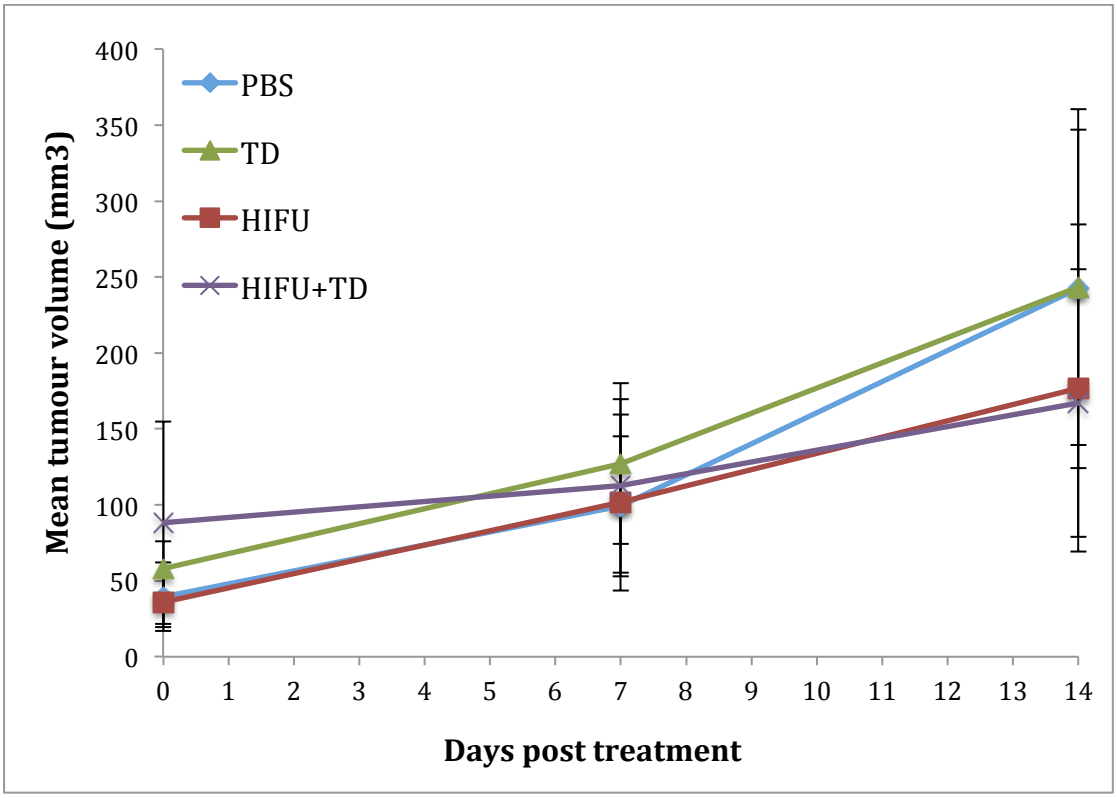

Figure 3-6: Graph showing the mean and standard deviation of tumour volume based on ultrasound imaging in different treatment groups against the number of days post treatment. PBS= phosphate buffer solution, TD= Thermodox only, HIFU= High intensity focused ultrasound only and HIFU+TD= combined treatment with High intensity focused ultrasound and Thermodox.

In order to overcome the observed initial heterogeneity in baseline tumour volume in the different treatment groups, the results of the ultrasound based tumour volume measurement from different treatment groups were re-analysed to identify the mean percentage change in tumour volume from baseline.

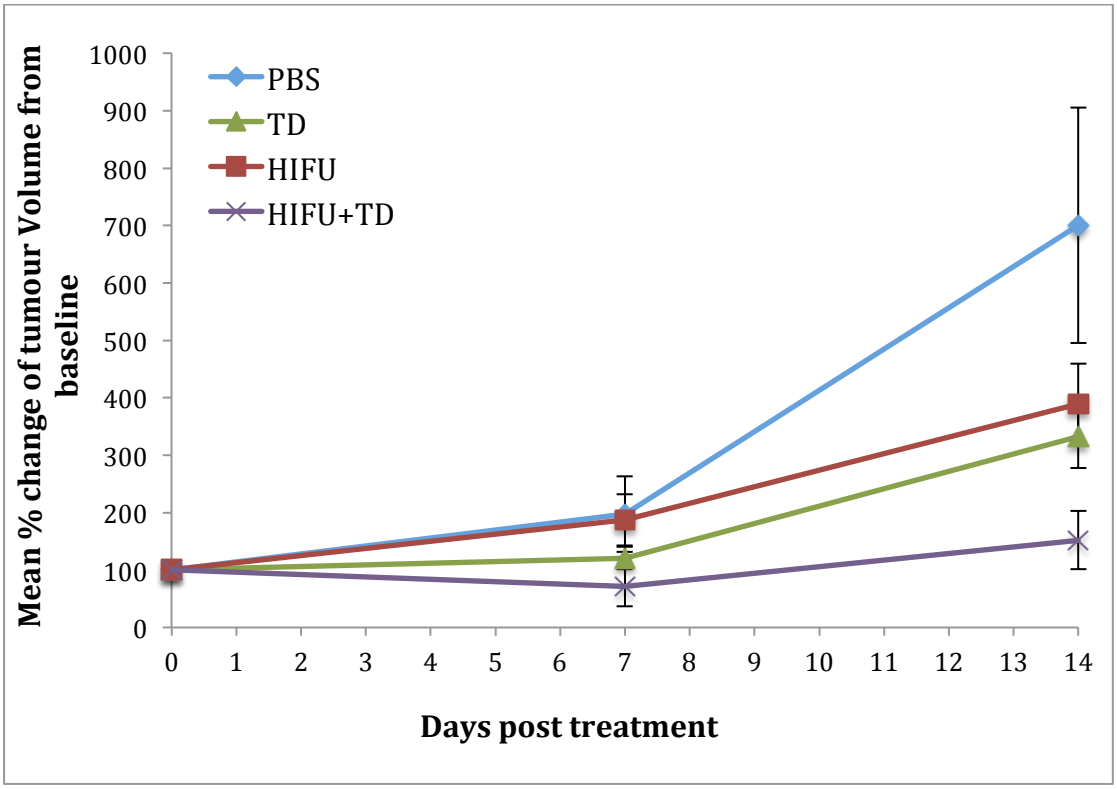

Figure 3-7: Graph showing the mean and standard deviation of percentage of tumour volume changes from baseline based on ultrasound imaging in different treatment groups against the number of days post treatment. PBS= phosphate buffer solution, TD= Thermodox only, HIFU= High intensity focused ultrasound only and HIFU+TD= combined treatment with High intensity focused ultrasound and Thermodox.

An initial reduction in mean tumour volume was again seen in the combined HIFU and TD group at day 7, when compared to baseline (**Figure 3-7**). Subsequent growth rate of tumours in this group was reduced until the end of the study when compared to the other treatment groups. Reduced growth rate of tumours treated with TD only was demonstrated up to day 7-post treatment compared to those in the PBS or HIFU only groups. While the growth rate of tumours in the PBS group significantly increased after day 7 post treatment, the growth rate of tumours in both the TD only and HIFU

only groups were found to be lower, though remained higher than those in the combined HIFU and TD group.

Based on this initial analysis of mean tumour size and mean percentage change of tumour size from baseline in the different treatment groups, the different treatment protocols in this experiment did not produce the differential tumour responses to treatment that was initially anticipated. Despite tumours in the combined HIFU and TD group receiving the optimal treatment, there was only modest reduction in the mean tumour volume, which was demonstrated with caliper measurement and re-calculation of tumour volume change from baseline. There was also persistent reduction in tumour growth rate in the combined HIFU and TD group, compared to the other treatment groups suggesting possible retarded growth resulting from the treatment. Rather than being classified as response to treatment, it could be argue that the retard growth would indicate stability of the tumours in this treatment group, and not strictly responding to the chemotherapy. In the remaining treatment groups, there was only interval growth of tumour at day 7 and day 14-post treatment from the baseline, although the rate of growth appeared to be lower in the HIFU only group based on caliper measurement, and TD only group based on recalculation of mean percentage interval change of tumour volume from baseline. Tumours in these groups were therefore regarded as non-responsive or progressive on chemotherapy. This analysis confirmed that all the ultrasound data collected from this experiment originated only from tumours that remained stable or progressed on treatment.

3.5.2. Mean percentage of pre-Rayleigh regions within the tumour volume in different treatment groups

Despite the findings from the initial analysis, the analysis was extended to identify any difference in the mean %PRR in the tumour volume between different treatment groups throughout the experiment. The baseline %PRR within the tumour volume was heterogeneous between different treatment groups with a lower mean %PRR in tumours treated with combined HIFU and TD (**Figure 3-8**). Reduction in the mean %PRR at day 7 and day 14-post treatment was seen across all treatment groups. However, the rate of reduction in mean %PRR in tumours from the combined HIFU and TD group between baseline and day 7-post treatment was less compared with the other treatment groups.

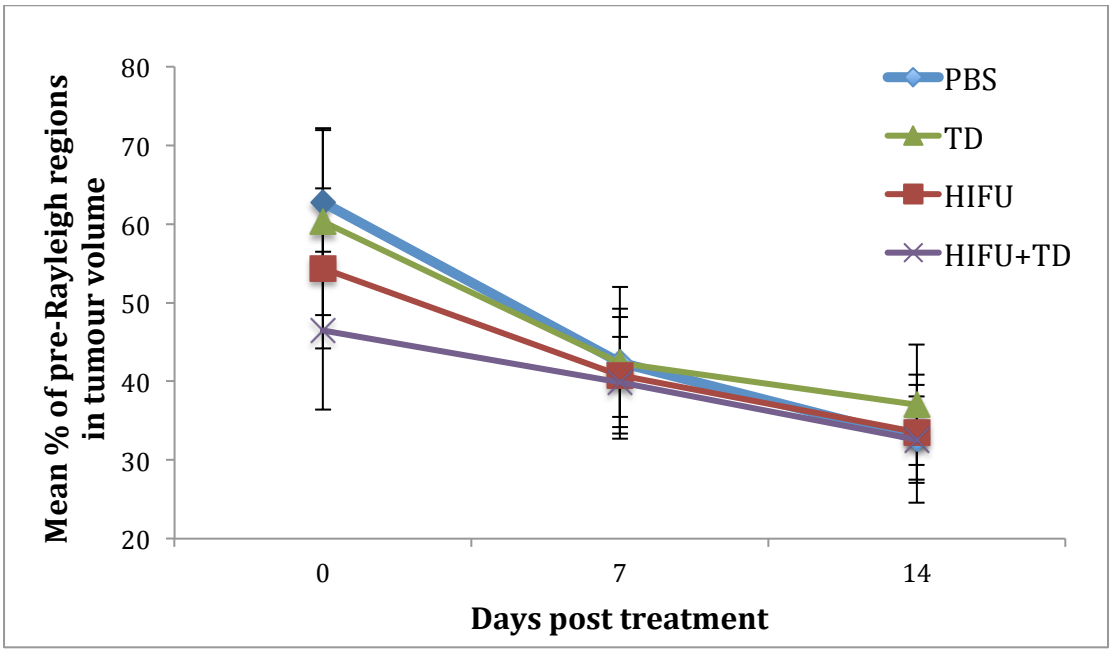

Figure 3-8: Graph showing the mean and standard deviation of %PRR regions in the tumour volume treated in different groups against the number of days post treatment. PBS= phosphate buffer solution, TD= Thermodox only, HIFU= High intensity focused ultrasound only and HIFU+TD= combined treatment with High intensity focused ultrasound and Thermodox.

Although this analysis confirms the %PRR from the tumour volume decreased in tumours from all the treatment groups, the gradient of the best fit lines suggests the rate of reduction to be reduced in the group of tumours designate as having stable

disease, i.e. combined HIFU and TD group, compared to tumour from the other treatment designated as non-responders or progressive disease. In addition, the observed heterogeneity of mean %PRR at baseline is concordant with the heterogeneity in tumour volume reported in our earlier analysis owing to the experimental protocol. These observations suggest the %PRR from tumour volume is likely to correlate with the size of the tumour. %PRR may be able to assess changes in tumour size, thus response to treatment by providing a quantitative assessment of the tumour tissue.

3.5.3. Correlation between ultrasound determined tumour volume and the percentage of pre-Rayleigh regions within the tumour volume

Based on the above results, the %PRR was plotted against ultrasound-determined tumour volume from all treatment groups. This confirmed an indirect correlation between the %PRR and tumour volume, where reduction in the %PRR correlated with an increase in the tumour volume (**Figure 3-9**). Furthermore, this correlation was observed across all treatment groups with or without TD as part of the treatment protocol (**Figure 3-10**). This latter observation suggest %PRR is unaffected by the presence of chemotherapy, validating this quantitative parameter as a reliable measure of true tissue change resulting from changes in tumour volume.

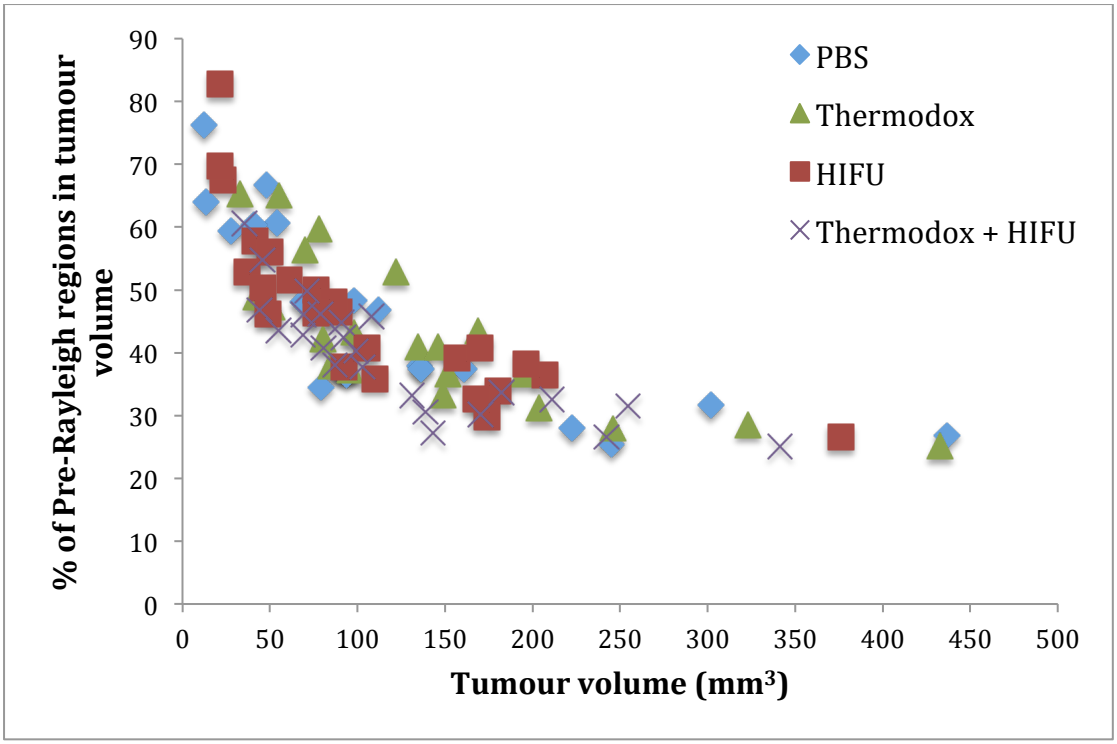

Figure 3-9. Graph showing the %PRR regions in the tumour plotted against the volume of tumour as determined by ultrasound imaging. PBS= phosphate buffer solution, TD= Thermodox only, HIFU= High intensity focused ultrasound only and HIFU+TD= combined treatment with High intensity focused ultrasound and Thermodox.

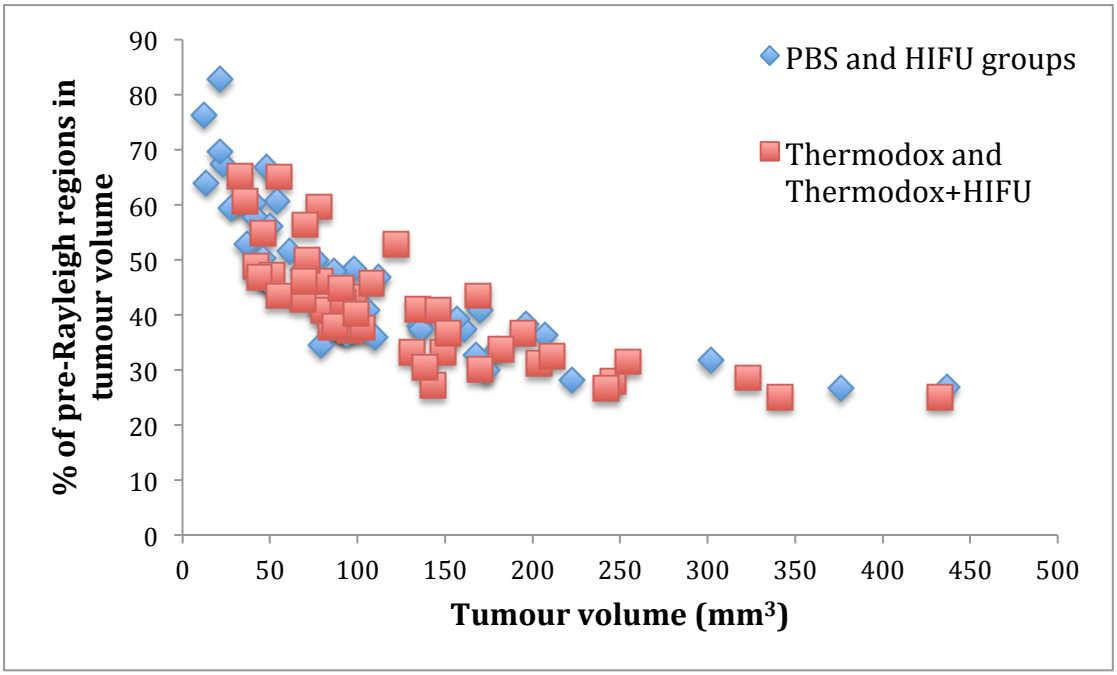

Fig. 3-10: Graph showing the %PRR regions in the tumour plotted against the volume of tumour as determined by ultrasound imaging. PBS= phosphate buffer solution, HIFU= High intensity focused ultrasound.

3.5.4. Interval change in the percentage of pre-Rayleigh regions from baseline between responders and non-responders

Having demonstrated the %PRR from tumour volume is related to tissue changes resulting from changes in tumour volume, the ultrasound dataset was reanalyzed in an attempt to reclassify tumours into responder and non-responder to treatment to establish if interval changes in %PRR from the tumour volume differ between the two groups. For the purpose this analysis, the treatment protocol employed was not taken into consideration. Tumours were ranked in order of response to treatment, based on percentage change in tumour volume from baseline. Tumours that demonstrated response better than the median were then classified as responders, with the remainder classified as non-responders. The interval change in %PRR of the tumour volume from baseline was compared between responders and non-responders. The reduction in %PRR at 7 and 14 days-post treatment was greater in tumours that were classed as non-responders, p=0.012 and 0.006 respectively (**Figure 3-11**).

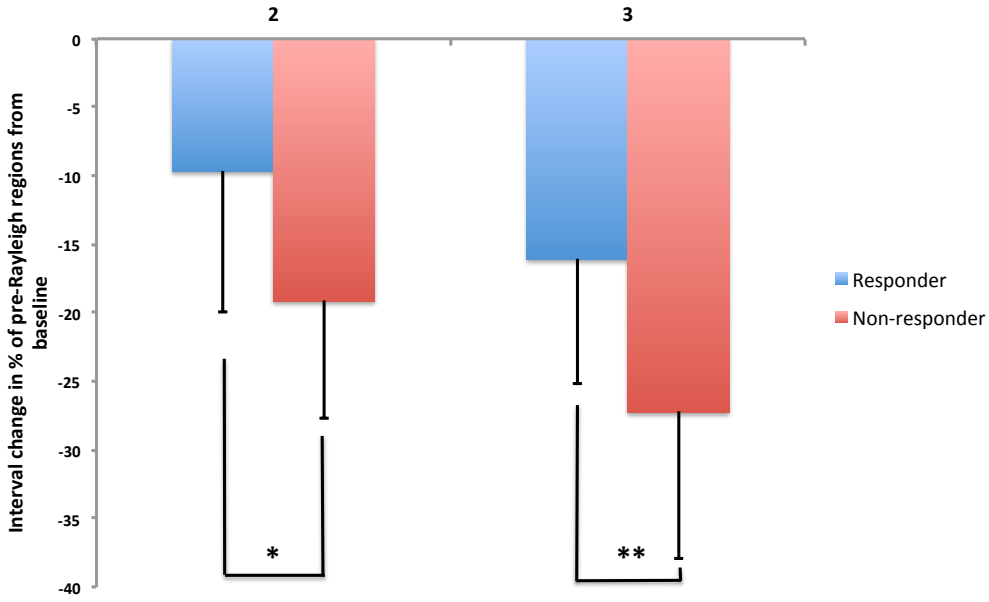

Figure 3-11: Graph showing the mean and standard deviation of the interval change in the %PRR regions in the tumour volume between responders and non-responders when compared to the baseline at different time points. Time points: 2= 7 days-post treatment, 3= 14 days-post, * and ** represents p-value of 0.012 and 0.006 respectively.

3.6. Discussion

The technique of Nakagami imaging, previously used for two-dimensional tissue characterization was adapted to provide a volumetric tissue assessment technique to assess ultrasound data from the entire tumour volume. The adapted technique provides a more accurate comparison of data from the entire tumour volume, overcoming potential bias associated with sampling error and heterogeneous tumour response when monitoring tumour tissue at multiple time points. The %PRR was selected as a quantitative parameter that can be obtained from volume tissue assessment based on deviation in backscattered envelope statistics towards pre-Rayleigh observed in previous studies of malignant breast tumour [77] and liver fibrosis [133]. This parameter allows objective comparison of data from different time point during the course of treatment. Further analysis demonstrated this parameter is related to tissue changes as tumour size changes. Further analysis confirmed interval change in %PRR of tumour volume was significantly different between tumours classified as responders and non-responders.

Xenograft tumours implanted and grown on the hindleg of mice underwent different treatment protocols as part of an ongoing study to investigate HIFU mediated release of chemotherapy, namely doxorubicin from lyso-thermosensitive liposomal doxorubicin (ThermoDox®, Celsion Corp.), by inducing mild hyperthermia. The experiment provided a platform from which ultrasound data could be acquired from animal tumours subjected to different treatment protocols resulting in differential tumour response to treatment. The initial analysis confirmed that none of the treatment protocols resulted in persistent reduction in tumour size that would conclusively indicate response to treatment. However, tumours in the combined HIFU and TD group did demonstrate an initial modest reduction in mean tumour volume,

followed by tumour growth with a reduced rate comparing to the remaining treatment groups (**Figure 3-5, 3-6, and 3-7**). Based on this observation, it was determined that tumours from this group could be classified as stable disease, while the remaining tumour in the other treatment groups were classified as non-responder or progressive disease.

This observation supports the experimental hypothesis that HIFU induced hyperthermia facilitates the release of chemotherapy encapsulated in TD, in turn causing a reduction in tumour volume, albeit modest in the current experiment. Since treatment was only performed on a single occasion at day 0 of the experiment, unlike the repeated chemotherapy administration of a normal clinical course, this may account for subsequent growth of the tumour following the initial reduction at day 7, rather than a continual reduction.

Having confirmed the responders of different tumour group, automated analysis of the dataset was performed with the adapted Nakagami imaging based volumetric tissue assessment technique. While reduction in %PRR of tumour volume was observed in all treatment groups, the rate of reduction in tumours treated with combined HIFU and TD was lower compared to the other treatment groups (**Figure 3-8)**, correlating with the reduced tumour growth rate demonstrated previously. This observation coupled with heterogeneity of %PRR at baseline correlating with the baseline heterogeneity of tumour size related to experimental protocol, led to the hypothesis that %PRR is related to tissue changes resulting from tumour size change. An indirect correlation between %PRR and tumour volume was subsequent confirmed. Further analysis also confirmed the %PRR was unaffected by the presence of chemotherapy, i.e. doxorubicin, validating its potential as a quantitative parameter to detect tissue changes (**Figure 3-10**). Following reclassification of the ultrasound dataset into

'responder' and 'non-responder' based on the percentage change in tumour volume from baseline, interval change in %PRR of the tumour volume from baseline at day 7 and 14-post treatment was compared between the two response groups. A significant difference was identified with greater reduction in %PRR identified in non-responders. This analysis provided further evidence supporting the use of this new quantitative parameter to assess tissue changes.

Since the Nakagami parameter changes with respect to the scattering conditions in the assessed tissues [124], the observed relationship between %PRR of the tumour volume with the tumour size may be secondary to alteration in scatterer densities or alignment. Previous research had hypothesized that the shift towards a pre-Rayleigh distribution for pathological tissues is due to increasing structural organization in breast tumours [77], and extracellular matrix deposition in liver fibrosis [133]. A similar explanation can thus be given for the observed reduction in %PRR with tumour growth. Larger tumours have increased vasculature, as well as proliferating extracellular support network due to growth and development, which in turn increases the proportion of the tumour with post-Rayleigh distribution owing to possible increased organization of scatterers secondary to changes within the tumour.

3.7. Summary

Despite the failure of the experimental protocol to provide an ultrasound dataset from tumours exhibiting a clear response to treatment, the mean %PRR of xenograft tumour volume was found to change at different rates between tumours in the different treatment groups. Further analysis demonstrated an indirect correlation between %PRR and tumour volume, while %PRR was also found to be unaffected by the presence of chemotherapy. %PRR was subsequent found to be significantly different amongst 'responding' and 'non-responding' tumours. The analysis in this

chapter has demonstrated the potential of the adapted Nakagami imaging based volumetric tissue assessment technique to quantitatively assess tissue changes. In particular, changes in the percentage of pre-Rayleigh regions (%PRR) within the tumour may be a suitable predictor of tumour response to chemotherapy.

Application of the technique to detect early tumour response to chemotherapy is subsequently investigated using clinical ultrasound datasets obtained from patients undergoing chemotherapy for liver metastasis, as described in the next chapter.

CHAPTER 4

CLINICAL VALIDATION OF NAKAGAMI IMAGING-BASED VOLUMETRIC ASSESSMENT OF TUMOUR RESPONSE

4. Clinical validation of Nakagami imaging-based volumetric assessment of tumour response

4.1. Introduction

By contrast to conventional ultrasonic tumour sizing, the volumetric Nakagami imaging based technique developed in the previous chapter had shown promising results in detecting xenograft tumour tissue changes in response to chemotherapy. To ensure accurate assessment of liver tumours throughout a course of chemotherapy, a volumetric approach to the ultrasound assessment technique remains vital, and this is further discussed in this chapter. However, unlike subcutaneous xenograft tumours, which are more accessible to ultrasound imaging, liver tumours are comparatively more challenging to image, due to deeper location from the skin surface, limitation of imaging window, and tumour movement related to breathing during data acquisition. Further adaptations of the data acquisition and analysis techniques to accommodate liver tumours in the clinical setting were necessary, and the reliability of these adapted techniques were evaluated.

4.1.1. Clinical need for volumetric ultrasound assessment

Previous studies using Nakagami imaging have determined underlying tissue characteristics based on a single cross section through the tissue, normally through the largest cross sectional area, at a single time point [77, 128]. In order to detect changes in tumour tissue characteristics during chemotherapy, serial assessment has to be performed throughout the duration of treatment. If the single cross-section Nakagmi technique was employed to monitor tumour tissue characteristics, the same tumour cross-section would have to be imaged at each time point by the operator during the monitoring period. This is necessary to ensure any tumour heterogeneity is not erroneously interpreted as treatment-related tissue change. Since changes in tumour

volume do not follow a regular pattern, e.g. increase or decrease spherically, identifying the same tumour cross section at each time point during monitoring with concurrent changes in tumour volume would be challenging.

Since CT and MRI offer superior three-dimensional visualisation of tumours, the use of commercially available software to fuse the previously acquired CT or MRI with real-time ultrasound may assist operators in identifying the same tumour cross section at each time point. A previous study has reported an error of up to 11.53 ± 8.38mm in the spatial location of colorectal metastasis on CT compared to real time US following fusion [140]. It was also reported that the spatial location error reduced if the time interval between preceding CT and real time ultrasound was shorter, or when the registration procedure was performed with the patient under general anaesthesia in preparation for a procedure, e.g. thermal ablation. The authors attributed their findings to patient motion and respiratory excursion between the preceding CT and real time ultrasound. Besides spatial location error associated with CT/US fusion, cross sectional CT or MRI of tumours do not always coincide with patient visits when ultrasound imaging could be used for monitoring. As a result, although fusion software may assist operators in imaging the correct tumour cross section for monitoring, the CT or MRI used for fusion may have been acquired some time ago, increasing the potential for spatial location error as illustrated in the previous study.

The potential error and limitation of multimodality imaging fusion means the single cross-section Nakagami imaging technique cannot be reliably used to monitor tumour characteristic changes in response to chemotherapy. In order to accurately detect changes in tumour characteristic during chemotherapy, ultrasound data from the entire tumour volume needs to be acquired for analysis at each follow-up time point. By capturing data from the entire tumour volume, the analysis would be more

standardised with improved repeatability. Due to the limitation of current three dimensional ultrasound techniques, an alternative approach was developed to acquire volumetric ultrasound data.

4.1.2. Limitation of three-dimensional ultrasound techniques

The location of the liver, being partially shielded by the rib cage, limits the use of commercially available three-dimensional ultrasound techniques to acquire volumetric ultrasound data. The two types of commercially available techniques for three-dimensional ultrasound acquisition include mechanical sweeping or acquisition using a two-dimensional transducer array. The former involves mounting a conventional 2D transducer inside a housing with mechanical movement through a known trajectory, resulting in the acquisition of multiple conventional 2D scans covering a fixed 3D volume (**Figure 4-1a**). The alternative less mature technique involves acquisition using a 2D transducer array where the piezoelectric elements are arranged in a square or rectangular pattern (**Figure 4-1b**).

3D ultrasound transducers have larger enclosures (**Figure 4-2**), requiring a larger area of contact with the patient's skin surface at the time of imaging. With the rib cage overlying a large proportion of the liver (**Figure 4-3**), imaging in the intercostal space, i.e. between the ribs, may be necessary depending on the tumour's location within the liver, since the ribs act as a strong reflector of ultrasound, preventing its transmission into the body. The small distances of intercostal spaces are too small to accommodate 3D ultrasound transducers, precluding volumetric data acquisition with existing techniques. An alternative method using conventional 2D ultrasound transducers was therefore necessary for volumetric ultrasound acquisition of liver tumours to facilitate monitoring during chemotherapy.

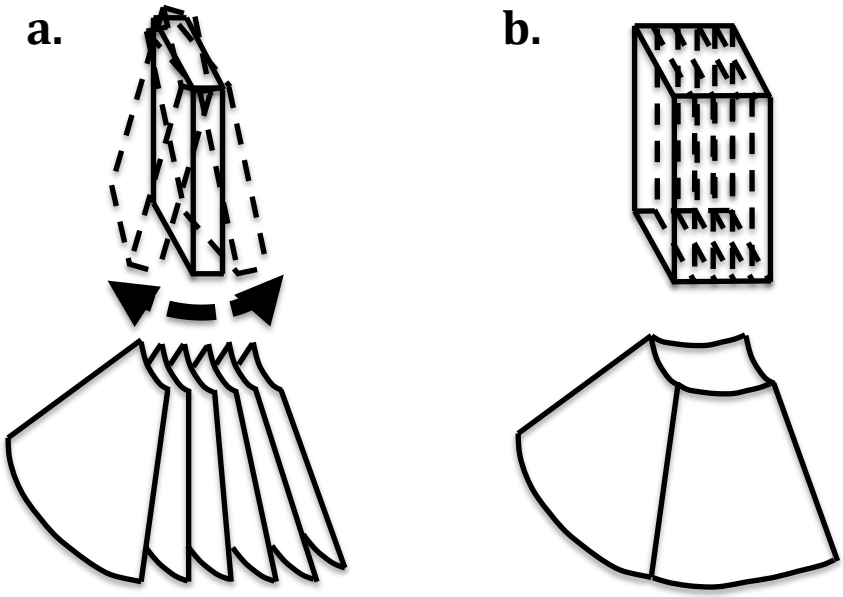

Figure 4-1: Diagram demonstrating commercially available 3D ultrasound techniques. a.) Mechanically swept transducer with acquisition of 2D images over a volume and b.) 2D transducer array stacked to create a square or rectangular array to acquire data over a pyramidal volume.

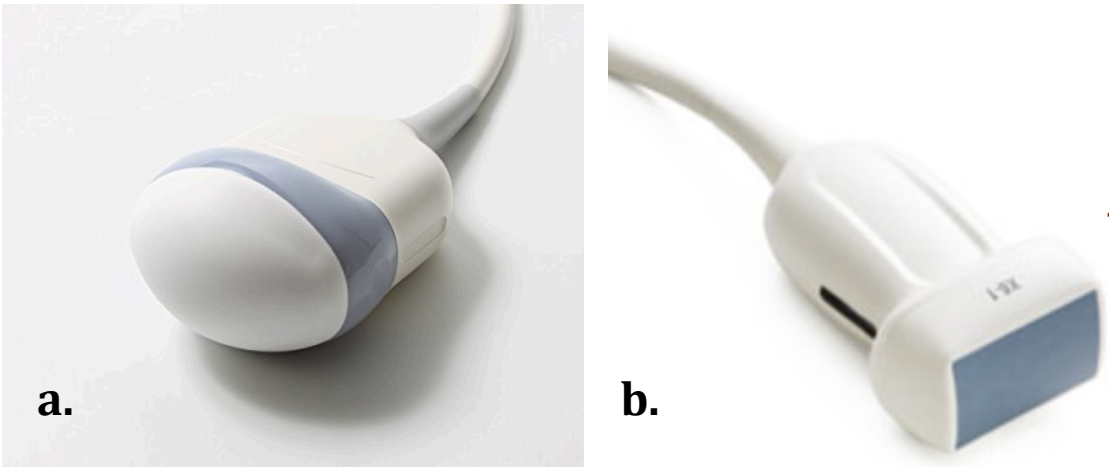

Figure 4-2: 3D ultrasound transducers. a.) General electric RAB4-8-RS 3D/4D convex ultrasound transducer, utilising the mechanical sweeping technique for 3D data acquisition. b.) Philips X6-1 PureWave xMatrix transducer with 3D acquisition using 2D transducer array.

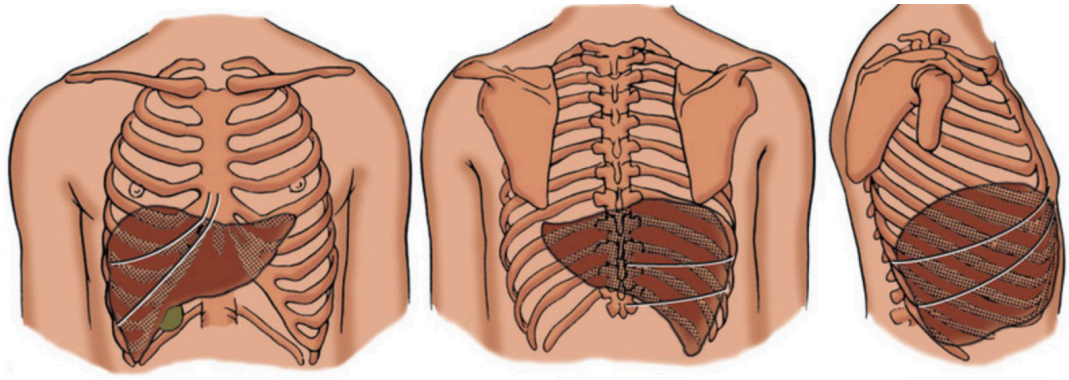

Figure 4-3: The relationship between the rib cage and liver (left to right) from anterior, posterior and lateral view. Image adapted from www.healthfixit.com.

4.1.3. Adapted freehand 3D ultrasound technique

A freehand 3D ultrasound protocol was developed to capture volumetric ultrasound data from liver tumours in order to compensate for the limitations of commercially available techniques. The term freehand 3D ultrasound is used to describe the acquisition of a sequence of 2D brightness mode (B-mode) ultrasound, which is combined into a volume dataset following post processing. Although research efforts have focused on reconstructing the volume dataset accurately by tracking the transducer's movement during scanning, this step is not necessary for the current application.

Based on the results from animal experiments detailed in chapter 3, the %PRR within the tumour volume is hypothesised to relate to changes in tumour tissue characteristics in response to chemotherapy and could therefore be used as an indicator of early response to treatment. Since the quantitative parameter being studied is the %PRR within the tumour volume, accurately reconstructing the imaged volume from the sequence of 2D B-mode images is not necessary. Instead, freehand 3D ultrasound of the target tumour may suffice to obtain volumetric ultrasound data from each time point during the monitoring period for analysis. The adapted method involves initial identification of the tumour target on 2D B-mode ultrasound. The

transducer is then angled to image either the most cranial or left lateral aspect of the tumour (**Figure 4-4**). Whilst the operator maintains stable contact with the patient's skin surface, the transducer is tilted towards either most caudal or right lateral aspect of the tumour in a smooth and steady sweeping motion (**Figure 4-4**). The imaging protocol results in a sequence of 2D cross sectional B-mode images through the tumour at various angles. Although the number of tumour cross sectional images will vary with each sweeping motion, due to variation in the smoothness and speeding of the sweeping action (**Figure 4-5**), provided the analysis is based upon all available images in the sequence containing the tumour, the %PRR within the tumour volume should be unaffected. In order to prevent any liver tumour movement secondary to breathing relation distortion of the liver, patients were asked to hold their breath during transducer sweeping and data acquisition.

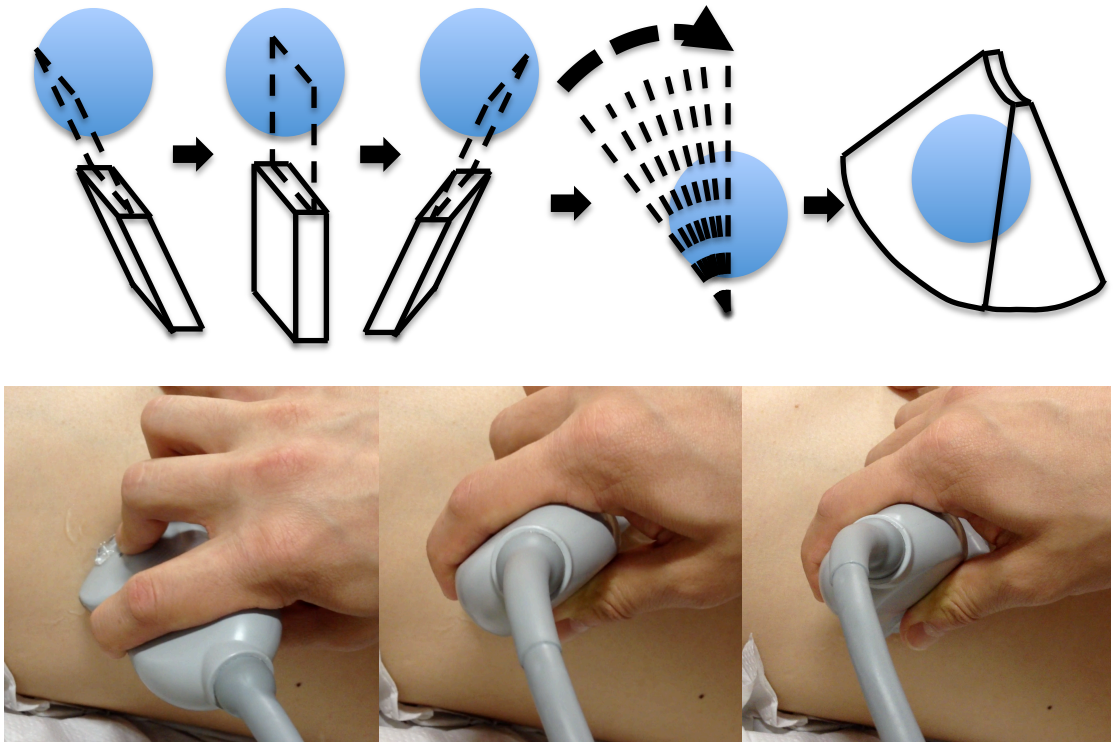

Figure 4-4: Diagram and photographs demonstrating the adapted freehand 3D ultrasound technique. Diagram in the top row illustrating the tumour being imaged in cross section at multiple angles as the transducer is swept. Photograph in the bottom row demonstrating the sweeping motion of the transducer as skin contact is maintained.

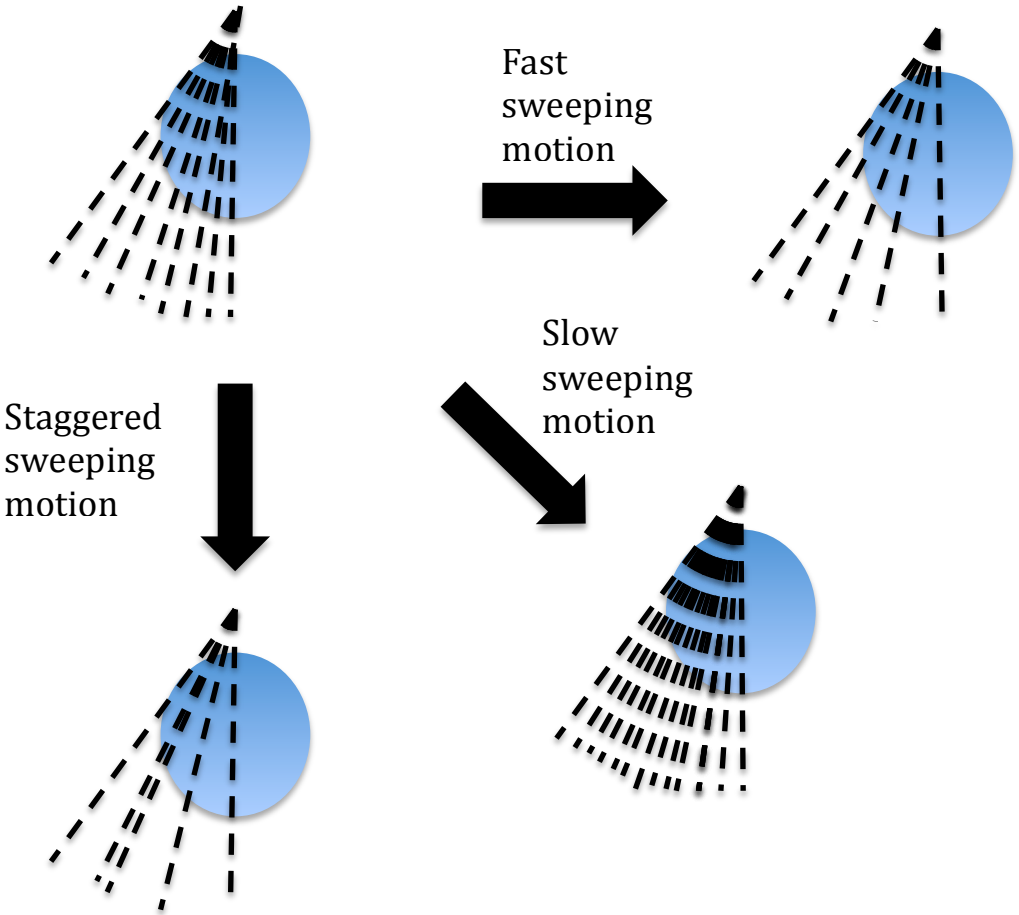

Figure 4-5: Diagram illustrating the effect of B-mode images sequence with variation in sweeping motion.

4.2. Gap in knowledge

The analysis of volumetric ultrasound data from the entire tumour volume is likely to offer the most accurate method to detect chemotherapy-related tumour tissue changes. An adapted freehand 3D ultrasound technique is developed to overcome the limitations of commercially available techniques to capture volumetric ultrasound data from liver tumours. This technique in combination with the adapted Nakagami imaging based technique developed in earlier animal experiments may facilitate the detection of chemotherapy-related tumour tissue changes to indicate response to treatment.

4.3. Aims

- To determine if the %PRR obtained from the analysis of freehand 3D ultrasound datasets with the adapted Nakagami imaging based technique can detect tissue changes in responding and non-responding tumours.
- To determine if the %PRR with the tumour volume correlates with axial dimension of the tumour.
- To determine if interval change in the %PRR within the tumour volume from baseline differs between responding and non-responding tumours.
- To assess the reliability of %PRR within the tumour volume calculated from analysis of datasets obtained from repeated freehand 3D ultrasound, as well as freehand 3D ultrasound datasets obtained from different imaging angles.

4.4. Materials and methods

4.4.1. Regulatory approval

A prospective observation study was set up to investigate the aims of this chapter. Ethical approval was granted by the National Research Ethics Service South Central-Oxford A Research Ethic Committee (Reference no: 12/SC/0279). The University of Oxford Research and Development department provided sponsorship for the study.

4.4.2. Recruitment Criteria

Patients diagnosed with liver metastases from any solid organ primary tumour, either on the basis of biopsy or imaging appearances, due to undergo chemotherapy at the Oxford Cancer and Haematology Centre at the Churchill hospital site of the Oxford University Hospitals NHS Trust were recruited. Subjects had to comply with the study protocol and follow up imaging schedule in order to participate. It was made clear on the patient information sheet that the patient will not be able to take further part in the study if a suitable liver tumour could not be identified following an initial ultrasound study (Further details in section 4.4.4.).

4.4.3. Patient recruitment and enrolment

Written referrals are made to the chemotherapy day unit outlining the proposed course of chemotherapy following decision by the respective cancer type specific multidisciplinary team meetings. Potential participants were identified from their oncologist's referrals to the treatment unit. Following confirmation of their diagnosis from pathology reports and prior imaging, patient information sheets (Appendix A) detailing the research procedure, including potential risks and benefits, were sent to suitable patients accompanying their appointment letters for their first treatment visit. In order to prevent any additional hospital visit resulting from patient participation,

those undergoing chemotherapy requiring multiple hospital attendances were particularly targeted for recruitment.

Patients were given at least 24 hours to consider the information and were telephoned to establish their wish to participate. Patients who agreed were asked to attend for a scan appointment an hour prior to their scheduled treatment. During this scan appointment, written consent was obtained prior to commencement of study ultrasound scans outlined in the protocol. It was made clear at this appointment that patients were free to withdraw from the study at any time and any data collected up to that point was used in the analyses.

4.4.4. Initial B-mode ultrasound assessment

After obtaining written information consent from the patient, a B-mode ultrasound study was performed of the whole liver to identify suitable tumour(s) for assessment. A suitable tumour in the current context was defined as one that is easily identifiable on B-mode ultrasound, and close to a stable anatomical location for ease of repeat scanning at subsequent time points during the monitoring period. If a suitable tumour could not be identified, resulting in the potential for poor repeatability, the patient was informed and withdrawn from the remainder of the study. Details of this initial ultrasound assessment were made clear on the patient information sheet, and patients were informed that the failure to identify a suitable tumour for assessment is due to the limitations of the imaging technique with no implication on their diagnosis or subsequent treatment.

4.4.5. Ultrasound study schedule

Following initial identification of a suitable liver tumour for monitoring, volumetric ultrasound dataset of the tumour will be captured using the technique described earlier

(Further details in section 4.1.3.). At the end of the patient's treatment visit, the ultrasound study was repeated once again with the aim of detecting any immediate changes to the tumour tissue characteristics.

This ultrasound scan schedule is then repeated during the patient's next scheduled treatment appointment to detect any early changes to tumour tissue characteristics.

Further ultrasound scans were repeated to coincide with subsequent patient visits for routine diagnostic imaging to assess their response to the chemotherapy, usually performed half way through and at the end of the chemotherapy course. During these visits, ultrasound scans were only performed on a single occasion either before or after the diagnostic imaging. These later ultrasound scans facilitated detection of late changes in tumour tissue in response to chemotherapy. Concurrent routine imaging also allowed correlation between ultrasound and routine diagnostic imaging findings.

4.4.6. Ultrasound imaging technique

Ultrasound data was acquired using a diagnostic ultrasound system (Z.one, Zonare Medical Systems, Mountain View, CA, USA) with a 4 MHz curvilinear transducer (Zonare C6-2 curved array probe). The transducer beam was directed through the target liver tumour in the intercostal, subcostal or longitudinal plane, based upon the optimal acoustic window for visualisation as determined at the time of initial B-mode ultrasound assessment. The same imaging window was then used for all subsequent follow up studies.

Volumetric 3D ultrasound scans of liver tumours were acquired using the freehand sweeping motion described earlier. Using a smooth movement and constant speed, the transducer was angled whilst maintaining a stable skin contact position to capture sequential 2D cross-sectional images of the target liver tumour, subsequently used to construct the 3D data set for analysis.

During each scheduled protocol ultrasound scan, freehand 3D ultrasound of the target liver tumour was repeated at least three times for assessment of reliability. In patients where the target tumour could be visualised from different imaging windows, volumetric datasets were collected from different imaging windows to assess the effect of scanning angle on the reliability of the data.

4.4.7. Ultrasound data analysis

The image analysis method described in this section was carried out in collaboration with Dr. Omar Al-Kadi and Dr. Amalia Cifor. Their contribution to the development of the software for automated image analysis was instrumental to the success of these experiments

Manual segmentation of the target liver tumour was performed on sequential 2D cross sectional images obtained from the freehand 3D ultrasound datasets. Similar to the prior animal experiment, it was challenging to ensure accurate segmentation of the small parts of the tumour without erroneous inclusion of normal tissue, owing to image artefacts, as well as the often ill-defined borders of tumours. In order to prevent inaccurate analysis, a similar elimination step was performed with removal from analysis of tumour cross sectional images with area less than the median area of all cross sectional images from the same volume dataset.

Following the elimination step, the remaining cross sectional images for each volumetric ultrasound datasets were subjected to the analysis using the Nakagami imaging based volumetric assessment technique developed in the previous animal experiment. A mean %PRR was obtained for each tumour at each ultrasound time point. Interval change in this quantitative parameter during the course of chemotherapy was correlated against change in tumour size at the end of the chemotherapy course compared to baseline as determined on routine clinical imaging

with CT or MRI, using the Response Evaluation Criteria in Solid Tumour (RECIST 1.1) [48]. For the purpose of the current study, tumour that responded to treatment were those that completely resolved or demonstrate reduction in axial diameter of >30% from baseline. Tumours that were classed as unresponsive to treatment if their axial diameter remained unchanged or increased by >20%.

4.4.8. Reliability of percentage of pre-Rayleigh regions obtained with freehand 3D ultrasound

The intra-observer variability of the %PRR obtained from each tumour at each monitoring time point was evaluated using intra-class correlation coefficients. Datasets obtained from patients with target tumours visible from different imaging window were evaluated for intra-observer variability using intra-class correlation coefficient. This evaluation will provide an assessment into the effect of imaging angle on the %PRR within the tumour volume.

4.4.9. Statistical analysis

Interval change in %PRR from baseline was considered as parametric data and different response groups were compared using the Student independent-sample t test. A P value of 0.05 or lower was considered significant. Intra-class correlation coefficient was used to assess intra-observer reliability of %PRR obtained from the adapted freehand 3D ultrasound sweeps. Data were analysed using commercially available statistical software (version 20.0; SPSS, Chicago, Illinois).

4.5. Results

4.5.1. Patient demographics

Patient enrolment occurred between October 2012 and June 2014. During this period 21 patients were recruited. 16 male and 5 female with a mean age of 64 years (range 29-84 years). Two patients had liver tumours that were not visible on initial B-mode ultrasound assessment. Eight patients, 2 female and 6 male with mean age of 57.9 years, completed the full schedule of ultrasound scans throughout their course of chemotherapy (Table 4-1) with a mean follow up duration of 118.6 ± 45.8 days. Five patients did not complete the full course of chemotherapy due to disease progression on chemotherapy. One patient withdrew from the study after the baseline study. Six patient's datasets could not be analysed due to difficult segmentation owing to poorly visible tumour.

Patient number	Age	Sex	Primary tumour site	Chemotherapy regime	Response on routine imaging
0	69	F	Colorectal	Capecitabine and Oxaliplatin	PR
1	43	M	Pancreas	Streptozocin	SD
5	79	M	Colorectal	Capecitabine and Oxaliplatin	PR
7	73	M	Colorectal	Capecitabine and Oxaliplatin	SD
9	29	M	Colorectal	Capecitabine and Oxaliplatin	PR
10	67	F	Cholangiocarcinoma	Gemcitabine and cisplatin	PD
14	44	M	Small cell lung cancer	Cisplatin and Etoposide	PD
17	61	M	Lung	Gemcitabine and Cisplatin	PR

Table 4-1: Patients who completed all scheduled ultrasound scans

Nine liver tumours from the eight patients who completed all the scheduled ultrasound scans were analysed. These consisted of four secondary tumours from

colorectal cancer, three from lung cancer, 1 each from pancreatic cancer and cholangiocarcinoma. The response of these tumours as determined on routine clinical imaging were partial response in five, stable disease in two and progressive disease in two. The tumours that showed stable or progressive disease were classified as non-responders in the subsequent analysis.

Data from patients who did not complete the full complement of scheduled ultrasound scans were used where possible to assess the intra-observer variability for freehand 3D ultrasound.

4.5.2. Correlation of percentage of pre-Rayleigh regions with tumour response to chemotherapy

The mean number of tumour cross sectional images per freehand 3D ultrasound sweep of the target liver tumour was 20.6. Following manual segmentation and automated analysis, the mean %PRR within the tumour volume from at least three freehand ultrasound sweeps was calculated for each scheduled ultrasound time point. Interval increase in %PRR regions was demonstrated in liver tumours that responded to chemotherapy during the monitoring period (**Figure 4-6**). The %PRR remained stable or decreased in tumours that did not respond to chemotherapy (**Figure 4-7**).

Comparison of ultrasound datasets collected pre and post treatment appointments demonstrated no significant difference in the %PRR within the tumour volume ($p=0.612$). This finding may be attributed to the lack of significant change in tumour tissue characteristics immediately post treatment. Alternatively, the degree of tumour tissue changes immediate post treatment was below the limit that can be detected with the ultrasound technique. Since significant changes in tumour tissue immediately post treatment was thought to be unlikely, results from datasets collected during the same treatment visit were combined for the subsequent analysis.

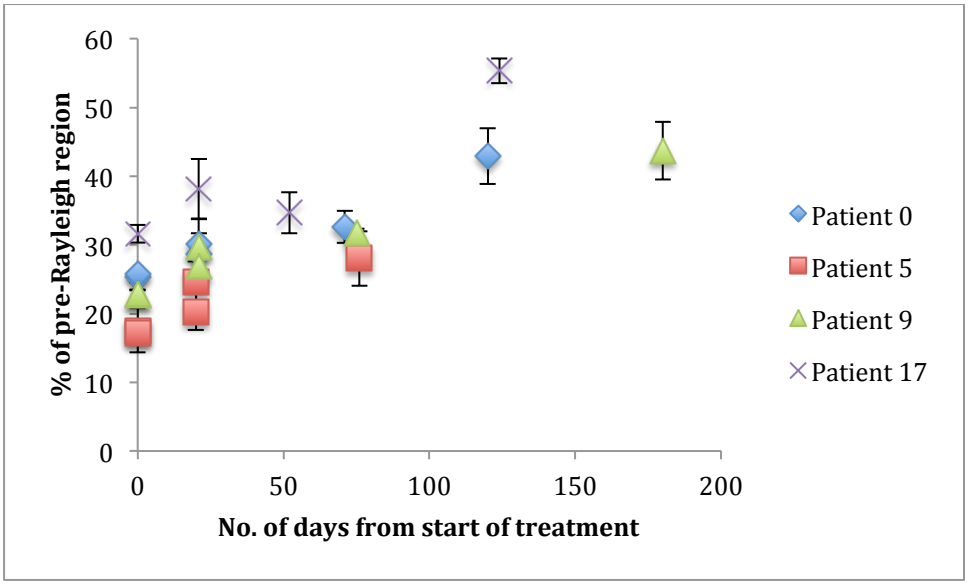

Figure 4-6: Graph showing the mean and standard deviation of the %PRR in the tumour volume plotted against the number of days from the start of treatment for tumours that demonstrated response to treatment on routine clinical imaging.

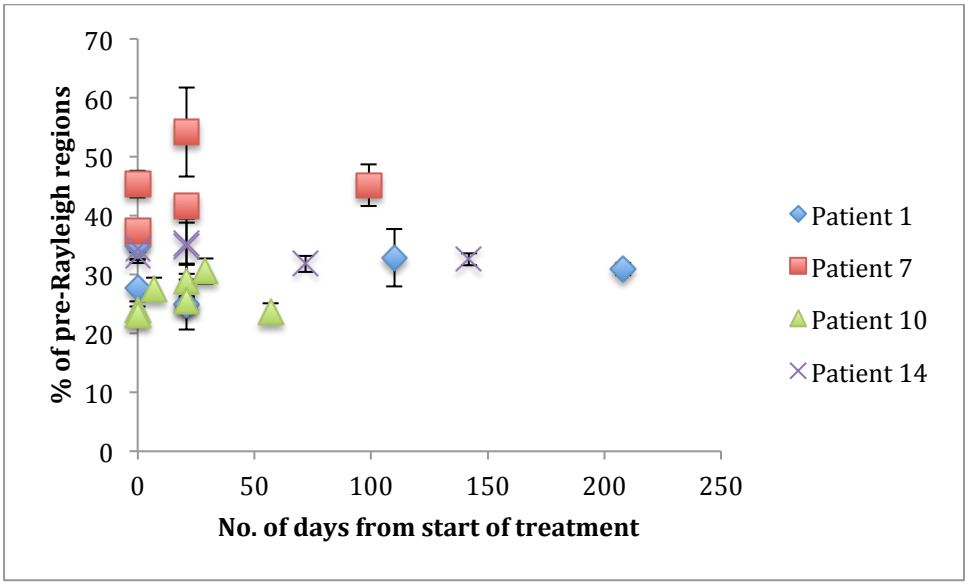

Figure 4-7: Graph showing the mean and standard deviation of the %PRR regions in the tumour volume plotted against the number of days from the start of treatment for tumours that demonstrated no response to treatment on routine clinical imaging.

Despite the observed difference between responders and non-responders, the actual %PRR appeared to cluster around the 20 – 50% throughout treatment with no significant changes. Since a correlation between the %PRR and tumour volume was demonstrated in the animal experiments described in Chapter 3, the clinical data was

re-analysed to see if a similar correlation exist between %PRR and the tumour axial dimension.

4.5.3. Correlation of percentage of pre-Rayleigh regions with axial dimension of tumour

A direct inverse relationship was demonstrated with reduction in the %PRR within a tumour volume as the axial diameter of tumour on CT increases (**Figure 4-8**). This replicates the relationship previously observed during the earlier animal experiment detailed in Chapter 3. In view of this observed correlation, this provided reassurance that despite the small changes in %PRR observed in tumours that responded to chemotherapy, the %PRR remains a possible indicator of response to treatment. This hypothesis was further examined by comparing the interval change in %PRR at different time points during the chemotherapy course between responding and non-responding tumours.

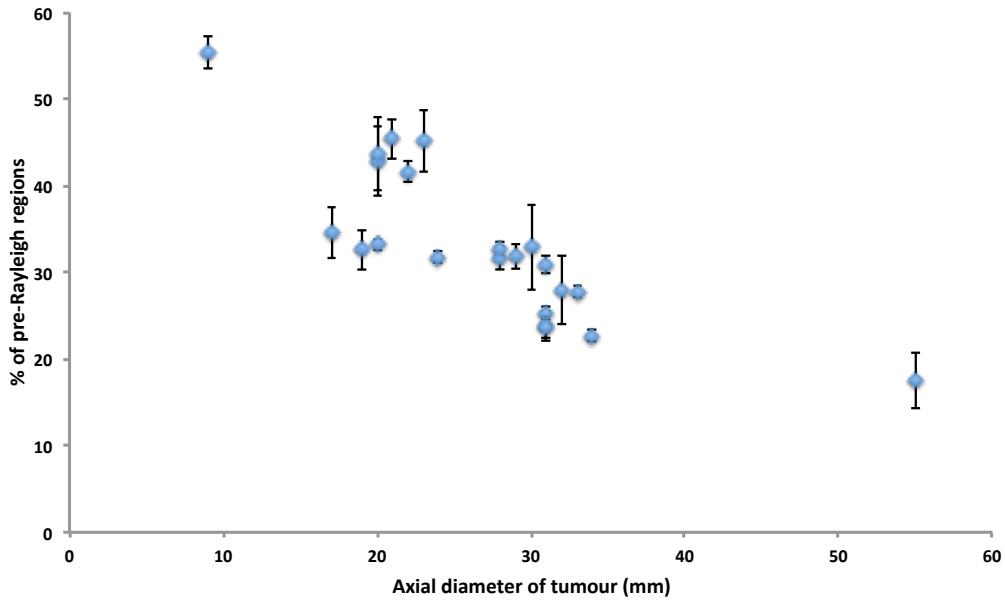

Figure 4-8: Graph showing the mean and standard deviation of the %PRR in the tumour volume plotted against the axial diameter of tumour on CT.

4.5.4. Interval change in the percentage of pre-Rayleigh regions from baseline between responders and non-responders

Datasets of all tumours that responded and those that did not respond to chemotherapy were combined into their respective groups. Interval changes in the %PRR from baseline at the different time point during monitoring for all tumours were calculated and compared between responders and non-responders. The increase in %PRR at halfway through and at completion of the chemotherapy compared to baseline were significantly higher in tumours that responded to chemotherapy, p= 0.047 and p=<0.001 respectively (**Figure 4-9**). On the other hand, interval increases in the %PRR at the second treatment visit compared to baseline was not significantly different between responders and non-responders (p=0.71).

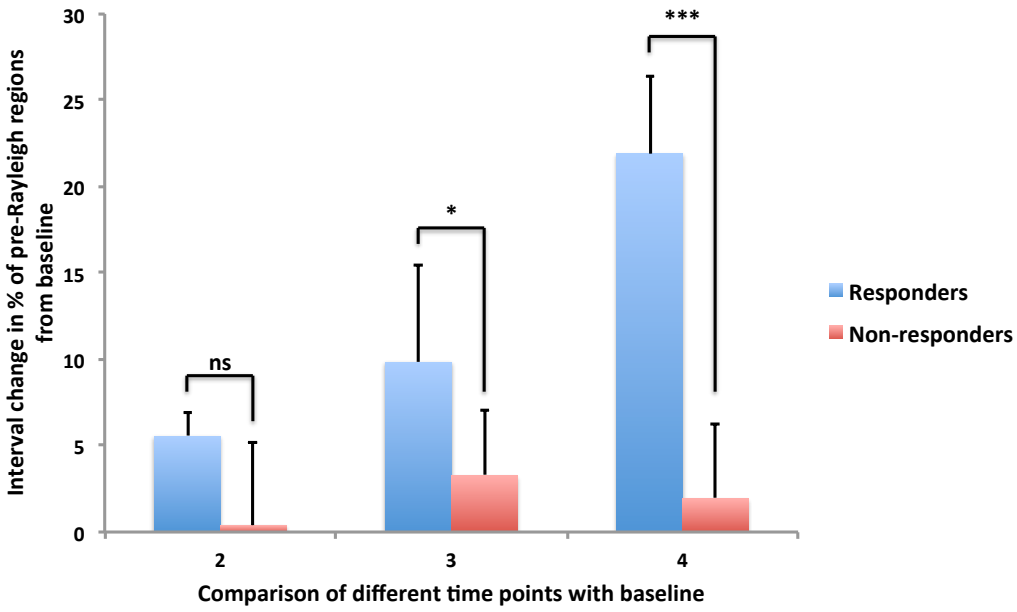

Figure 4-9: Graph showing the mean and standard deviation of the interval change in the %PRR in the tumour volume between responders and non-responders when compared to the baseline at different time points. Time points: 2= pre and post 2nd hospital visit for chemotherapy, 3= pre or post routine imaging halfway through chemotherapy course, 4= pre or post routine imaging at completion of chemotherapy course. * and * represents p-value of <0.05 and 0.001 respectively.**

4.5.5. Reliability of percentage of pre-Rayleigh regions obtained with freehand 3D ultrasound

The intra-rater reliability to obtain the same %PRR within the tumour volume using different freehand 3D ultrasound sweeps during the same follow up time point was calculated using datasets from 82 different time points when at least three freehand 3D ultrasound datasets from different sweeps were analysed from the same target tumour. There was excellent intra-rater reliability with intra-class correlation coefficient of 0.969, and 95% confidence interval of 0.955-0.979.

The reliability of obtaining the same %PRR within the tumour volume using datasets from different angles was calculated using data from 16 different mean %PRR calculated from freehand 3D ultrasound datasets obtained from the same target tumour using two different imaging windows. The analysis confirms good reliability with intra-class correlation coefficient of 0.857, and 95% confidence interval of 0.457-0.955. The wide 95% confidence interval range suggests the level of reliability ranges from fair to excellent.

4.6. Discussion

The adapted freehand 3D ultrasound developed in this chapter facilitated the collection of volumetric ultrasound dataset at multiple time points during a course of chemotherapy. The technique was not limited by the tumour's location within the liver or the imaging window necessary for visualisation, thus overcoming the potential limitations of commercially available 3D ultrasound techniques.

Analysis of these clinical volumetric datasets confirmed the validity of the adapted Nakagami imaging based technique developed in the earlier animal experiment. The %PRR within the tumour volume increased during the course of chemotherapy in tumours that responded to treatment (**Figure 4-6**). Conversely, in tumours that did not respond to treatment, the %PRR was stable or decreased (**Figure 4-7**). Despite only small changes in %PRR in tumours that responded to treatment, this observation was confirmed on further analysis, demonstrating an indirect correlation between %PRR within the tumour volume and axial diameter on CT (**Figure 4-8**). This finding is analogous to the correlation seen in our previous animal study with the same indirect correlation between the tumour volume and the %PRR within a tumour volume (**Figure 3-12**). The observations from animal and clinical datasets suggest the %PRR within a tumour volume is a quantitative parameter of tumour tissue characteristics that change as the tumour size changes.

These findings were supported by significantly greater interval increase in the mean %PRR within the tumour volume of responding tumours from baseline when results from responding and non-responding tumours were pooled for analysis. However, statistically significant difference in this interval increase from baseline was only seen with datasets at or after halfway through the course of chemotherapy. When datasets collected immediate following the first treatment appointment, and those collected at

the second treatment visit were compared with the baseline, there were no statistical significant difference in the interval increase in mean %PRR from baseline between responding and non-responding tumours. Based on the results, interval increase in the %PRR within a tumour volume from baseline appears to be significantly higher in tumours that respond to treatment (**Figure 4-9**). This observation was however only apparent after halfway through the chemotherapy course, while datasets analysed from earlier time point did not provide similar results. Nevertheless, it is important to note that the protocol ultrasound schedule for the current observational study did not include any ultrasound scans between the second treatment appointment and the patient's next attended for routine clinical follow up imaging. This time interval ranged from 31-89 days, and more frequent monitoring with additional ultrasound scans during this time period may identify an earlier time point when interval increase in %PRR is significant different between responding and non-responding tumours, thus providing a mean of identifying tumour responding to treatment prior to routine follow up imaging.

This quantitative parameter derived from ultrasound datasets therefore offers an alternative measurement of tumour development beyond size of the tumour obtained from routine clinical imaging. The histological basis of this finding remains unconfirmed based on the current results; however, the interval increase in the %PRR amongst responding tumour volume may represent changes in scatterer's arrangement. As tumour size reduces in response to treatment, the chaotic vasculature and the disorganised extracellular support network may normalise, resulting in scatterer arrangements moving from post-Rayleigh towards pre-Rayleigh distribution.

The ability of the adapted freehand 3D ultrasound technique to reliably produce this quantitative parameter on repeated sweeps was found to have excellent intra-observer

reliability. Although similar level of reliability was also seen when comparing datasets obtained from different imaging windows, this was found to have a wide 95% confidence interval, reducing to only fair reliability in some cases thus scanning in the same imaging window will be necessary for increased accuracy. Although, there is high intra-observer reliability, it will be necessary to also determine the inter-observer reliability prior to wider application of this technique for tumour response monitoring.

The inclusion in this study of different types of secondary liver tumours undergoing different chemotherapy regimens may affect the validity of our observations. Our results may be inaccurate due to possible differences in scatterer density and arrangement between tumours with different histology. Additionally, tumour response to different chemotherapy regimens may result in different changes to the scatterer density or arrangement within the tumour. Since the analysis method requires direct internal comparison on a tumour-by-tumour basis, rather than against an external reference standard, the heterogeneity in tumour histology and treatment is unlikely to influence the results. Therefore, the analysis technique has the potential to monitor response to treatment in a variety of liver tumours treated with different chemotherapy regimes.

The number of patients that completed the entire schedule of protocol scans was low compared to the overall patient enrolment (8/21), owing to patient factors including withdrawal of treatment due to disease progression, as well as withdrawal of consent. A large number of datasets were also not analysable due to difficulty in segmentation of the target tumour due to image artefact or the quality of imaging secondary to tumour location. It is envisaged that this barrier may be overcome in the future with further development in automated segmentation technique using features, such as the

radiofrequency data [141], bypassing subjectivity of manual segmentation. The development of automated segmentation techniques may also increase the practical application of this technique, since manual segmentation of individual cross sectional images is necessary prior to automated analysis. Future work to understand the histological changes underpinning the observed changes in %PRR within tumours volumes in response to treatment is perhaps also necessary prior to broader clinical adoption of this technique. Finally as only a single liver tumour is monitored owing to the current time consuming nature of the technique and the analysis, response in this tumour to chemotherapy may not be indicative of disease response to treatment elsewhere in the patient. Testing of this monitoring technique in tumours, accessible by ultrasound imaging, elsewhere in the body may allow the response of multiple tissue sites to chemotherapy to be monitored simultaneously, thus providing a broader understanding of the patient's overall response to treatment.

4.7. Summary

Despite analysis of a restricted number of complete datasets with the full complement of scheduled protocol freehand 3D ultrasound scans, the %PRR within the tumour volume was found to increase in tumours that responded to chemotherapy. The analysis also corroborate previous animal experiment findings, demonstrating the potential of the adapted Nakagami imaging based volumetric assessment to detect tissue changes as the tumour size changes in response to chemotherapy. This trend was further confirmed with significantly greater increase in the %PRR from baseline in responding tumour compared to non-responding tumours. Excellent intra-observer reliability to reproduce this novel quantitative ultrasound parameter from freehand 3D ultrasound datasets provided further evidence of its potential to be translated into clinical use.

CHAPTER 5

CONCLUSIONS AND FUTURE WORK

5. Conclusions and future work

The ability to detect early response of liver tumour to chemotherapy could conver significant benefits to patient care. Treatment success could be confirmed much earlier than can be achieved currently, providing patients with reassurance. For patients who are found to be unresponsive to treatment, ineffective treatments can be terminated early to avoid unnecessary side effects, enabling earlier switching to alternative therapies with a greater chance of success.

The main objective of this thesis was twofold: firstly, to investigate whether fractal analysis of contrast-enhanced CT images of colorectal liver metastases could be used as to detect early treatment response; secondly, to develop a novel Nakagami imaging-based technique capable of detecting early liver tumour response to chemotherapy by analysing back-scattered ultrasound signals, which are routinely acquired during conventional B-mode ultrasound scanning.

In chapter 1, the burden of liver cancer was discussed, followed by a brief overview of the mechanisms of chemotherapy as well as their side effect. This was followed by an extensive review of the current and novel imaging techniques that can quantitatively assess different pathophysiology of tumours to detect interval changes that can determine tumour response to treatment. The literature review identified a number of CT and US based techniques not previous investigated for their potential in detecting early response of liver tumour to chemotherapy. In the case of CT, fractal analysis demonstrated promise in detecting treatment response by assessing CT image texture, a marker of tumour heterogeneity. Since it can be directly applied to the existing

CT-scanning regimen without the need for additional cost or patient exposure to ionizing radiation, this was an attractive technique for further investigation and was subsequently explored in greater detail in Chapter 2.

Additionally, ultrasound, which is easy to perform, relatively low-cost, with no radiation risk, was found to be underexplored as a tool for assessing tumour response to treatment. Leaving aside dynamic contrast enhanced US with drawbacks including the need for intravenous access and cost associated with contrast, tumour texture analysis using US backscattered signal was explored as a potential indicator of treatment response. The technique was investigated further using ultrasound datasets from animal and clinical studies in Chapters 3, and 4 respectively.

The concept of CT texture analysis was introduced in Chapter 2, including the theories supporting its use in quantifying tumour heterogeneity. This was supported by a review of studies confirming its ability to detect changes in tumour, as well as its potential as a method to detect early liver tumour response to chemotherapy. Fractal analysis was then applied to contrast enhanced CT images of colorectal liver metastases at baseline, prior to commencement of conventional cytotoxic chemotherapy and at first follow up. The interval changes in mean FD were not found to correlate with the final tumour response to treatment at the end of chemotherapy. However, mean FD was found to be unaffected by the tumour size, the degree of tumour necrosis or the presence of chemotherapy. These findings confirm the mean FD of liver tumours as a potential reliable biomarker to detect changes in tumour tissue resulting from chemotherapy. Although not successfully validated in the current setting, future work may involve investigating fractal analysis of different types of liver tumour

treated with anti-angiogenic therapy. Its application may alternatively be tested in colorectal liver metastasis treated with anti-angiogenic. This suggestion stems from the proposal of previous study authors, suggesting FD might in fact be a marker of tumour angiogenesis, or normalisation of vasculature owing to the presumed fractal geometry of vascular growth and development.

Using a mouse xenograft tumour model that underwent treatment as part of an on-going investigation of high-intensity focus ultrasound mediated release of chemotherapy from thermosensitive liposomes, backscattered ultrasound RF signals were used to develop a Nakagami-imaging based volumetric tissue assessment technique. The Nakagami-imaging based technique was found to be unaffected by the presence of chemotherapy, namely doxorubicin in this case, further confirming its ability to detect true tissue changes in response to treatment. Although the response of the xenograft tumours to different treatment protocols were not consistent with our prediction, with no definite response to treatment in any of the treatment groups, a correlation was found between the tumour volume and the percentage of pre-Rayleigh regions (%PRR) within the tumour volume. Based on this finding, it was hypothesised that the %PRR regions may provide an indicator of tumour internal architecture, which is directly dependent on the stage of development of the tumour and therefore tumour size. The parameter was therefore found to hold considerable promise for detection of early tumour changes in response to chemotherapy.

Building on the findings of the animal study, a prospective observation study was set up in order to apply the Nakagami-imaging based technique for tissue volume assessment to patients with liver metastases treated with chemotherapy. To ensure ultrasound data was collected from the entire tumour volume for

analysis, thus reducing erroneous measurement secondly to selection bias associated with single cross-section analysis, a freehand 3D ultrasound technique was developed. Similar to the findings in the prior animal study, analysis of the ultrasound dataset from the whole tumour volume demonstrated a correlation between the %PRR in the tumour volume and the axial dimension of the tumour. Interval changes in the %PRR at follow up imaging compared to baseline was found to be significantly different between responding and non-responding tumours ($p=0.047$, between baseline and first follow up imaging and $p= <0.001$, when comparing interval changes from baseline to end of treatment). The %PRR obtained with datasets from different freehand 3D ultrasound sweeps acquiring during the same scanning session was found to have excellent intra-observer reproducibility with intra-class correlation coefficient of 0.969.

Based on the result of the clinical study, interval change in the %PRR within the tumour volume from baseline is a promising quantitative method of detecting tumour tissue changes in response to treatment. This finding, though significant, was identified from a small dataset owing to the limited number of patients completing the full schedule of protocol ultrasound. Our analysis confirmed the difference in interval change from baseline in %PRR within responding and non-responding tumour reached statistical significance after half the chemotherapy course had been completed. It is possible that this difference between responding and non-responding tumours could be detected at an earlier time point. However, this could not be validated based on analysis of the available dataset. Future studies could be designed to address this question by performing more frequent ultrasound scanning during the early part of the chemotherapy course, however this needs to be balanced against inconvenience to participants

associated with frequent scanning. Prior to wider clinical use, there are additional areas that require future investigation. Firstly, correlation of %PRR within the tumour volume with histological changes of the tumour should be performed, potentially with the use surgically resected specimens following neoadjuvant therapy. Attributing a histological basis to changes in %PRR would provide further supportive evidence for its clinical use and potentially extend the use of this quantitative parameter to other areas of tissue characterisation. Since this is an ultrasound derived quantitative parameter, it will also be interesting to correlate the %PRR within the tumour volume with other characteristics that can be assessed with ultrasound techniques including vascularity and perfusion with dceUS, and stiffness with ultrasound elastography. Although intra-observer reproducibility has been confirmed, inter-observer reproducibility also needs to be assessed prior to translation into clinical practice, since the same operator may not be available to perform serial studies for response. Currently, manual segmentation is necessary prior to automated analysis; development of ultrasound tumour segmentation techniques will permit more rapid tumour assessment, with the aim of bypassing the need for image post processing offline with parameters being made available at the time of image acquisition.

REFERENCES

References

1. Liver cancer incidence statistics- Cancer Research UK. In, 2015
2. Torre LA, Bray F, Siegel RL, Ferlay J, Lortet‐Tieulent J, Jemal A. Global cancer statistics, 2012. *CA Cancer J Clin* 2015; 65:87-108
3. Taylor-Robinson SD, Foster GR, Arora S, Hargreaves S, Thomas HC. Increase in primary liver cancer in the UK, 1979–94. *The Lancet* 1997; 350:1142-1143
4. El-Serag HB, Mason AC. Rising incidence of hepatocellular carcinoma in the United States. *N Engl J Med* 1999; 340:745-750
5. El-Serag HB, Mason AC. Risk factors for the rising rates of primary liver cancer in the United States. *Arch Intern Med* 2000; 160:3227-3230
6. Davila J, Morgan R, Shaib Y, McGlynn K, El-Serag H. Diabetes increases the risk of hepatocellular carcinoma in the United States: a population based case control study. *Gut* 2005; 54:533-539
7. Cancer incidence for common cancers- Cancer Research UK. In, 2015
8. Hoe A, Royle G, Taylor I. Breast liver metastases—incidence, diagnosis and outcome. *J R Soc Med* 1991; 84:714-716
9. Steele Jr G, Ravikumar T. Resection of hepatic metastases from colorectal cancer. Biologic perspective. *Ann Surg* 1989; 210:127
10. Llovet JM, Fuster J, Bruix J. Intention‐to‐treat analysis of surgical treatment for early hepatocellular carcinoma: Resection versus transplantation. *Hepatology* 1999; 30:1434-1440
11. Hoffmann K, Bulut S, Tekbas A, Hinz U, Büchler MW, Schemmer P. Is Hepatic Resection for Non-colorectal, Non-neuroendocrine Liver Metastases Justified? *Ann Surg Oncol* 2015:1-10
12. Dittmar Y, Altendorf-Hofmann A, Schüle S, et al. Liver resection in selected patients with metastatic breast cancer: a single-centre analysis and review of literature. *J Cancer Res Clin Oncol* 2013; 139:1317-1325
13. Fong Y, Fortner J, Sun RL, Brennan MF, Blumgart LH. Clinical score for predicting recurrence after hepatic resection for metastatic colorectal cancer: analysis of 1001 consecutive cases. *Ann Surg* 1999; 230:309
14. Mayo SC, de Jong MC, Pulitano C, et al. Surgical management of hepatic neuroendocrine tumor metastasis: results from an international multi-institutional analysis. *Ann Surg Oncol* 2010; 17:3129-3136
15. Bismuth H, Adam R, Lévi F, et al. Resection of nonresectable liver metastases from colorectal cancer after neoadjuvant chemotherapy. *Ann Surg* 1996; 224:509
16. Doci R, Gennari L, Bignami P, Montalto F, Morabito A, Bozzetti F. One hundred patients with hepatic metastases from colorectal cancer treated by resection: analysis of prognostic determinants. *Br J Surg* 1991; 78:797-801
17. Adam R, Avisar E, Ariche A, et al. Five-year survival following hepatic resection after neoadjuvant therapy for nonresectable colorectal [liver] metastases. *Ann Surg Oncol* 2001; 8:347-353

18. Adam R, Delvart V, Pascal G, et al. Rescue surgery for unresectable colorectal liver metastases downstaged by chemotherapy: a model to predict long-term survival. *Ann Surg* 2004; 240:644
19. Livraghi T, Meloni F, Di Stasi M, et al. Sustained complete response and complications rates after radiofrequency ablation of very early hepatocellular carcinoma in cirrhosis: is resection still the treatment of choice? *Hepatology* 2008; 47:82-89
20. Lencioni R, Cioni D, Crocetti L, et al. Early-stage hepatocellular carcinoma in patients with cirrhosis: long-term results of percutaneous image-guided radiofrequency ablation. *Radiology* 2005; 234:961-967
21. Solbiati L, Ahmed M, Cova L, Ierace T, Brioschi M, Goldberg SN. Small liver colorectal metastases treated with percutaneous radiofrequency ablation: local response rate and long-term survival with up to 10-year follow-up. *Radiology* 2012; 265:958-968
22. Bruix J, Sherman M. Management of hepatocellular carcinoma: an update. *Hepatology* 2011; 53:1020-1022
23. Malhotra V, Perry MC. Classical chemotherapy: mechanisms, toxicities and the therapeutc window. *Cancer Biol Ther* 2003; 2:1-3
24. Hanahan D, Weinberg RA. Hallmarks of cancer: the next generation. *Cell* 2011; 144:646-674
25. Sullivan LA, Brekken RA. The VEGF family in cancer and antibody-based strategies for their inhibition. *mAbs* 2010; 2:165-175
26. Hinnen P, Eskens FA. Vascular disrupting agents in clinical development. *Br J Cancer* 2007; 96:1159-1165
27. Ciardiello F, Tortora G. EGFR antagonists in cancer treatment. *N Engl J Med* 2008; 358:1160-1174
28. Jones KL, Buzdar AU. Evolving novel anti-HER2 strategies. *Lancet Oncol* 2009; 10:1179-1187
29. Hudis CA. Trastuzumab--mechanism of action and use in clinical practice. *N Engl J Med* 2007; 357:39-51
30. LoPiccolo J, Blumenthal GM, Bernstein WB, Dennis PA. Targeting the PI3K/Akt/mTOR pathway: effective combinations and clinical considerations. *Drug Resist Updat* 2008; 11:32-50
31. Sleijfer S, Wiemer E, Verweij J. Drug Insight: gastrointestinal stromal tumors (GIST)--the solid tumor model for cancer-specific treatment. *Nat Clin Pract Oncol* 2008; 5:102-111
32. El Saghir NS, Tfayli A, Hatoum HA, Nachef Z, Dinh P, Awada A. Treatment of metastatic breast cancer: state-of-the-art, subtypes and perspectives. *Crit Rev Oncol Hematol* 2011; 80:433-449
33. Heidenreich A, Bastian PJ, Bellmunt J, et al. EAU guidelines on prostate cancer. Part II: treatment of advanced, relapsing, and castration-resistant prostate cancer. *Eur Urol* 2014; 65:467-479
34. Coates A, Abraham S, Kaye SB, et al. On the receiving end—patient perception of the side-effects of cancer chemotherapy. *Eur J Cancer Clin Oncol* 1983; 19:203-208
35. Allan JM, Travis LB. Mechanisms of therapy-related carcinogenesis. *Nature Reviews Cancer* 2005; 5:943-955
36. Kabbinavar F, Hurwitz HI, Fehrenbacher L, et al. Phase II, randomized trial comparing bevacizumab plus fluorouracil (FU)/leucovorin (LV) with

FU/LV alone in patients with metastatic colorectal cancer. *J Clin Oncol* 2003; 21:60-65
37. Kilickap S, Abali H, Celik I. Bevacizumab, bleeding, thrombosis, and warfarin. *J Clin Oncol* 2003; 21:3542-3542
38. Cunningham D, Humblet Y, Siena S, et al. Cetuximab monotherapy and cetuximab plus irinotecan in irinotecan-refractory metastatic colorectal cancer. *N Engl J Med* 2004; 351:337-345
39. Ranson M, Hammond LA, Ferry D, et al. ZD1839, a selective oral epidermal growth factor receptor–tyrosine kinase inhibitor, is well tolerated and active in patients with solid, malignant tumors: results of a phase I trial. *J Clin Oncol* 2002; 20:2240-2250
40. Robert F, Blumenschein G, Herbst RS, et al. Phase I/IIa study of cetuximab with gemcitabine plus carboplatin in patients with chemotherapy-naïve advanced non–small-cell lung cancer. *J Clin Oncol* 2005; 23:9089-9096
41. Vincenzi B, Santini D, Rabitti C, et al. Cetuximab and irinotecan as third-line therapy in advanced colorectal cancer patients: a single centre phase II trial. *Br J Cancer* 2006; 94:792-797
42. Ewer MS, Vooletich MT, Durand J-B, et al. Reversibility of trastuzumab-related cardiotoxicity: new insights based on clinical course and response to medical treatment. *J Clin Oncol* 2005; 23:7820-7826
43. Robert C, Soria J-C, Spatz A, et al. Cutaneous side-effects of kinase inhibitors and blocking antibodies. *The lancet oncology* 2005; 6:491-500
44. Desai J, Yassa L, Marqusee E, et al. Hypothyroidism after sunitinib treatment for patients with gastrointestinal stromal tumors. *Ann Intern Med* 2006; 145:660-664
45. Alberts SR, Horvath WL, Sternfeld WC, et al. Oxaliplatin, fluorouracil, and leucovorin for patients with unresectable liver-only metastases from colorectal cancer: a North Central Cancer Treatment Group phase II study. *J Clin Oncol* 2005; 23:9243-9249
46. Abou-Alfa GK, Schwartz L, Ricci S, et al. Phase II study of sorafenib in patients with advanced hepatocellular carcinoma. *J Clin Oncol* 2006; 24:4293-4300
47. Kim H, Folks KD, Guo L, et al. Early therapy evaluation of combined cetuximab and irinotecan in orthotopic pancreatic tumor xenografts by dynamic contrast-enhanced magnetic resonance imaging. *Mol Imaging* 2011; 10:153
48. Eisenhauer EA, Therasse P, Bogaerts J, et al. New response evaluation criteria in solid tumours: revised RECIST guideline (version 1.1). *Eur J Cancer* 2009; 45:228-247
49. Byrne M, Nowak A. Modified RECIST criteria for assessment of response in malignant pleural mesothelioma. *Ann Oncol* 2004; 15:257-260
50. Marcus CD, Ladam-Marcus V, Cucu C, Bouche O, Lucas L, Hoeffel C. Imaging techniques to evaluate the response to treatment in oncology: current standards and perspectives. *Crit Rev Oncol Hematol* 2009; 72:217-238
51. Benjamin RS, Choi H, Macapinlac HA, et al. We should desist using RECIST, at least in GIST. *J Clin Oncol* 2007; 25:1760-1764
52. Chun YS, Vauthey JN, Boonsirikamchai P, et al. Association of computed tomography morphologic criteria with pathologic response and survival

in patients treated with bevacizumab for colorectal liver metastases. *JAMA: The Journal of the American Medical Association* 2009; 302:2338-2344
53. Choi H, Charnsangavej C, Faria SC, et al. Correlation of computed tomography and positron emission tomography in patients with metastatic gastrointestinal stromal tumor treated at a single institution with imatinib mesylate: proposal of new computed tomography response criteria. *J Clin Oncol* 2007; 25:1753-1759
54. Rubbia-Brandt L, Giostra E, Brezault C, et al. Importance of histological tumor response assessment in predicting the outcome in patients with colorectal liver metastases treated with neo-adjuvant chemotherapy followed by liver surgery. *Ann Oncol* 2007; 18:299-304
55. O'Connor JP, Jackson A, Asselin MC, Buckley DL, Parker GJ, Jayson GC. Quantitative imaging biomarkers in the clinical development of targeted therapeutics: current and future perspectives. *Lancet Oncol* 2008; 9:766-776
56. Deshpande N, Pysz MA, Willmann JK. Molecular ultrasound assessment of tumor angiogenesis. *Angiogenesis* 2010; 13:175-188
57. Miles K. Molecular imaging with dynamic contrast-enhanced computed tomography. *Clin Radiol* 2010; 65:549-556
58. Padhani A, Leach M. Antivascular cancer treatments: functional assessments by dynamic contrast-enhanced magnetic resonance imaging. *Abdom Imaging* 2005; 30:325-342
59. Lassau N, Chami L, Benatsou B, Peronneau P, Roche A. Dynamic contrast-enhanced ultrasonography (DCE-US) with quantification of tumor perfusion: a new diagnostic tool to evaluate the early effects of antiangiogenic treatment. *European Radiology Supplements* 2007; 17:89-98
60. Lassau N, Koscielny S, Chami L, et al. Advanced hepatocellular carcinoma: early evaluation of response to bevacizumab therapy at dynamic contrast-enhanced US with quantification—preliminary results. *Radiology* 2011; 258:291-300
61. Averkiou M, Lampaskis M, Kyriakopoulou K, et al. Quantification of tumor microvascularity with respiratory gated contrast enhanced ultrasound for monitoring therapy. *Ultrasound Med Biol* 2010; 36:68-77
62. Xiong HQ, Herbst R, Faria SC, et al. A phase I surrogate endpoint study of SU6668 in patients with solid tumors. *Invest New Drugs* 2004; 22:459-466
63. Ng CS, Charnsangavej C, Wei W, Yao JC. Perfusion CT findings in patients with metastatic carcinoid tumors undergoing bevacizumab and interferon therapy. *AJR* 2011; 196:569-576
64. Kim DH, Kim SH, Im SA, et al. Intermodality comparison between 3D perfusion CT and 18F-FDG PET/CT imaging for predicting early tumor response in patients with liver metastasis after chemotherapy: Preliminary results of a prospective study. *Eur J Radiol* 2012;
65. Hirashima Y, Yamada Y, Tateishi U, et al. Pharmacokinetic parameters from 3‐Tesla DCE‐MRI as surrogate biomarkers of antitumor effects of bevacizumab plus FOLFIRI in colorectal cancer with liver metastasis. *Int J Cancer* 2012; 130:2359-2365

66. Hayano K, Yoshida H, Zhu AX, Sahani DV. Fractal Analysis of Contrast-Enhanced CT Images to Predict Survival of Patients with Hepatocellular Carcinoma Treated with Sunitinib. *Dig Dis Sci* 2014; 59:1996-2003
67. Padhani AR, Liu G, Mu-Koh D, et al. Diffusion-weighted magnetic resonance imaging as a cancer biomarker: consensus and recommendations. *Neoplasia* 2009; 11:102-125
68. Afaq A, Andreou A, Koh D. Diffusion-weighted magnetic resonance imaging for tumour response assessment: why, when and how? *Cancer Imaging* 2010; 10:S179
69. Padhani AR, Koh D-M. Diffusion MR imaging for monitoring of treatment response. *Magn Reson Imaging Clin N Am* 2011; 19:181-209
70. Cui Y, Zhang XP, Sun YS, Tang L, Shen L. Apparent diffusion coefficient: potential imaging biomarker for prediction and early detection of response to chemotherapy in hepatic metastases. *Radiology* 2008; 248:894-900
71. Insana MF, Wagner RF, Brown DG, Hall TJ. Describing small-scale structure in random media using pulse-echo ultrasound. *J Acoust Soc Am* 1990; 87:179-192
72. Bamber J, Hill C. Acoustic properties of normal and cancerous human liver—I. Dependence on pathological condition. *Ultrasound Med Biol* 1981; 7:121-133
73. Bamber J, Hill C, King J. Acoustic properties of normal and cancerous human liver—II Dependence on tissue structure. *Ultrasound Med Biol* 1981; 7:135-144
74. Mohana Shankar P. A general statistical model for ultrasonic backscattering from tissues. *IEEE Trans Ultrason Ferroelectr Freq Control* 2000; 47:727-736
75. Shankar PM, Dumane V, Reid JM, et al. Classification of ultrasonic B-mode images of breast masses using Nakagami distribution. *Ultrasonics, Ferroelectrics and Frequency Control, IEEE Transactions on* 2001; 48:569-580
76. Shankar P. Statistical modeling of scattering from biological media. *Acoustical Society of America Journal* 2002; 111:2463-2463
77. Tsui PH, Yeh CK, Liao YY, et al. Ultrasonic Nakagami imaging: a strategy to visualize the scatterer properties of benign and malignant breast tumors. *Ultrasound Med Biol* 2010; 36:209-217
78. Jain RK. Normalizing tumor vasculature with anti-angiogenic therapy: a new paradigm for combination therapy. *Nat Med* 2001; 7:987-989
79. DeWall RJ, Bharat S, Varghese T, Hanson ME, Agni RM, Kliewer MA. Characterizing the compression-dependent viscoelastic properties of human hepatic pathologies using dynamic compression testing. *Phys Med Biol* 2012; 57:2273-2286
80. Tong RT, Boucher Y, Kozin SV, Winkler F, Hicklin DJ, Jain RK. Vascular normalization by vascular endothelial growth factor receptor 2 blockade induces a pressure gradient across the vasculature and improves drug penetration in tumors. *Cancer Res* 2004; 64:3731-3736
81. Jain RK. Normalization of tumor vasculature: an emerging concept in antiangiogenic therapy. *Science* 2005; 307:58-62

82. Sarvazyan AP, Rudenko OV, Swanson SD, Fowlkes JB, Emelianov SY. Shear wave elasticity imaging: a new ultrasonic technology of medical diagnostics. *Ultrasound Med Biol* 1998; 24:1419-1435
83. Masuzaki R, Tateishi R, Yoshida H, et al. Assessing liver tumor stiffness by transient elastography. *Hepatology international* 2007; 1:394-397
84. Bercoff J, Tanter M, Fink M. Supersonic shear imaging: a new technique for soft tissue elasticity mapping. *IEEE Trans Ultrason Ferroelectr Freq Control* 2004; 51:396-409
85. Davies G, Koenen M. Acoustic radiation force impulse elastography in distinguishing hepatic haemangiomata from metastases: preliminary observations. *Br J Radiol* 2011; 84:939-943
86. Gallotti A, D'Onofrio M, Romanini L, Cantisani V, Pozzi Mucelli R. Acoustic Radiation Force Impulse (ARFI) ultrasound imaging of solid focal liver lesions. *Eur J Radiol* 2012; 81:451-455
87. Ying L, Lin X, Xie ZL, Tang FY, Hu YP, Shi KQ. Clinical utility of acoustic radiation force impulse imaging for identification of malignant liver lesions: a meta-analysis. *Eur Radiol* 2012;
88. Guibal A, Boularan C, Bruce M, et al. Evaluation of shearwave elastography for the characterisation of focal liver lesions on ultrasound. *Eur Radiol* 2012;
89. Shuang-Ming T, Ping Z, Ying Q, Li-Rong C, Ping Z, Rui-Zhen L. Usefulness of acoustic radiation force impulse imaging in the differential diagnosis of benign and malignant liver lesions. *Acad Radiol* 2011; 18:810-815
90. Cho SH, Lee JY, Han JK, Choi BI. Acoustic radiation force impulse elastography for the evaluation of focal solid hepatic lesions: preliminary findings. *Ultrasound Med Biol* 2010; 36:202-208
91. Hoyt K, Warram JM. Quantitative elasticity measurements reveal intratumoral changes in response to antiangiogenic therapy-preliminary results. In: *Ultrasonics Symposium (IUS), 2009 IEEE International*: IEEE, 2009:1443-1446
92. Patel C, Goldstone A, Chowdhury F, Scarsbrook A. FDG PET/CT in oncology:"raising the bar". *Clin Radiol* 2010; 65:522-535
93. Wahl RL, Jacene H, Kasamon Y, Lodge MA. From RECIST to PERCIST: Evolving Considerations for PET response criteria in solid tumors. *J Nucl Med* 2009; 50 Suppl 1:122S-150S
94. Hendlisz A, Golfinopoulos V, Garcia C, et al. Serial FDG-PET/CT for early outcome prediction in patients with metastatic colorectal cancer undergoing chemotherapy. *Ann Oncol* 2012; 23:1687-1693
95. Nelson DA, Tan TT, Rabson AB, Anderson D, Degenhardt K, White E. Hypoxia and defective apoptosis drive genomic instability and tumorigenesis. *Genes Dev* 2004; 18:2095-2107
96. Dexter DL, Kowalski HM, Blazar BA, Fligiel Z, Vogel R, Heppner GH. Heterogeneity of tumor cells from a single mouse mammary tumor. *Cancer Res* 1978; 38:3174-3181
97. Hockel M, Knoop C, Schlenger K, et al. Intratumoral pO2 predicts survival in advanced cancer of the uterine cervix. *Radiother Oncol* 1993; 26:45-50
98. Hockel M, Schlenger K, Aral B, Mitze M, Schaffer U, Vaupel P. Association between tumor hypoxia and malignant progression in advanced cancer of the uterine cervix. *Cancer Res* 1996; 56:4509-4515

99. Yang Z, Tang LH, Klimstra DS. Effect of tumor heterogeneity on the assessment of Ki67 labeling index in well-differentiated neuroendocrine tumors metastatic to the liver: implications for prognostic stratification. *Am J Surg Pathol* 2011; 35:853-860
100. Castellano G, Bonilha L, Li LM, Cendes F. Texture analysis of medical images. *Clin Radiol* 2004; 59:1061-1069
101. Al-Kadi OS, Watson D. Texture analysis of aggressive and nonaggressive lung tumor CE CT images. *IEEE Trans Biomed Eng* 2008; 55:1822-1830
102. Ganeshan B, Goh V, Mandeville HC, Ng QS, Hoskin PJ, Miles KA. Non-small cell lung cancer: histopathologic correlates for texture parameters at CT. *Radiology* 2013; 266:326-336
103. Kido S, Kuriyama K, Higashiyama M, Kasugai T, Kuroda C. Fractal analysis of internal and peripheral textures of small peripheral bronchogenic carcinomas in thin-section computed tomography: comparison of bronchioloalveolar cell carcinomas with nonbronchioloalveolar cell carcinomas. *J Comput Assist Tomogr* 2003; 27:56-61
104. Kido S, Kuriyama K, Higashiyama M, Kasugai T, Kuroda C. Fractal analysis of small peripheral pulmonary nodules in thin-section CT: evaluation of the lung-nodule interfaces. *J Comput Assist Tomogr* 2002; 26:573-578
105. Huang YL, Chen JH, Shen WC. Diagnosis of hepatic tumors with texture analysis in nonenhanced computed tomography images. *Acad Radiol* 2006; 13:713-720
106. Goh V, Sanghera B, Wellsted DM, Sundin J, Halligan S. Assessment of the spatial pattern of colorectal tumour perfusion estimated at perfusion CT using two-dimensional fractal analysis. *Eur Radiol* 2009; 19:1358-1365
107. Cui C, Cai H, Liu L, Li L, Tian H, Li L. Quantitative analysis and prediction of regional lymph node status in rectal cancer based on computed tomography imaging. *Eur Radiol* 2011; 21:2318-2325
108. Goh V, Ganeshan B, Nathan P, Juttla JK, Vinayan A, Miles KA. Assessment of response to tyrosine kinase inhibitors in metastatic renal cell cancer: CT texture as a predictive biomarker. *Radiology* 2011; 261:165-171
109. Yip C, Davnall F, Kozarski R, et al. Assessment of changes in tumor heterogeneity following neoadjuvant chemotherapy in primary esophageal cancer. *Dis Esophagus* 2015; 28:172-179
110. Cross SS. Fractals in pathology. *J Pathol* 1997; 182:1-8
111. Mandelbrote B. *The fractal geometry of nature.*: W.H.Freeman and Company, New York, 1983
112. Buczkowski S, Kyriacos S, Nekka F, Cartilier L. The modified box-counting method: analysis of some characteristic parameters. *Pattern Recognition* 1998; 31:411-418
113. Feng J, Lin W-C, Chen C-T. Fractional box-counting approach to fractal dimension estimation. In: *Pattern Recognition, 1996., Proceedings of the 13th International Conference on*: IEEE, 1996:854-858
114. Keller JM, Chen S, Crownover RM. Texture description and segmentation through fractal geometry. *Computer Vision, Graphics, and Image Processing* 1989; 45:150-166
115. Sarkar N, Chaudhuri B. An efficient differential box-counting approach to compute fractal dimension of image. *Systems, Man and Cybernetics, IEEE Transactions on* 1994; 24:115-120

116. Traina C, Traina A, Wu L, Faloutsos C. Fast feature selection using fractal dimension. 2000;
117. Goldberg RM, Sargent DJ, Morton RF, et al. A randomized controlled trial of fluorouracil plus leucovorin, irinotecan, and oxaliplatin combinations in patients with previously untreated metastatic colorectal cancer. *J Clin Oncol* 2004; 22:23-30
118. Tournigand C, André T, Achille E, et al. FOLFIRI followed by FOLFOX6 or the reverse sequence in advanced colorectal cancer: a randomized GERCOR study. *J Clin Oncol* 2004; 22:229-237
119. Nordlinger B, Van Cutsem E, Gruenberger T, et al. Combination of surgery and chemotherapy and the role of targeted agents in the treatment of patients with colorectal liver metastases: recommendations from an expert panel. *Ann Oncol* 2009; 20:985-992
120. Wells P, Halliwell M. Speckle in ultrasonic imaging. *Ultrasonics* 1981; 19:225-229
121. Chivers R. The scattering of ultrasound by human tissues—some theoretical models. *Ultrasound Med Biol* 1977; 3:1-13
122. Destrempes F, Cloutier G. A critical review and uniformized representation of statistical distributions modeling the ultrasound echo envelope. *Ultrasound Med Biol* 2010; 36:1037-1051
123. Holfman H. *Statistical methods on radio wave propagation*: New York: Pergamon, 1960
124. Shankar P. A general statistical model for ultrasonic backscattering from tissues. *IEEE Trans Ultrason Ferroelectr Freq Control* 2000; 47:727-736
125. Mamou J, Oelze M. *Quantitative ultrasound in soft tissues*: New York: Springer, 2013
126. Tsui PH, Chang CC. Imaging local scatterer concentrations by the Nakagami statistical model. *Ultrasound Med Biol* 2007; 33:608-619
127. Zhou Z, Wu S, Wang CY, Ma HY, Lin CC, Tsui PH. Monitoring radiofrequency ablation using real-time ultrasound Nakagami imaging combined with frequency and temporal compounding techniques. *PLoS ONE* 2015; 10:e0118030
128. Tsui PH, Huang CC, Chang CC, Wang SH, Shung KK. Feasibility study of using high-frequency ultrasonic Nakagami imaging for characterizing the cataract lens in vitro. *Phys Med Biol* 2007; 52:6413-6425
129. Tsui PH, Yeh CK, Chang CC, Liao YY. Classification of breast masses by ultrasonic Nakagami imaging: a feasibility study. *Phys Med Biol* 2008; 53:6027-6044
130. Tsui PH, Liao YY, Chang CC, Kuo WH, Chang KJ, Yeh CK. Classification of benign and malignant breast tumors by 2-d analysis based on contour description and scatterer characterization. *IEEE Trans Med Imaging* 2010; 29:513-522
131. Ho MC, Lee YH, Jeng YM, Chen CN, Chang KJ, Tsui PH. Relationship between ultrasound backscattered statistics and the concentration of fatty droplets in livers: an animal study. *PLoS ONE* 2013; 8:e63543
132. Ho MC, Lin JJ, Shu YC, et al. Using ultrasound Nakagami imaging to assess liver fibrosis in rats. *Ultrasonics* 2012; 52:215-222

133. Yamada H, Ebara M, Yamaguchi T, et al. A pilot approach for quantitative assessment of liver fibrosis using ultrasound: preliminary results in 79 cases. *J Hepatol* 2006; 44:68-75
134. Lin YH, Huang CC, Wang SH. Quantitative assessments of burn degree by high-frequency ultrasonic backscattering and statistical model. *Phys Med Biol* 2011; 56:757-773
135. Yang X, Rossi P, Bruner DW, Tridandapani S, Shelton J, Liu T. Noninvasive evaluation of vaginal fibrosis following radiotherapy for gynecologic malignancies: a feasibility study with ultrasound B-mode and Nakagami parameter imaging. *Med Phys* 2013; 40:022901
136. Yang X, Tridandapani S, Beitler JJ, et al. Ultrasonic Nakagami-parameter characterization of parotid-gland injury following head-and-neck radiotherapy: a feasibility study of late toxicity. *Med Phys* 2014; 41:022903
137. Marusyk A, Almendro V, Polyak K. Intra-tumour heterogeneity: a looking glass for cancer? *Nat Rev Cancer* 2012; 12:323-334
138. Toraya-Brown S, Fiering S. Local tumour hyperthermia as immunotherapy for metastatic cancer. *Int J Hyperthermia* 2014; 30:531-539
139. Al-Kadi OS, Chung DY, Carlisle RC, Coussios CC, Noble JA. Quantification of ultrasonic texture intra-heterogeneity via volumetric stochastic modeling for tissue characterization. *Med Image Anal* 2015; 21:59-71
140. Hakime A, Deschamps F, De Carvalho EG, Teriitehau C, Auperin A, De Baere T. Clinical evaluation of spatial accuracy of a fusion imaging technique combining previously acquired computed tomography and real-time ultrasound for imaging of liver metastases. *Cardiovasc Intervent Radiol* 2011; 34:338-344
141. Noble JA. Ultrasound image segmentation and tissue characterization. *Proc Inst Mech Eng H* 2010; 224:307-316

APPENDIX

Appendix A: Clinical study protocol

Below is the synopsis for the clinical study mentioned in chapter 4 of this thesis.

Study Title	Pilot observation study to assess the utility of liver tumour ultrasound imaging parameters in detecting response to treatment.
Ethics ref. no.	12/SC/0279
Study Design	Pilot observation study
Study Participants	Patients diagnosed with liver metastases from any solid cancer, who are receiving systemic therapy at the Oxford University Hospitals NHS Trust.
Number of Participants	50 patients
Planned Study Period	Recruitment will continue for 2 years with the aim of 50 patients completing the proposed study schedule and final imaging study at the end of their chemotherapy course.
Primary Objective	To assess if changes in radiofrequency echo ultrasound data of liver tumours throughout chemotherapeutic treatment correlate with response to treatment.
Secondary Objectives	1. To assess if changes in contrast enhanced ultrasound data, Doppler ultrasound data and ultrasound elastography data of liver tumours throughout chemotherapeutic treatment correlate with response to treatment. 2. To test existing methods for automated segmentation and registration of liver tumours in order to facilitate operator-independent comparison between ultrasound and CT imaging data.
Primary Endpoint	Changes in radiofrequency echo ultrasound data of liver tumours throughout chemotherapeutic treatment will be correlated with measured response on CT or MRI scans performed to assess response to treatment using RECIST 1.1 criteria.
Secondary Endpoints	1. Changes in contrast-enhanced ultrasound data, Doppler ultrasound data and ultrasound elastography data of liver tumours throughout chemotherapeutic treatment will be correlated with measured response on CT or MRI scans performed to assess response to treatment using RECIST 1.1 criteria. 2. Comparing degree of overlap of liver tumours as measured by the operator and estimated by automated registration and segmentation methods on ultrasound images from different time points, and between different imaging modalities using Dice coefficient.